Manipulating polymers and composites from the nanoscopic to microscopic length scales.

MANIPULATING POLYMERS AND COMPOSITES FROM THE NANOSCOPIC TO MICROSCOPIC LENGTH SCALES

A Dissertation Presented

by

SURESH GUPTA

Submitted to the Graduate School of the
University of Massachusetts Amherst in partial fulfillment
of the requirements for the degree of

DOCTOR OF PHILOSOPHY

May 2008

Polymer Science and Engineering

MANIPULATING POLYMERS AND COMPOSITES FROM THE NANOSCOPIC TO MICROSCOPIC LENGTH SCALES

A Dissertation Presented

by

SURESH GUPTA

Approved as to style and content by:

_____

Prof. Thomas P. Russell, Chair

_____

Prof. David A. Hoagland, Member

_____

Prof. Anthony D. Dinsmore, Member

_____

Prof. Shaw Ling Hsu, Department Head
Department of Polymer Science and Engineering

MANIPULATING POLYMERS AND COMPOSITES FROM THE NANOSCOPIC TO MICROSCOPIC LENGTH SCALES

A Dissertation Presented

by

SURESH GUPTA

Approved as to style and content by:

Prof. Thomas P. Russell, Chair

Prof. David A. Hoagland, Member

Prof. Anthony D. Dinsmore, Member

Prof. Shaw Ling Hsu, Department Head
Department of Polymer Science and Engineering

ABSTRACT

MANIPULATING POLYMERS AND COMPOSITES FROM THE NANOSCOPIC TO MICROSCOPIC LENGTH SCALES

MAY 2008

SURESH GUPTA

B.Tech. INDIAN INSTITUTE OF TECHNOLOGY, DELHI

M.S. UNIVERSITY OF MASSACHUSETTS AMHERST

Ph.D. UNIVERSITY OF MASSACHUSETTS AMHERST

Directed by: Professor Thomas P. Russell

This thesis focuses on the manipulation of polymers and composites on length scales ranging from the nanoscopic to microscopic. In particular, on the microscopic length scale electric fields were used to produce instabilities at the air surface and at polymer interfaces that lead to novel three dimensional structures and patterns. On the nanoscopic length scale, the interaction of ligands attached to nanoparticles and polymer matrix were used to induce self-assembly processes that, in turn, lead to systems that self-heal, self-corral, or are patterned.

For manipulation at the micron length scale, electrohydrodynamic instabilities were used in trilayer system composed of a layer of poly(methyl methacrylate) (PMMA), a second layer of polystyrene (PS) and a third layer of air. Dewetting of the polymer at the substrate at the polymer/polymer interface under an applied electric field was used to generate novel three dimensional structures. Also, electrohydrodynamic instabilities were used to pattern thin polymer films in conjunction with ultrasonic vibrations and patterned upper electrodes.

Self-assembly processes involving polymers and nanoparticles offer a unique means of generating pattern materials or materials that self heal. Simple polymer/nanoparticle composites were investigated. Here, in the absence of interactions between the poly(ethylene oxide) ligands attached to the nanoparticles and PMMA polymer matrix, the opportunity to generate self-healing systems was opened. The size of the nanoparticle was varied and the effect on diffusion of nanoparticle in the polymer matrix was studied. CdSe nanorods were also assembled on a substrate templated with or guided by microphase separated diblock copolymers. The nanorods were incorporated in the diblock copolymer thin films by spin coating the co-solution of nanorods and polymer, surface adsorption of nanorods on to the patterned diblock copolymer films and surface reconstruction of PS/PMMA diblock copolymer thin film. Further, the interactions between the PMMA polymer matrix and the tri n-octyl phosphine oxide ligands attached to an anisotropic nanoparticle, i.e. nanorods, were used to influence the dispersion of the nanorods in the polymer. This led to a novel assembly, termed self-corralling where under an applied electric field highly oriented, highly ordered arrays of nanorods form. Further, self corralling of nanorods was directed by chemically patterned substrates.

TABLE OF CONTENTS

LIST OF TABLES

LIST OF FIGURES

CHAPTER 1

INTRODUCTION

In past few decades, polymers have become an integral part of research in various fields of science and technology. It may be in the field of medical devices and implants, semiconductor technology or energy, polymers have become material of choice for the researchers due to their versatility and potentially cheap sources to obtain them. In order to further increase the popularity and use of polymers, new approaches have been developed. One of the approaches has been to blend inorganic materials with the polymers and hence modify their mechanical, electronic, magnetic and optical properties. Particles of varying characteristics; sizes from micron length scale to nano length scale, metallic to ceramic, conducting to insulators; have been blended with polymers to make composite materials and to obtain properties not present inherently in the polymeric materials. In addition to blending, there are other ways to manipulate polymers so as to further enhance their functionality and use in technology. Patterning of polymer thin films using light have been one of them. But recently non-photolithographic techniques are also becoming popular to pattern polymer thin films like nano-imprint lithography, dip pen lithography etc. Use of electric field has also been proposed to be one of the ways to obtain patterned films. By using a patterned electrode and applying electric field, pattern can be replicated onto the polymer film.

In this thesis, effect of electric field on polymer thin films is studied and structures at micron length scale are patterned onto polymer films. Further, at nano length scale, polymer-nanoparticle composites are studied where the interactions

between nanoparticles and polymer are manipulated to develop composites that self heal as well as composites that have potential applications in photovoltaic devices.

In this chapter the electrohydrodynamic instabilities are introduced. These instabilities result when an electric field is applied across thin polymer films. Also, nanoparticle-polymer composites are introduced later on in this chapter.

1.1 Electrohydrodynamic instability

Non-photolithographic patterning techniques have been extensively studied in the past two decades. This includes patterning with microphase separated diblock copolymers[1], contact printing techniques,[2] and imprint lithography.[3] Patterns have also been generated based on instabilities in thin polymer films on a substrate. Van der Waals forces,[4] mechanical stresses,[5] thermal gradients,[6] and electric field gradients[7] are examples of destabilizing fields that have been used to generate patterned films. Electric field gradients are advantageous, since the size scale of the pattern can be controlled simply by adjusting the strength of the electric field. The process of pattern generation with an electric field gradient can easily be coupled with the dewetting of thin polymer films to generate novel structures. With dewetting of thin polymer films, the instability is generated by van der Waals forces. Thermal fluctuations at the free polymer surface are amplified and, hence, lead to dewetting, depending upon the surface energies of the fluid and underlying substrate.[8] In an electric field, the instability is produced by the stresses at the interface between two dielectric fluids due to uncompensated displacement charges. This imbalance makes the system unstable to fluctuations of a specific wavelength, and patterns are generated with a wavelength determined by the

interfacial energy and the electric field gradient at the interface. Structure formation at polymer/air (single layer),[7] polymer/polymer (bilayer),[9] and polymer/polymer/air (trilayer)[10] interfaces has been well-studied. Typically, experiments are performed between two parallel electrodes separated by a well-defined distance.

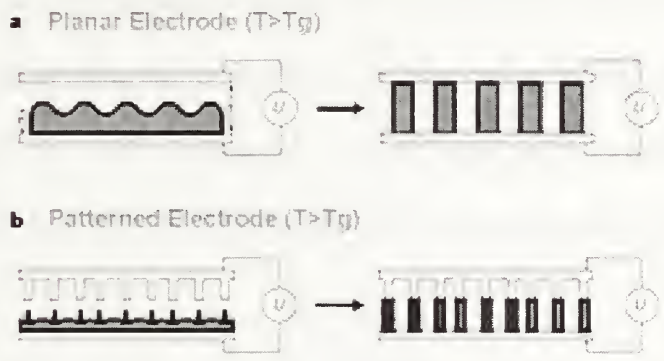

Figure 1.1: Schematic for experiment to study electrohydrodynamic instabilities[7]

Figure 1.1 shows the schematic diagram of the experiment. In this schematic, there is a thin polymer film between two electrodes separated by an air gap. The electric field is applied by applying potential difference between the two electrodes. Generally the gap between the two electrodes is about 1 -10 micrometer and the voltage is applied in the range of 10-100 volts. This gives the field strengths in the range of 10^7 volts/m. When electric field is applied across the polymer film/ air interface, instabilities at the interface are produced. The origin of the instabilities is due to the Maxwell stress generated at the interface which pulls the interface towards the electrode. These stresses are opposed by the Laplace pressure which tends to make the interface flat. Instabilities lead to the formation of pillars which grow until they impinge the upper electrode. The spacing between the pillars is determined by these two competing pressures.

Schaeffer et al. suggested that the overall pressure distribution at the film surface is expressed by,[7,11]

$$p = p_0 - \gamma \frac{\partial^2 h}{\partial x^2} + p_{el}(h) + p_{dis}(h) \quad \textbf{(1.1)}$$

with p_0 being the atmospheric pressure. The second term, the Laplace pressure, stems from the surface tension γ and the fourth term, the disjoining pressure p_{dis}, arises from van der Waals interactions between the polymer and the substrate. The electrostatic pressure for a given electric field in the polymer film is given by,

$$p_{el} = -\varepsilon_0 \varepsilon_p (\varepsilon_p - 1) E_p^{\ 2}$$

where,

$$E_p = \frac{U}{\{\varepsilon_p d - (\varepsilon_p - 1)h\}}$$

ε_0 is the electric constant, ε_p is the dielectric constant of the polymer, E_p is the electric field inside polymer, d is the separation between the two electrodes, h is the polymer film thickness and U is the voltage applied.

In order to do the stability analysis of the system, a small sinusoidal perturbation of h is introduced in the equation 1.1. Here, we have ignored the disjoining pressure as we are discounting the effect of polymer dewetting on the substrate. On doing the linear perturbation analysis, the fastest growing wavelength that comes from the dispersion relation is given by[12]

$$\lambda = 2\pi \sqrt{\frac{\gamma U}{\varepsilon_0 \varepsilon_p (\varepsilon_p - 1)^2}} E_p^{\ -\frac{3}{2}} \quad \textbf{(1.2)}$$

and the waves of this wavelength is unstable i.e. the wave amplitude grows with time. This wavelength determines the separation between the pillars and as shown in the equation 1.2 can be varied by: 1) changing the interfacial tension between two layers and 2) changing the electric field strength. On further analysis of the equation it can be seen that the electrohydrodynamic instabilities are analogous to phase separation in polymer blends. In the latter system, phase domains develop with time with a periodicity equal to the dominant wavelength of concentration fluctuations in the system. The wavelength of these fluctuations is dictated by a balance between thermodynamics and kinetics. Thermodynamics, which is governed by the interfacial tension produced by formation of phases, favors the growth of large domains, while kinetics favor the growth of smaller phases. The kinetics of phase separation in polymer blends, i.e. the rate at which fluctuations grow at early stages of the phase separation, is characterized by an exponential growth, as described by linearized Cahn-Hilliard arguments.[13] However, at the later stages, deviations from this behavior are seen and the hydrodynamics associated with the flow of the polymers must be considered. The growth of fluctuations at the air-polymer interface in an electric field also follow a similar pattern, as it is similarly governed by a balance between surface tension and Maxwell stress. The linearized theory of Schaffer et al. predicts that the rate of growth in the amplitude of the dominant wavelength should be exponential. However, deviations from this should be expected as the flow of the polymer in the thin films becomes dominant.

1.1.1 Eletrohydrodynamic instabilities in multilayer polymer systems

The electrohydrodynamic instabilities of liquid/liquid interfaces have also been studied extensively by Russell and coworkers.[10] The reduction in the difference in the dielectric constants and the reduction in the interfacial tension results in a change in the characteristic wavelength of EHD instabilities at a liquid/liquid interface. The electrohydrodynamic instabilities of PMMA/PS/air were examined. Lin et al. investigated the PMMA (Mw = 95 kg/mol, layer thickness = 228 nm)/PS (Mw = 96 kg/mol, 284 nm)/air interface under different electric field strengths where the electrode spacing was varied.[14] The growth of surface fluctuations and pillar formation in the upper PS layer on the underlying PMMA layer could be seen by the removal of the PS layer with a selective solvent. After removing the PS layer with cyclohexane, a line scan of the PMMA surface, corresponding to the interface between the PS and PMMA, was featureless. Consequently, the PS/air interface deforms much more readily than the PMMA/PS interface. Qualitatively, the PS/air surface is expected to deform much more rapidly than the PMMA/PS interface, and the viscous damping for the deformation of a free surface is much smaller than that of a polymer-polymer interface.

Further, Lin et al. characterized the structure formation at the interface of liquid/liquid bilayers.[9] A good agreement between theory and experiment was found over many orders of magnitude in reduced wavelength and field strength using no adjustable parameters, regardless of the polymers. The following systems were investigated: PS (Mw=30 kg/mol, 550 nm)/PDMS (η=10,000 cSt, 570 nm); PS

(Mw=96 kg/mol, 730 nm)/PMMA (Mw=27 kg/mol, 290 nm); and PMMA (Mw=27 kg/mol, 290 nm)/PDMS (η=10,000 cSt, 730 nm) where the molecular weight of the polymer as well as the film thickness is mentioned in the parentheses .

The PS/PDMS bilayer after 1 day at 170 °C under 44 V/μm showed pillars of PS penetrating through the upper PDMS layer. The distribution of the center-to-center distances of adjacent pillars was determined and the average separation distance was 12.9 μm. Substituting the parameters for the PDMS/PS bilayer into Eq. (1.2) yielded a characteristic distance of 15.8 μm, which agreed well with the 12.9 μm value measured experimentally. In a second set of experiments, the upper PDMS layer was replaced by a PMMA layer to form PS/PMMA bilayer. Since the interfacial tension between PS and PMMA (1.7 mN/m at 170 °C) is smaller than that for a PS/PDMS bilayer (6.1 mN/m at 170 °C) at any given temperature, it would be expected that the characteristic wavelength would decrease. PMMA pillars formed within the PS layer. Experiments on PMMA/PDMS bilayers showed essentially the same behavior as that of the PS/PDMS bilayers. The film thickness of underlying PMMA layer was much thinner than that of the upper PDMS

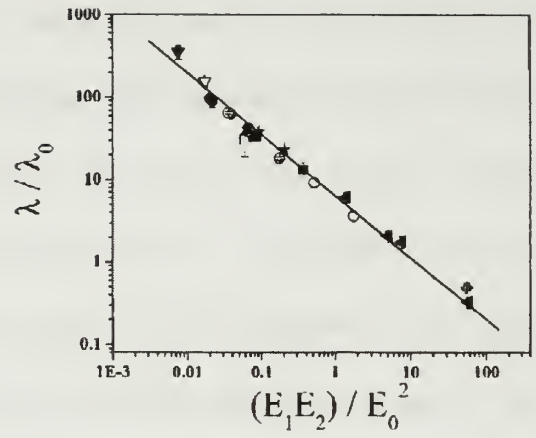

Figure 1.2: Master curve of the typical distance λ in varieties of thin film and bilayer experiments as a function of the electric field strength in layer 1 and layer 2. The different symbols corresponded to 10 data sets: (♦) PS/PMMA bilayer with hPS=730 nm; (d - hPS)PMMA=290 nm, U) 30 V; (▼) PMMA/PDMS bilayer with hPMMA=180-290 nm, (d - hPMMA)PDMS=690-1030 nm, U=19-50 V; (★) PS/PDMS bilayer with hPS=305 nm, (d - hPS)PDMS=400 nm and 720 nm respectively, U=50 V; (▲) PS/PDMS bilayer with hPS=550 nm, (d - hPS)PDMS=570 nm and 700 nm respectively, U=50 V; (o) PSBr/air single layer with hPSBr=740 nm, d=1.66-1.98 μm, U=20-60 V; (●) dPS/air single layer with hdPS=530 nm, d=1.06-1.85 μm, U=30 V. E1 and E2 are the electric field strength in layer 1 and 2. Other data sets (▼, ∇, ■, □) are measurements from ref. [12]

layer, therefore the PMMA pillars were obtained. Most importantly, there was excellent agreement between experiment and theory over four orders of magnitude in the reduced wavelength and reduced field strength. A master curve (Figure 1.2) was shown to describe the results from a wide range of systems over many orders of magnitude in reduced field strength and distance with no adjustable parameters[9].

In Chapter 1, the electrohydrodynamic instabilities in multilayered polymer films are studied where in combination with a preferential wetting of the top electrode by one of the polymers, leads to unique three-dimensional structures, where one polymer can be encased within another, whereas, in the absence of preferential wetting of the top electrode by one polymer, different structures are obtained in which one

polymer is not completely encased in the other. PMMA/PS/air trilayer generate fluctuations first at the PS/air interface, with the PMMA film remaining relatively unperturbed. In those experiments, the wavelength of the fastest growing fluctuation amplified by the electric field defined the characteristic spacing of a well-ordered array of PS pillars, spanning the electrodes. Although the electric field creates a destabilizing force at both the PS/air interface and the PMMA/PS interface, due to dielectric contrast in the materials, the time scale of pillar formation is much faster at the PS/air interface. This is largely due to the low viscous resistance at the air interface, combined with the tendency of PS to dewet PMMA, allowing for interfacial slip.

1.1.2 Pattern replication using electrohydrodynamic instabilities

The physical basis of this electrohydrodynamic patterning technique is the amplification of fluctuations at a fluid/fluid interface by a destabilizing force generated when an electric field is applied normal to the surface of a thin film. Electrohydrodynamic pattern formation can be spatially controlled by introducing heterogeneity into the electric field. One simple case is a single elevated point protruding from the top electrode. Figure 1.3 shows the progress of an instability initiated at a single point. The nucleated pillar is surrounded by a radial wave propagating outward from the nucleation point (0 min). The rim develops a lateral undulation, leading to the formation of pillars along the rim (7–70 min). Once the first shell of pillars is complete, this process is continued radially outward: rims surrounding the pillars lead to the nucleation of further pillars. For sufficiently long times, this nucleated pillar formation process competes with the pattern formation caused by the

homogeneous field. The preferred induction of electrohydrodynamic instabilities at locations of highest electric field lies at the base of the electrohydrodynamic lithography. A common methodology is the use of topographically patterned top electrodes. To explore the process of pattern replication, Voicu *et al.* studied electrohydrodynamic instabilities induced by a topographic line grating as the top electrode.[15] Figure 1.4 shows the instability produced by an electrode with an array of lines. After annealing for 108 min (t=0) undulations appear under the lines protruding from the electrode surface. With time the pillars make contact with the electrode, resulting in linear arrays of pillars. Figure 1.4b shows, in comparison, the simulations by Verma *et al.*[16] for a system with filling ratio of 0.5. The simulations are qualitatively similar to the experimental results.

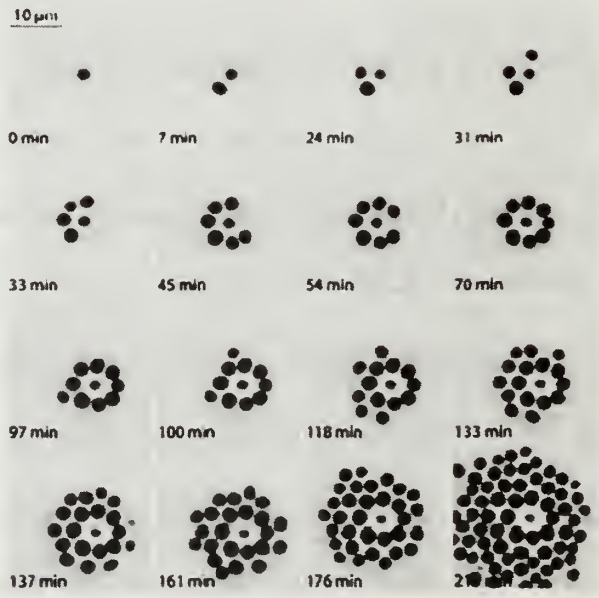

Figure 1.3: Nucleated pattern formation in an electric field. The images show a 125 nm PSBr film (filling ratio 0.5) at 10 V at 164 °C. From ref [15]

Since the wavelength of the intrinsic instability is larger by a factor of two compared to the periodicity of the grating in Figure 1.4b, only every second line of the

grating is replicated. The patterned electrode can have a topographic pattern or a pattern of conducting material on an insulating material. This will create different electric field strengths laterally and the pattern will be replicated in the polymer film as the areas under higher electric field will destabilize first.

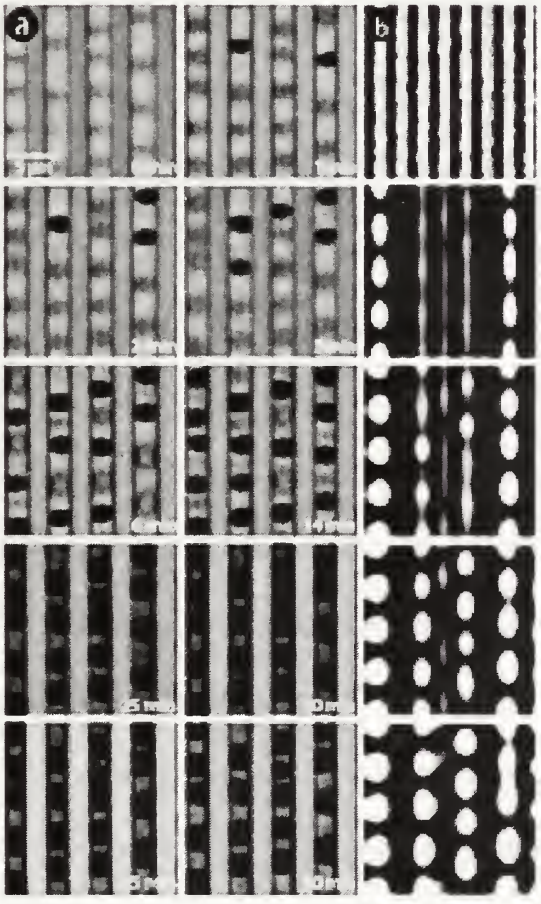

Figure 1.4: Nucleation of columns induced by an electrode with an array of lines. a) A 125 nm PSBr film (filling ratio 0.25) annealed under 30 V at 170 °C. b) Simulation results of Verma et al.[16] for filling ratio of 0.5.

In Chapter 2, experiments to replicate patterns with 30 nm features are discussed. The pattern on the electrode is produced by microphase separated PS-*b*-

PMMA diblock copolymers with different morphologies. A PS-*b*-PMMA diblock copolymer, with lamellae oriented normal to surface gives line patterns, while in the case of cylinders oriented normal to surface, hexagonally packed circles are produced on the top electrode.

Since there is a contrast in the dielectric constant of PS ($\varepsilon \sim 2$) and PMMA ($\varepsilon \sim 6$) at ~100 ^{o}C, the electric field strength is different, such that the area under the PMMA domains experience greater electric field strength. As predicted by both simulations and calculations, the larger electric field will increase the rate of structure growth. Therefore, the areas under the PMMA are pulled towards the patterned electrode initially. This gives us a means to translate a pattern having a dielectric constant contrast into patterned topography on the ~10 nm length scale. The major limitation to this technique is that the contrast in the electric field strength under PMMA and PS is reduced as the separation between the polymer film on the lower electrode and the top patterned electrode increases. Therefore, the separation gap between the two electrodes has to be similar to the size scale of the pattern. This limits the height of the patterns generated on the non-patterned film.

Pillar formation occurs when the destabilizing force is sufficiently large to overcome the stabilizing forces acting at the interface, such as surface tension, gravity, etc. The pillars thus formed are hexagonally packed but not well ordered over large areas. To obtain large areas of well ordered patterned pillars we want to couple ultrasound induced surface vibrations and freeze them with electric field and these experiments are also described in Chapter 2.

It is well known that the ultrasonic vibrations produce square packed structures on the surface of a liquid which vibrate at the same frequency as that of ultrasound.[17] The wavelength of the pattern can be controlled by varying the frequency of the ultrasound and is given by Kelvin's equation

$$\lambda = \sqrt[3]{\frac{8\pi\sigma}{f^2\rho}}$$

where ρ is the density of the liquid, f is the frequency of the ultrasound, λ is the wavelength of the pattern and σ is the surface tension of the liquid. The origin of these standing surface waves on the liquid can be understood in terms of forces applied at liquid surface which is accelerated and decelerated by vibrations.[18] The acceleration or deceleration of surface depends upon the square of the frequency of the ultrasound. These inertial forces tend to destabilize the surface while the surface tension works to stabilize the surface. Therefore, the wavelength of the standing surface waves results from the interplay between surface tension and the frequency of the ultrasonic vibrations. The aim of this study is to generate patterns on the surface of a polymer film with ultrasonic vibrations and then apply an electric field so as to amplify the patterns towards the top electrode and, hence, form stationary square packed structures.

1.2 Nanoparticle-polymer composites

The push to increase the sustainability of materials and reduce energy costs is driving researchers to rethink the design and fabrication of materials. Two key issues are rising to the forefront in the design of sustainable, energy-efficient systems. First, there is a critical need for materials that can automatically respond to environmental

changes and perform a specific function without external intervention. This is particularly important with respect to mechanical damage[19,20,21], where responsive systems could prevent catastrophic failure and thus, enhance the survivability and lifetime of the materials. Second, there is a vital need for lightweight materials that exhibit multi-functional behavior. Significant progress has been made in addressing these needs by combining polymers with inorganic nanoparticles, which impart the desired optical, electromagnetic and mechanical properties. In particular, researchers have established means of harnessing both enthalpic and entropic interactions to control the particle distribution in the polymer matrix and thereby tailor the macroscopic behavior of the composite. For example, by varying the nature of the ligands on the particles (and thus, the enthalpic interactions in the system), these solid additives can be preferentially localized at either the edges or interiors of specific domains within diblock copolymers [22], leading to distinct control over the optical properties of the nanocomposite[23,24]. Moreover, by exploiting variations in the conformational entropy of the chains, the particles can be localized within the core of cylindrical domains[25,26], opening the possibility of producing conductive nanowires or mechanically reinforcing rods that extend through the system[27]. Thus, there has been significant success in fabricating composites that integrate the desired functionality of the particles and weight advantages of the polymers. Metallic, semiconductor and magnetic nanoparticles are of great interest in nanoscience and nanotechnology due to the novel electronic, luminescent and magnetic properties that are not present in the bulk[28,29,30,31,32]. The combination of the unique properties of nanoparticles with their small size leads to a wide range of applications that could be realized from high density arrays of these

functional components. Nanoparticles can be made in various shapes, e.g. spherical, cylindrical, pyramidal, or star-like; moreover, a significant control over nanoparticle size and size distribution can be achieved[32]. However, optimal utilization of the unique properties of nanoparticles requires a positional control on the nanometer length scale enabled by self-assembly.

1.2.1 Self healing materials

Biological organisms have an amazing ability to automatically initiate self-healing and self-repair when they sustain damage. To replicate this ability in physical materials have so far remain a challenge. Such self healing materials could be of particular use in structures that are at present impractical or impossible to repair, such as electronic circuit boards, implanted medical devices or spacecraft. Self-repairing materials would have a massive impact on virtually all industries, lengthening product lifetimes, increasing safety, and lowering product costs by reducing maintenance requirements. Nanotechnology has empowered us to realize such materials. Recently two approaches have been developed to make self healing surfaces: 1) the fabrication of active composite-layered systems in which the passive coating matrix is alternated with layers bearing an active coating component (e.g., corrosion inhibitor, lubricant)[33] or 2) the integration of nanoscale containers (carriers) loaded with the active components into existing traditional coatings[34]. In other words nanocontainers are embedded in a matrix so that they release encapsulated active materials in a controlled way, leading to a new family of self-repairing coatings. These approaches have

significant shortcomings with regard to stability and self-repairing activity of the coating. Moreover, spontaneous leakage from the surface can occur during aging.

In Chapter 4, we will exploit both the ability to tailor the ligands on the nanoparticles and the entropic interactions between the particles and polymers to create a self-healing hybrid material. We focus on a multilayer system that encompasses a brittle film and an underlying nanoparticle-filled polymer. Multilayered composites of ductile polymers and brittle films (ceramics or metals) are essential for microelectronics packaging, coatings, solid-state devices, and biomedical applications. However, when subjected to high temperatures, brittle films form cracks that lie transverse to the polymer layers[35,36]. Here, when such a crack is introduced into the brittle layer, the location of the nanoparticles will be studied.

1.2.2 Nanoparticle- block copolymer composites

A variety of approaches have been undertaken towards the controlled assembly of spherical nanoparticles, ranging from assembly into close-packed superlattices[37], to particle assemblies within host matrices achieved by lithography[38] as well as self-assembly[39] . When nanoparticle assembly is performed within a host matrix, such as a polymer material, the ligands attached to the nanoparticles control the interactions of the nanoparticles with the surrounding material. Variation of the nature of the ligands can thus be used to finely tune the dispersion of nanoparticles in molten polymers, as well as other types of fluids. The effect of ligands on assemblies is well demonstrated in nanoparticle-block copolymer mixtures, where the ligand/segment interactions can be manipulated so that the nanoparticles reside in one of the microphase separated domains

of the copolymer or at the interface between the microdomains [40]. Alternatively, unfavorable interactions between the nanoparticles and polymer, coupled with packing constraints of the polymer around the nanoparticle, can lead to their expulsion from a polymer film. This latter behavior has been used to design self-orienting, self-assembling composite systems, where diblock copolymer morphology is controlled by the nanoparticle-polymer interactions[26]. Capillary force[41,42,38] and electrophoretic deposition[43] have also been used to assemble spherical nanoparticles into arrays on patterned diblock copolymer templates. In this case, the areal density of the nanoparticles can be tuned by the experimental conditions (i.e., nanoparticle concentration, choice of solvent, deposition time, and/or voltage) chosen for the particular assembly technique.

The influence of ligands on nanoparticle properties is not limited to spherical particles, but rather extends across a wide variety of particle composition and shape. Changing the shape of nanoparticles from isotropic spheres to anisotropic rods can dramatically change their properties[44]. For example, anisotropic CdSe nanorods are deemed interesting for photovoltaic applications, since the long axis of the rod may provide a continuous channel for electron transfer, and provide an advantage over spherical nanoparticles, where electron hopping is required to move electrons[45]. However, effective methods to manipulate nanorods are few and limited in scope. CdSe nanorods have been shown to self-assemble into liquid crystalline phases in a manner similar to rigid rod molecules, due to their anisotropic shape[46,47,48]. Alternatively, Au nanorods have been shown to assemble into strings, where multi-wall carbon nanotubes serve as templates[49]. However, to use nanorods to their full potential

for applications, further control is needed over their assembly, such as lateral distribution, and positional and orientational correlation between the nanorods. In Chapter 5, we demonstrate a novel route to nanorod assembly that enables both positional and orientational control over the rods. A polystyrene-*block*-poly(methyl methacrylate) (PS-*b*-PMMA) diblock copolymer thin film is used to generate templates having hollow cylindrical pores perpendicular to an underlying substrate, or narrow channels lying parallel to an underlying substrate[43]. Thurn-Albrecht, *et al.* previously showed that the cylindrical pores (approximately 15 nm in diameter) in identical polymer templates can be filled by direct current electro deposition, to give extremely dense arrays of cobalt nanowires standing parallel to an underlying substrate, and separated by defined distances[50]. However, electro deposition cannot be used to generate nanocrystalline materials with the nanoscale shapes and properties that can be achieved by solution synthesis of nanoparticles.[51] Thus, to introduce the desired nanoscopic properties of the particles into the self-assembled polymer matrix, nanoparticle synthesis and assembly are optimally performed as separate steps.

1.2.3 Composites for bulk heterojunction photovoltaic devices

In order to address the growing global energy need, energy directly from sunlight can be harvested using photovoltaic technology. This will also minimize detrimental effects on the environment by reducing 'green house' gas emissions. A photovoltaic device, or solar cell, converts absorbed photons directly into electrical charges that are used to energize an external circuit. A typical conventional solar cell is fabricated from an inorganic semiconductor material, such as crystalline Si, that is

doped to form a p–n junction. The p side contains an excess of positive charges (holes), and the n side contains an excess of negative charges (electrons). The crystalline Si based photovoltaic devices have high photoconversion efficiencies but due to inhibitively expensive cost of the processing, these devices are not considered viable to replace the conventional energy sources. Therefore, organic based photovoltaic devices have gained importance in recent times. Some key advantages for organic photovoltaic devices are that organic small-molecule and polymer materials are potentially inexpensive; they can have very high optical absorption coefficients that permit the use of films with thicknesses of only several hundred nanometers; they are compatible with plastic substrates; and they can be fabricated using high-throughput, low temperature approaches that employ one of a variety of well-established printing techniques in a roll-to-roll process. Organic photovoltaic devices can be characterized into dye sensitized solar cells, organic-inorganic solar cells and organic-organic solar cells. In dye sensitized solar cells, the photons are harvested by a transition metal based dye and charges are transported through inorganic/organic layers. Whereas in organic-inorganic and organic-organic solar cells donor-acceptor materials are used and photons are harvested by either or both acceptor-donor materials. Recently, fullerene-conducting polymer based solar cells have become very popular. Polymer–fullerene solar cells are among the first to utilize this bulk heterojunction principle.[52] Bulk heterojunction devices are fabricated by simply mixing the acceptor and donor materials and relying on the intrinsic tendency of polymer materials to phase-separate. This creates junctions throughout the bulk of the material that ensure quantitative dissociation of photogenerated excitons, irrespective of the thickness. However, this attractive solution

poses a new challenge. Photogenerated charges must be able to migrate to the collecting electrodes through this intimately mixed blend. Because holes are transported by the acceptor semiconductor and electrons by donor material, these materials should be preferably mixed into a discontinuous, interpenetrating network in which inclusions, or barrier layers are avoided. The development of organic–inorganic composites that self-assemble into ordered phases with pathways for efficient charge transport is a promising route to obtaining higher carrier mobilities. One way to achieve ordered pathways is to use inorganic semiconductor nanoparticles with asymmetric shape. These nanoparticles can provide ballistic transport for electrons to the electrode. Therefore, orienting and packing the nano-scale anisotropic objects like nanorods is highly desirable for inorganic–organic bulk heterojunction photovoltaic devices[45]. The nanorods tend to be randomly packed when they are deposited from a solution. By increasing the concentration of nanorods, liquid crystalline packing can be achieved in solution[46,47,48]. Also by adding a non-solvent to the solution of nanorods, crystalline aggregates of nanorods can be formed[37]. The deposition of these crystalline aggregates of nanorods give densely packed nanorods on a substrate, but the orientation of nanorods remains uncontrolled.

By using an external field, the orientation of anisotropic particles can be controlled. It has been shown in the case of block copolymer templates, that the domains can be oriented in a preferred direction by using an electric field due to the anisotropy in dielectric properties of two blocks[53]. Similarly, due to the presence of permanent dipole moment in CdSe nanorods as well as anisotropy in dielectric properties of CdSe nanorods and solution, electric field can align the nanorods along its

direction. Also, by addition of polymer in the solution of nanorods, the nanorods can be 'corralled' together because of the non-favorable interactions between the nanorods and polymer. Such interactions can be tailored by varying the polymer or surface ligands of the nanorods. This effect of the external field in combination with self corralling is investigated in Chapter 6 and is used to obtain densely packed nanorods with controlled orientation.

In summary, macroscopic structures are obtained in polymer thin films using electric field combined with internal forces and external forces. Van der Waals interaction of polymer with substrate which predicts wetting characteristics of the polymer thin film on substrate is the internal force. Novel 3-D structures are formed using such forces, while ultrasonic vibrations are used as external forces which in combination with electric field give regularly patterned surfaces. Further interaction of polymer with inorganic nanoparticles is controlled by choosing different ligands that are attached to the nanoparticles. By manipulating such interactions, novel self healing materials and nanocomposite materials for photovoltaic applications are prepared.

1.3 References

1. Black, C. T.; Guarini, K. W.; Milkove, K. R.; Baker, S. M.; Russell, T. P. and Tuominen, M. T., Integration of self-assembled diblock copolymers for semiconductor capacitor fabrication. *Applied Physics Letters* 2001, **79**, (3), 409-411.

2. Zhao, X. M.; Xia, Y. N. and Whitesides, G. M., Soft lithographic methods for nano-fabrication. *Journal of Materials Chemistry* 1997, **7**, (7), 1069-1074.

3. Colburn, M.; Bailey, T.; Choi, B. J.; Ekerdt, J. G.; Sreenivasan, S. V. and Willson, C. G., Development and advantages of step-and-flash lithography. *Solid State Technology* 2001, **44**, (7), 67-+.

4. Reiter, G., Unstable Thin Polymer-Films - Rupture and Dewetting Processes. *Langmuir* 1993, **9**, (5), 1344-1351.

5. Monch, W. and Herminghaus, S., Elastic instability of rubber films between solid bodies. *Europhysics Letters* 2001, **53**, (4), 525-531.

6. Schaffer, E.; Harkema, S.; Roerdink, M.; Blossey, R. and Steiner, U., Morphological instability of a confined polymer film in a thermal gradient. *Macromolecules* 2003, **36**, (5), 1645-1655.

7. Schaffer, E.; Thurn-Albrecht, T.; Russell, T. P. and Steiner, U., Electrically induced structure formation and pattern transfer. *Nature* 2000, **403**, (6772), 874-877.

8. Reiter, G., Dewetting of Thin Polymer-Films. *Physical Review Letters* 1992, **68**, (1), 75-78.

9. Lin, Z. Q.; Kerle, T.; Russell, T. P.; Schaffer, E. and Steiner, U., Structure formation at the interface of liquid liquid bilayer in electric field. *Macromolecules* 2002, **35**, (10), 3971-3976.

10. Morariu, M. D.; Voicu, N. E.; Schaffer, E.; Lin, Z. Q.; Russell, T. P. and Steiner, U., Hierarchical structure formation and pattern replication induced by an electric field. *Nature Materials* 2003, **2**, (1), 48-52.

11. Schaffer, E.; Thurn-Albrecht, T.; Russell, T. P. and Steiner, U., Electrohydrodynamic instabilities in polymer films. *Europhysics Letters* 2001, **53**, (4), 518-524.

12. Lin, Z. Q.; Kerle, T.; Baker, S. M.; Hoagland, D. A.; Schaffer, E.; Steiner, U. and Russell, T. P., Electric field induced instabilities at liquid/liquid interfaces. *Journal of Chemical Physics* 2001, **114**, (5), 2377-2381.

13. Cahn, J. W. and Hilliard, J. E., Free Energy of a Nonuniform System .1. Interfacial Free Energy. *Journal of Chemical Physics* 1958, **28**, (2), 258-267.

14. Lin, Z. Q.; Kerle, T.; Russell, T. P.; Schaffer, E. and Steiner, U., Electric field induced dewetting at polymer/polymer interfaces. *Macromolecules* 2002, **35**, (16), 6255-6262.

15. Voicu, N. E.; Harkema, S. and Steiner, U., Electric-field-induced pattern morphologies in thin liquid films. *Advanced Functional Materials* 2006, **16**, (7), 926-934.

16. Verma, R.; Sharma, A.; Kargupta, K. and Bhaumik, J., Electric field induced instability and pattern formation in thin liquid films. *Langmuir* 2005, **21**, (8), 3710-3721.

17. Lang, R. J., Ultrasonic Atomization of Liquids. *Journal of the Acoustical Society of America* 1962, **34**, (1), 6-&.

18. Miles, J. and Henderson, D., Parametrically Forced Surface-Waves. *Annual Review of Fluid Mechanics* 1990, **22**, 143-165.

19. Trau, M.; Saville, D. A. and Aksay, I. A., Assembly of colloidal crystals at electrode interfaces. *Langmuir* 1997, **13**, (24), 6375-6381.

20. White, S. R.; Sottos, N. R.; Geubelle, P. H.; Moore, J. S.; Kessler, M. R.; Sriram, S. R.; Brown, E. N. and Viswanathan, S., Autonomic healing of polymer composites. *Nature* 2001, **409**, (6822), 794-797.

21. Chen, X. X.; Dam, M. A.; Ono, K.; Mal, A.; Shen, H. B.; Nutt, S. R.; Sheran, K. and Wudl, F., A thermally re-mendable cross-linked polymeric material. *Science* 2002, **295**, (5560), 1698-1702.

22. Chiu, J. J.; Kim, B. J.; Kramer, E. J. and Pine, D. J., Control of nanoparticle location in block copolymers. *Journal of the American Chemical Society* 2005, **127**, (14), 5036-5037.

23. Buxton, G. A.; Lee, J. Y. and Balazs, A. C., Computer simulation of morphologies and optical properties of filled diblock copolymers. *Macromolecules* 2003, **36**, (25), 9631-9637.

24. Bockstaller, M. R. and Thomas, E. L., Proximity effects in self-organized binary particle-block copolymer blends. *Physical Review Letters* 2004, **93**, (16).

25. Thompson, R. B.; Ginzburg, V. V.; Matsen, M. W. and Balazs, A. C., Predicting the mesophases of copolymer-nanoparticle composites. *Science* 2001, **292**, (5526), 2469-2472.

26. Lin, Y.; Boker, A.; He, J. B.; Sill, K.; Xiang, H. Q.; Abetz, C.; Li, X. F.; Wang, J.; Emrick, T.; Long, S.; Wang, Q.; Balazs, A. and Russell, T. P., Self-directed self-assembly of nanoparticle/copolymer mixtures. *Nature* 2005, **434**, (7029), 55-59.

27. Lee, J. Y.; Buxton, G. A. and Balazs, A. C., Using nanoparticles to create self-healing composites. *Journal of Chemical Physics* 2004, **121**, (11), 5531-5540.

28. Alivisatos, A. P., Semiconductor clusters, nanocrystals, and quantum dots. *Science* 1996, **271**, (5251), 933-937.

29. Frank, S.; Poncharal, P.; Wang, Z. L. and de Heer, W. A., Carbon nanotube quantum resistors. *Science* 1998, **280**, (5370), 1744-1746.

30. Sun, S. H.; Murray, C. B.; Weller, D.; Folks, L. and Moser, A., Monodisperse FePt nanoparticles and ferromagnetic FePt nanocrystal superlattices. *Science* 2000, **287**, (5460), 1989-1992.

31. Maier, S. A.; Brongersma, M. L.; Kik, P. G.; Meltzer, S.; Requicha, A. A. G. and Atwater, H. A., Plasmonics - A route to nanoscale optical devices. *Advanced Materials* 2001, **13**, (19), 1501-+.

32. Cushing, B. L.; Kolesnichenko, V. L. and O'Connor, C. J., Recent advances in the liquid-phase syntheses of inorganic nanoparticles. *Chemical Reviews* 2004, **104**, (9), 3893-3946.

33. Shchukin, D. G.; Zheludkevich, M.; Yasakau, K.; Lamaka, S.; Ferreira, M. G. S. and Mohwald, H., Layer-by-layer assembled nanocontainers for self-healing corrosion protection. *Advanced Materials* 2006, **18**, (13), 1672-+.

34. Shchukin, D. G. and Mohwald, H., Self-repairing coatings containing active nanoreservoirs. *Small* 2007, **3**, (6), 926-943.

35. McGuigan, A. P.; Briggs, G. A. D.; Burlakov, V.; Yanaka, M. and Tsukahara, Y., An elastic-plastic shear lag model for fracture of layered coatings. *Thin Solid Films* 2003, **424**, (2), 219-223.

36. Tyagi, S.; Lee, J. Y.; Buxton, G. A. and Balazs, A. C., Using nanocomposite coatings to heal surface defects. *Macromolecules* 2004, **37**, (24), 9160-9168.

37. Talapin, D. V.; Shevchenko, E. V.; Murray, C. B.; Kornowski, A.; Forster, S. and Weller, H., CdSe and CdSe/CdS nanorod solids. *Journal of the American Chemical Society* 2004, **126**, (40), 12984-12988.

38. Cui, Y.; Bjork, M. T.; Liddle, J. A.; Sonnichsen, C.; Boussert, B. and Alivisatos, A. P., Integration of colloidal nanocrystals into lithographically patterned devices. *Nano Letters* 2004, **4**, (6), 1093-1098.

39. Lin, Y.; Skaff, H.; Emrick, T.; Dinsmore, A. D. and Russell, T. P., Nanoparticle assembly and transport at liquid-liquid interfaces. *Science* 2003, **299**, (5604), 226-229.

40. Bockstaller, M. R.; Lapetnikov, Y.; Margel, S. and Thomas, E. L., Size-selective organization of enthalpic compatibilized nanocrystals in ternary block copolymer/particle mixtures. *Journal of the American Chemical Society* 2003, **125**, (18), 5276-5277.

41. Yin, Y. D.; Lu, Y.; Gates, B. and Xia, Y. N., Template-assisted self-assembly: A practical route to complex aggregates of monodispersed colloids with well-defined sizes, shapes, and structures. *Journal of the American Chemical Society* 2001, **123**, (36), 8718-8729.

42. Misner, M. J.; Skaff, H.; Emrick, T. and Russell, T. P., Directed deposition of nanoparticles using diblock copolymer templates. *Advanced Materials* 2003, **15**, (3), 221-+.

43. Zhang, C. L.; Xu, T.; Butterfield, D.; Misner, M. J.; Ryu, D. Y.; Emrick, T. and Russell, T. P., Controlled placement of CdSe nanoparticles in diblock copolymer templates by electrophoretic deposition. *Nano Letters* 2005, **5**, (2), 357-361.

44. Hu, J. T.; Li, L. S.; Yang, W. D.; Manna, L.; Wang, L. W. and Alivisatos, A. P., Linearly polarized emission from colloidal semiconductor quantum rods. *Science* 2001, **292**, (5524), 2060-2063.

45. Huynh, W. U.; Dittmer, J. J. and Alivisatos, A. P., Hybrid nanorod-polymer solar cells. *Science* 2002, **295**, (5564), 2425-2427.

46. Kim, F.; Kwan, S.; Akana, J. and Yang, P. D., Langmuir-Blodgett nanorod assembly. *Journal of the American Chemical Society* 2001, **123**, (18), 4360-4361.

47. Li, L. S.; Walda, J.; Manna, L. and Alivisatos, A. P., Semiconductor nanorod liquid crystals. *Nano Letters* 2002, **2**, (6), 557-560.

48. Li, L. S. and Alivisatos, A. P., Semiconductor nanorod liquid crystals and their assembly on a substrate. *Advanced Materials* 2003, **15**, (5), 408-+.

49. Correa-Duarte, M. A.; Perez-Juste, J.; Sanchez-Iglesias, A.; Giersig, M. and Liz-Marzan, L. M., Aligning an nanorods by using carbon nanotubes as templates. *Angewandte Chemie-International Edition* 2005, **44**, (28), 4375-4378.

50. Thurn-Albrecht, T.; Schotter, J.; Kastle, C. A.; Emley, N.; Shibauchi, T.; Krusin-Elbaum, L.; Guarini, K.; Black, C. T.; Tuominen, M. T. and Russell, T. P., Ultrahigh-density nanowire arrays grown in self-assembled diblock copolymer templates. *Science* 2000, **290**, (5499), 2126-2129.

51. Peng, Z. A. and Peng, X. G., Nearly monodisperse and shape-controlled CdSe nanocrystals via alternative routes: Nucleation and growth. *Journal of the American Chemical Society* 2002, **124**, (13), 3343-3353.

52. Yu, G.; Gao, J.; Hummelen, J. C.; Wudl, F. and Heeger, A. J., Polymer Photovoltaic Cells - Enhanced Efficiencies Via a Network of Internal Donor-Acceptor Heterojunctions. *Science* 1995, **270**, (5243), 1789-1791.

53. Morkved, T. L.; Lu, M.; Urbas, A. M.; Ehrichs, E. E.; Jaeger, H. M.; Mansky, P. and Russell, T. P., Local control of microdomain orientation in diblock copolymer thin films with electric fields. *Science* 1996, **273**, (5277), 931-933.

CHAPTER 2

NOVEL 3-D STRUCTURES IN POLYMER FILMS BY ELECTROHYDRODYNAMIC INSTABILITIES

2.1 Electrohydrodynamic instabilities in air/PMMA/PS trilayer

2.2.1 Introduction

A promising approach to obtain patterned surfaces in condensed matter is to harness and tune the pattern formation methods which are found in nature. These include self-assembly, phase separation and dewetting processes and these can be used to obtain controlled patterns in thin polymer films. The mechanism and length scale of the process of dewetting of a thin liquid film from a nonwettable substrate depends on the film thickness, viscosity, and surface tension of the film, and van der Waals forces affecting the liquid-substrate interface[1,2]. Similarly, electric fields can be used to induce an instability that depends on these parameters, and the permittivity and conductivity of the liquid and the strength of the applied field. Several laboratories[3,4] have recently used electric fields to pattern polymer films on 100 nm length scales, with the potential to extend this technique to even smaller feature sizes, simply by tuning the properties of the material and the strength of the field.

The physical basis of this electrohydrodynamic patterning technique is the amplification of fluctuations at a fluid/fluid interface by a destabilizing force generated when an electric field is applied normal to the surface of a thin film as described in Chapter 1. Pillar formation occurs when the destabilizing force is sufficiently large to

overcome the stabilizing forces acting at the interface, such as surface tension and gravity. This force imbalance amplifies interfacial fluctuations until they eventually span the capacitor in the form of pillars, as shown in Figure 2.1. The characteristic spacing of these structures can be predicted using a linear stability analysis[5,6,ch1] or through the use of 3-D simulations[7]. Wetting plays a more subtle role in the amount of residual material between pillars[8].

Several variations of the experimental set-up shown in Figure 2.1 have been investigated. Bilayer systems have been studied in which the air above the film is replaced with a second film. Rational material selection results in lower interfacial tension between the two layers, allowing structures with smaller characteristic wavelengths to be formed[5,9].

There has only been one trilayer system reported in the literature, poly(methyl methacrylate) (PMMA) covered by polystyrene (PS) with an overlying air gap. Lin et al.[8] and Morariu et al.[9] showed that electrostatic forces applied to the PMMA/PS/air trilayer generate fluctuations first at the PS/air interface, with the PMMA film remaining relatively unperturbed. In those experiments, the wavelength of the fastest-growing fluctuation amplified by the electric field defined the characteristic spacing of a well-ordered array of PS columns, spanning the electrodes. Although the electric field creates a destabilizing force at both the PS/air interface and the PMMA/PS interface, due to dielectric contrast in the materials, the time scale of pillar formation is much faster at the PS/air interface. This is largely due to the low viscous resistance at the air interface, combined with the tendency of PS to dewet PMMA, allowing for interfacial slip. Qu et al.[10] used measurements of dewetting velocities to confirm quantitatively the

theoretical predictions about liquid/liquid bilayers made by Brochard-Wyart and coworkers[11]. These studies suggest that, for liquid/liquid dewetting where $\eta_A/\theta_E < \eta_B$ (η_A and η_B are the viscosities of the upper and lower layer respectively, and θ_E is the equilibrium contact angle between the two liquids), the upper layer dictates dewetting dynamics and morphology, while the lower layer displays solid-like behavior, similar to the situation observed for the PMMA/PS/air trilayers. However, for $\eta_A/\theta_E > \eta_B$, Brochard Wyart et al.[11] predicted a crossover to a regime in which viscous dissipation occurs mostly in the lower layer, which controls dewetting dynamics.

Here, multi-layered polymer films are used where pattern formation, in combination with a preferential wetting of the top electrode by one of the polymers, leads to unique three-dimensional structures, where one polymer can be encased within another. Whereas, in the absence of preferential wetting of the top electrode by one polymer, different structures are obtained in which one polymer is not completely encased in the other. Two different set of experiments were done. In one set, the PMMA layer was deposited on silicon wafer on which further a PS layer was further deposited. While in second set of experiments, PS layer was deposited on the substrate and PMMA layer was deposited on PS layer. The results for both set of experiments are discussed separately in this chapter.

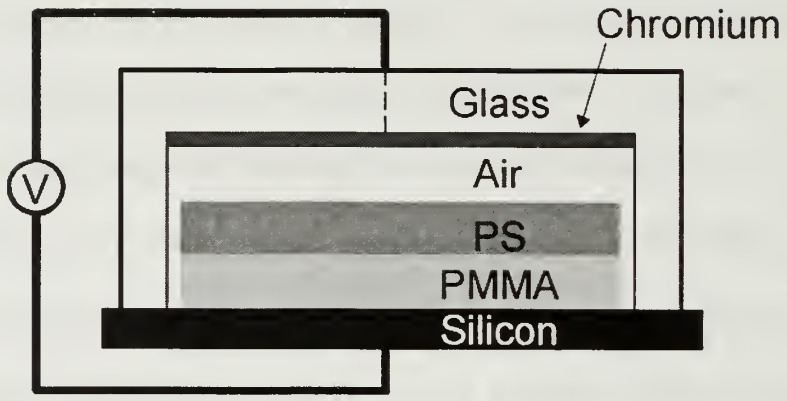

Figure 2.1: N-doped, backside aluminum coated silicon wafer serves as the substrate and chromium deposited on glass serve as the upper electrode. The setup is heated on a hotplate.

2.2.2 Experimental

A schematic diagram of the experimental geometry is shown in Figure 2.1. The two electrodes consisted of a doped silicon wafer and a chrome-coated glass slide. The glass slide had a 3.5 μm rectangular recess in the center. The recess was generated by etching the slide with buffered hydrofluoric acid, and the depth of the recess was determined by profilometry. A ~50 nm chromium layer was thermally evaporated on the recess to create upper electrode. The surface properties of the chromium surface were modified by coating with 3M HFE fluoropolymer, which makes the surface hydrophobic. The coating was applied by dipping the chrome layer in the fluoropolymer solution. Experiments were done with both fluoropolymer-coated and uncoated chrome layers. A ~l μm thick poly(methyl methacrylate) (PMMA) film was spin coated onto a silicon wafer from 10% solution in chlorobenzene. A ~0.7 μm thick polystyrene film was spin coated from 12.5% solution in toluene on top of the PMMA. The films were heated to 90 ^{0}C for 1 minute after each step to remove residual solvent. The edges of the

polymer film were removed with solvent and the two electrodes were clamped together, such that the layered polymer films were entirely under the recess. The resulting air gap was ~4 μm, as determined by measurement of the height of the structures formed after removal of the upper electrode. The system was heated to 120 ^{O}C on a hotplate and 200 V DC was applied across the two electrodes. This led to a destabilization of the layered polymer films, causing the initially transparent polymer bilayer to become translucent. This macroscopic change indicates the formation of microscopic structures on a size scale that scatters visible light. The temperature was then raised to 190 ^{O}C for 45 minutes, with the voltage being maintained. The system was then cooled to room temperature before removing the electric field. The silicon wafer was removed and divided into two parts. Electrode separation was facilitated by using a chromium etch solution to remove the evaporated chromium layer from both the treated and untreated chromium surfaces. This prevented the fracture of structures while removing the wafer from the glass slide. A section of the sample was imaged, without further treatment, by scanning electron microscopy (SEM), while another section was imaged after selectively removing the PS with cyclohexane, a non-solvent for PMMA.

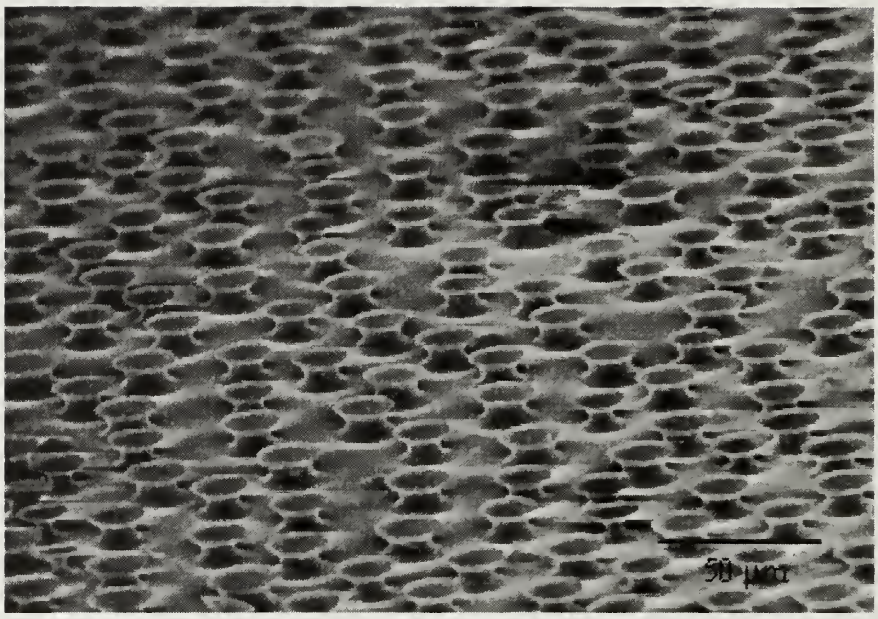

Figure 2.2: SEM image of the structures obtained after removing the upper electrode and without further treatment.

2.2.3 Results and Discussion

Figure 2.2 shows the structures formed in the case, where the chromium surface was not treated. These structures are similar to those obtained by electrohydrodynamic instabilities in a single layer of polymer. Columns of polymer are seen with concave walls and flat tops. From this image no distinction can be made between the different components, PS and PMMA. It is evident that these columnar structures are uniformly distributed over the surface and that the lateral size of the structures (~5 μm diameter tops) is uniform. By magnifying one column, the hour-glass shape of the structures was seen as shown in Figure 2.3. In addition, the exposure of the multi-component structure to an electron beam in the SEM degraded the PMMA without altering the PS. There is a recess on the top of the column, a distinct rim on the side wall at the top, and, what appear to be channels running vertically up the walls of the column. The

complement to this image was obtained by selectively removing the PS with cyclohexane. Shown in Figure 2.4a is a very unique cage-type structure made by the PMMA. Here, strands of PMMA spanned between the bottom layer of PMMA and a disk of PMMA that formed on the upper electrode. Note that the surface of this disk or ceiling was smooth since it was adjacent to the evaporated chromium layer on the upper electrode. In addition, around the ring of PMMA strands, there was an elevated rim of PMMA that corresponded to the diameter of the columns formed by the PS/PMMA bilayer. A cross-sectional SEM image of a cleaved cage-type structure is shown in Figure 2.4b where the diameter of the cage is ~16.5 μm with a height of 4 μm, the separation distance between the electrodes and the ceiling thickness is 1.2 μm.

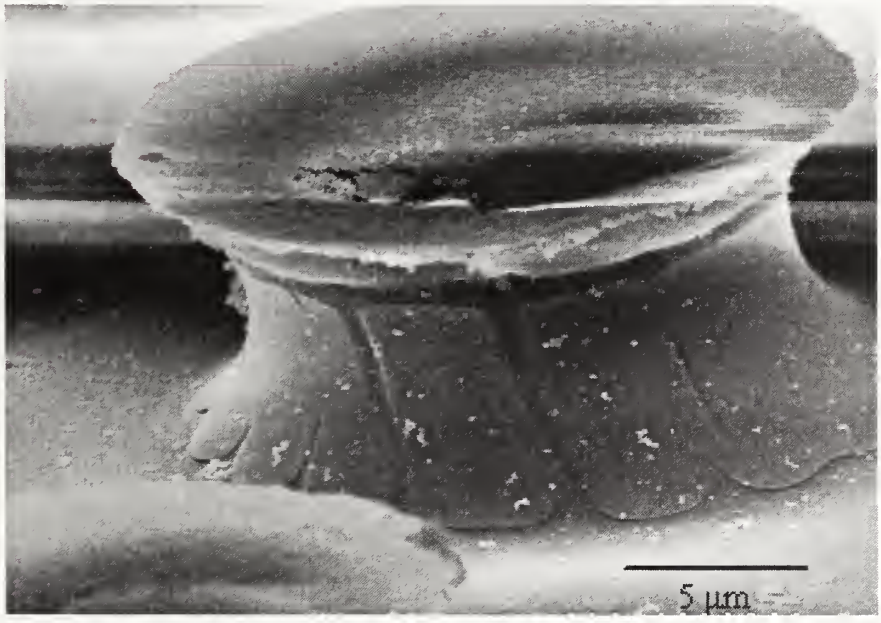

Figure 2.3: SEM image of a single structure. The dark recesses along the height of the pillar are due to PMMA that has been degraded because of e-beam exposure in the SEM.

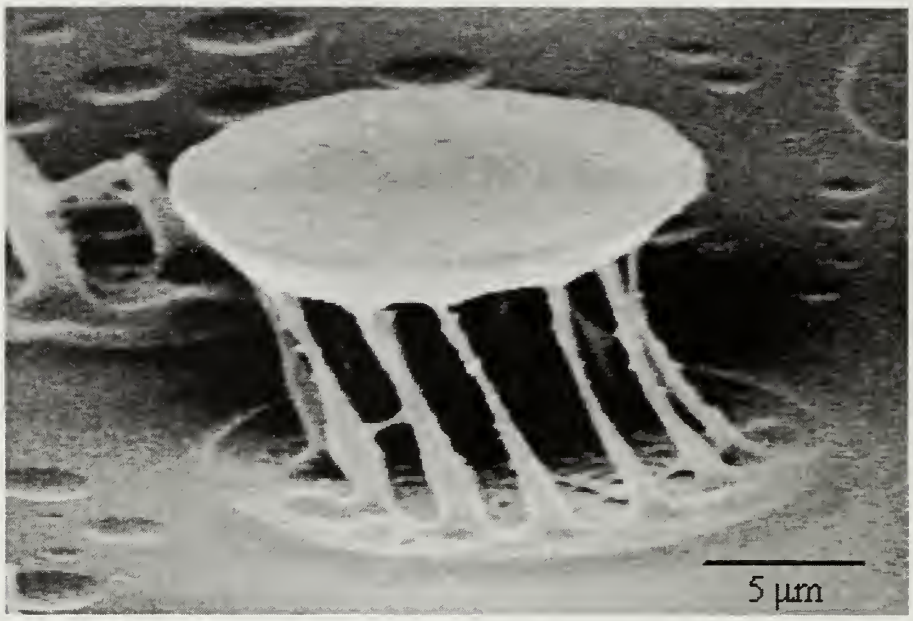

Figure 2.4: a) SEM image of a single 'cage'. Sample was cyclohexane washed to remove PS and close cell structure made of PMMA was obtained.

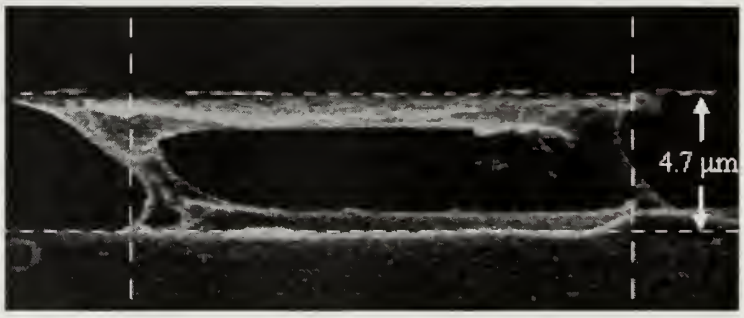

Figure 2.4: b) Cross-sectional SEM image of a cleaved single 'cage'. The dimension of a single close cell structure is shown.

The structure can be understood in the context of electrohydrodynamic instabilities. As shown previously,[9] the upper PS layer forms columnar structures on the lower layer of PMMA. The PMMA film acted like a substrate though it was above its glass transition temperature. This can be easily understood by comparing the short characteristic times required to initiate instabilities at the PS-air interface to the much longer characteristic times for instabilities to grow at the PMMA-PS interface.

Instabilities at the PS/PMMA interface require viscous flow in both layers, and therefore the time required to amplify fluctuations is large. After the growth of the PS structures, the contact line at PS/PMMA interface is locally deformed, forming a rim on the PMMA surface as shown in Figure 2.5b. The Neuman construction[11] can be used to determine the direction of surface forces at the contact line, and the uncompensated normal component of the surface tension leads to contact line deformation. In addition to surface tension, viscous stresses, due to lateral movement of the contact line during growth of the PS structures, lead to a deformation of the contact line.

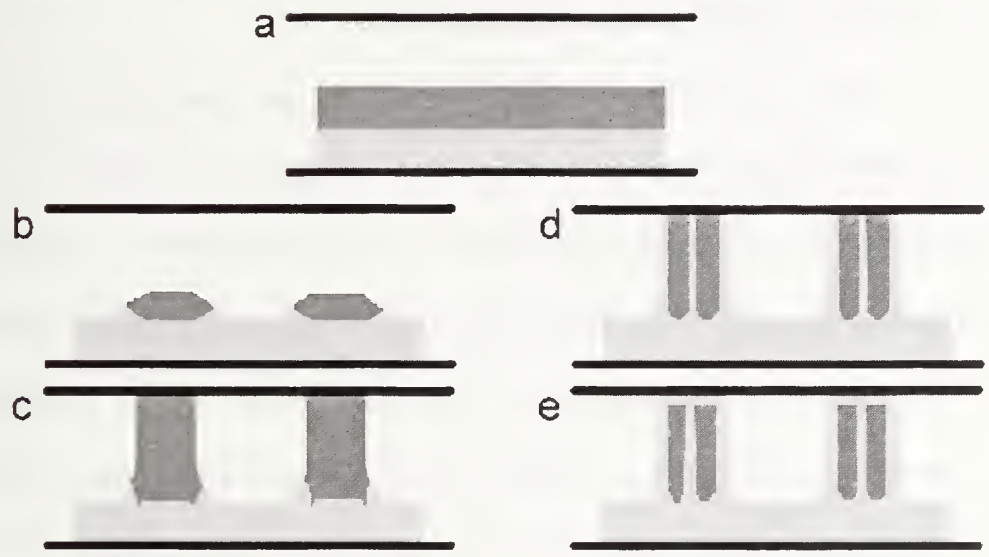

Figure 2.5: Schematic of the mechanism of the formation of 'cage structures. a) Initial smooth films. b) PS dewets the PMMA surface and form structures. c) These structures grow under electric field and touch the top electrode. d) PMMA 'fingers' climb up along the pillar under electric field and touch the top electrode. e) PMMA displaces PS from the top electrode and exerts downward pressure on PS due to electric field.

The electric field strength at the top of the rim was enhanced by the curvature of the structures. This led to the initiation of an instability and the rim was pulled upwards.

Morariu et al[9] observed that the rim was pulled up uniformly by the electric field, forming a sheath of PMMA around the PS column. In contrast, we observed the growth of a fingering instability along the circumference of the rim. This fingering instability arose from the flow of the thin film of PMMA on the PS pillar under the influence of electric field stresses. Since PMMA has a small contact angle (~23°) with PS[12], flow of PMMA induced an instability and led to the formation of fingers perpendicular to the direction of flow as shown in Figure 2.5d [13]. Once the fingering instability formed, the electric field amplified the instability and caused the formation of strands around the circumference of the PS columns already formed.

Once the strands of PMMA reached the top electrode, PMMA wetted the chromium surface displacing the PS, as shown in Figure 2.5e. This was experimentally confirmed by coating a film of PMMA on top of a PS film on a chromium surface. After annealing the films, PMMA was observed on the chromium surface under the microscope after removing the PS with cyclohexane. This is consistent with the observations of Harris et al.[12] where PS/PMMA bilayers on silicon oxide were studied. The energetic gain of replacing the PS/chromium interface with the more favorable PMMA/chromium interface caused the formation of a thin PMMA film between the PS and chromium. This thin PMMA film was the ceiling in the cage-like structure. The formation of this thin film requires that the strands of PMMA act like channels for the flow of PMMA from the lower layer to the upper electrode surface. The reduction in interfacial energy not only promoted the formation of the ceiling but, once formed, the higher dielectric constant of PMMA versus that of PS produced an electrostatic pressure

that pulled the PMMA/PS interface in the ceiling down to the lower electrode. This, in turn, caused the thickness of the ceiling to increase to ~1.2 μm.

This mechanism was further verified by using the surface treated chromium electrode. Figure 2.6 shows SEM image of the structures formed by keeping the same film thickness and electric field strength the same as in the previous experiment, but changing the surface of the chromium layer. The sample was treated with cyclohexane to remove PS selectively before imaging. It can be seen that the PMMA formed a sheath around PS pillar but had not encased the PS completely. Since the chromium was coated with a fluoropolymer (3M Novec HFE 7000), PMMA did not preferentially wet the surface and could not displace the PS from the electrode, and therefore, it does not form a ceiling in the structures. This demonstrates that the surface interactions which are inherent to the polymer coupled with external fields, like an electric field, can lead to formation of novel 3D structures.

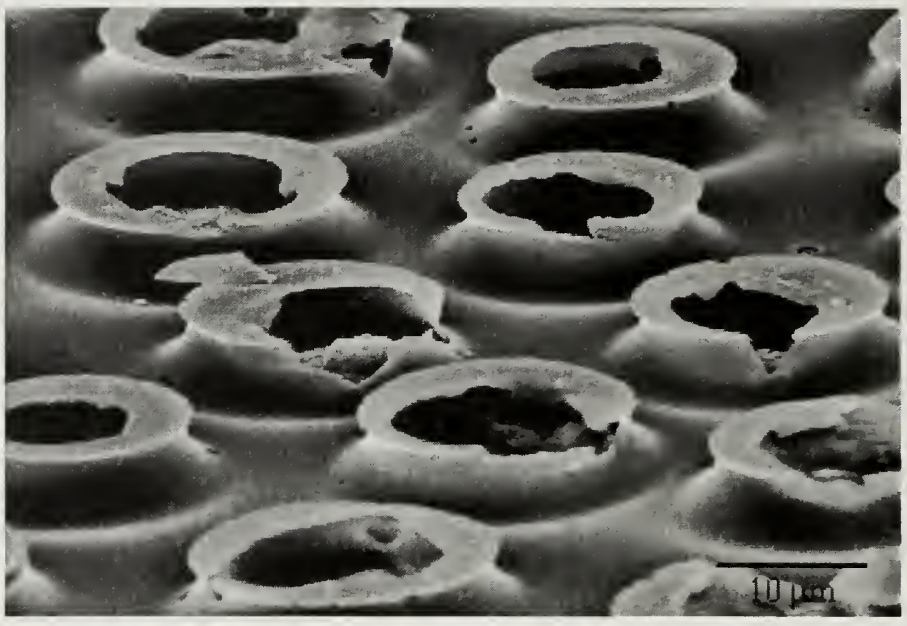

Figure 2.6: SEM image of structures obtained with hydrophobic chromium layer and treated with cyclohexane. The structures are hollow and do not have ceiling.

Patterned electrodes, as shown by Morariu et al. [10] can also be used, as opposed to uniform electrodes, to control structures laterally in films. By adjusting the geometry (film thickness, electrode separation distance and field strength) it should be possible to generate structures that range from the cage-like structures shown here, to fully encapsulated structures in a prescribed manner, so that closed structures can be obtained, which is nontrivial to achieve with current patterning techniques. The size scale of the patterns can also be tailored by adjusting the electric field strength.

2.2 Electrohydrodynamic instabilities in air/PS/PMMA trilayer

2.2.1 Introduction

In this section, the results from the inverted configuration of a PMMA film on a PS coated substrate are discussed. One might expect the dynamics of the PS/PMMA/air

trilayer system to mimic the PMMA/PS/air system, with PMMA forming an array of pillars on top of the underlying PS, followed by concentric growth of PS around the PMMA pillars. However, in the inverted system (PS/PMMA/air) structure surprisingly resembles that of the non-inverted system (PMMA/PS/air). Despite the resemblance in the final structure, the mechanism by which the pillars form is completely different due to changes in interfacial forces resulting from the inverted configuration, as shown in Figure 2.2.

The change in system dynamics resulting from placement of PMMA in the middle of the trilayer is a downward electrostatic force at the PMMA/PS interface. At the PMMA/air interface, there is an upward force (i.e. toward the upper electrode) since PMMA has a higher dielectric constant than air. This is akin to the force acting on the PS layer in the non-inverted system. The downward electrostatic force at the PMMA/PS interface is due to PMMA having a larger dielectric constant than PS, which is a rational, yet non-intuitive, and can have an impact on the system dynamics.

In addition to altering the electrostatic forces, the inverted trilayer system creates new dewetting interfaces. The previously studied PMMA/PS/air trilayer has one dewetting interface, PS/PMMA. In contrast, the inverted system of PS/PMMA/air has two interfaces that energetically favor dewetting, the PS/PMMA interface and the PS/silicon substrate (with 2 nm thick native oxide) interface. Thus, the dewetting of the bottom PS layer is highly favored. Although the films are relatively thick (~500 nm), dewetting can be initiated by electric-field amplified surface undulations. Thus, the electrostatic forces and the interfacial energies work in tandem to dewet the underlying

PS layer, as shown schematically in Figure 2.7, which ultimately affects the final structure morphology.

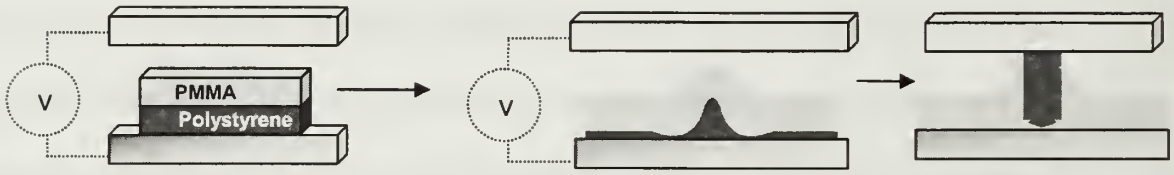

Figure 2.7: Schematic of trilayer "inversion" with PMMA on top of PS. The dielectric constant of PMMA is larger than PS, creating a downward electrostatic force at the PMMA/PS interface. The tendency of PS to dewet both the substrate and PMMA accelerates the structures formation. The PMMA displaces the PS and the PS emerges towards the upper electrode.

The complex concerted effects of dewetting and electrostatic pressure acting at the polymer/polymer and polymer/air interfaces in the PS/PMMA/air system is discussed here along with the effects of viscosity on the final structure. The combined effects of increasing polymer mobility by lowering viscosity and of changing polymer-electrode surface interactions strongly enhance the kinetics of structure formation, resulting in much faster patterning than realized in prior studies.

2.2.2 Experimental

Films of PS and PMMA, having the molecular weights shown in Table 1, were spin coated onto polished silicon substrates from solution in toluene or, when a selective solvent was required to deposit the upper layer, cyclohexane and acetic acid, respectively. Prior to spin coating, the silicon substrates were cleaned in concentrated sulfuric acid mixed with inorganic oxidizers. All of the polymer films were uniformly smooth (±1 nm over the 1 x 1 cm^2 sample area) and had thicknesses of 500 nm

(±10nm), measured by spectral interferometry. Trilayer systems were assembled using the silicon substrate as one electrode and a soda-lime glass slide coated with chromium for the other. Using a polymer mask at the edges of the slide, a rectangular well was etched by immersion in buffered hydrofluoric acid. The electrode spacing was varied between experiments by varying the etching time to control the depth of the well, which was measured using a contact probe profilometer (Veeco Dektak 3). Soda-lime glass contains mobile sodium ions, which prevent the decay of the electric field over the thickness of the glass slide, so that the electric field gradient is entirely across the air gap and polymer films. Furthermore, flow of electronic current, which could result in degradation of the polymer, is prevented. The voltage was applied and the films heated to 170°C, above their glass transition temperatures, for 1.5 to 3 hours. Following each experiment, the upper electrode was removed and the film on the silicon substrate was broken into three sections for selective solvent washing. One section was rinsed with acetic acid to remove the PMMA component, another was rinsed with cyclohexane to remove the PS component, and the third was not rinsed. Finally, the structures were imaged using scanning electron microscopy (SEM) and comparisons were made between each set of three images to determine the overall morphology.

Table 2.1: Characteristics of the Polymers Used In This Study

	M_w (g/mol)	M_w/M_n	Viscosity (Pa s) at 170C *	Dielectric Constant
PS	8,000	1.09	24	2.95
PS	157,000	1.04	7.3×10^4	2.95
PMMA	32,000	1.61	2.3×10^5	5.24
PMMA	99,000	1.04	9.2×10^5	5.24

* PS viscosities calculated from reference [14]; PMMA viscosities measured using a TA Instruments AR2000 Rheometer.

2.2.3 Results and Discussion

Figure 2.8a and 2.8b show SEM images of the pattern of structures formed when the electric field was applied across PS/PMMA/Air trilayer. 8 kg/mol molecular weight PS and 32 kg/mol molecular weight PMMA were used for these experiments and the film thickness for each layer was 0.5 μm. The air gap was 2-4 μm and 136 volts were applied across the two electrodes. The spacing between the generated structures is observed to be ~ 20 μm from the image.

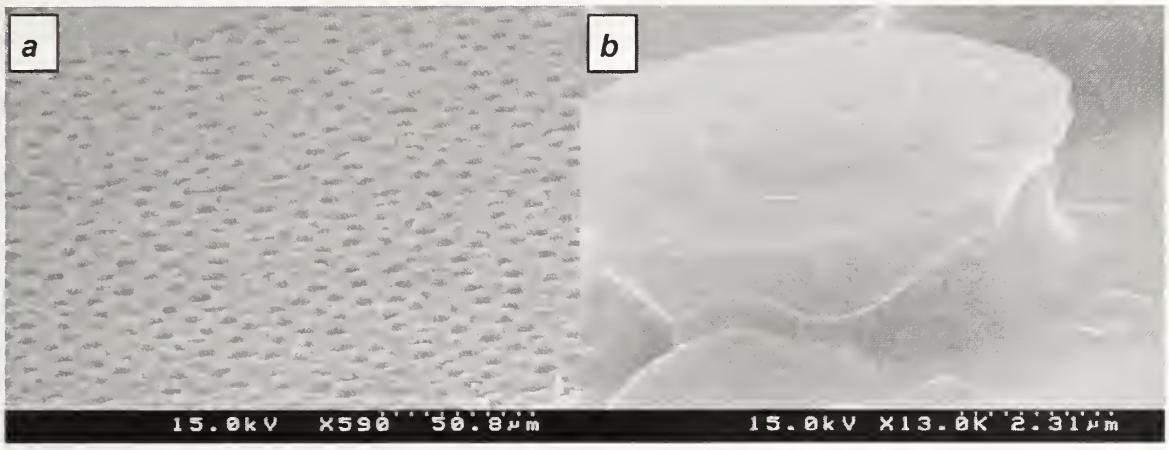

Figure 2.8: a) Overview of 32 kg/mol PMMA on 8 kg/mol PS b) PS core surrounded by PMMA sheath.

Figure 2.9a further shows the structures after removing the PMMA with acetic acid which does not remove PS, while Figure 2.9b shows the structure after selectively removing the PS with a cyclohexane rinse. These images show that the PS has formed the core of the structures while PMMA forms the sheath.

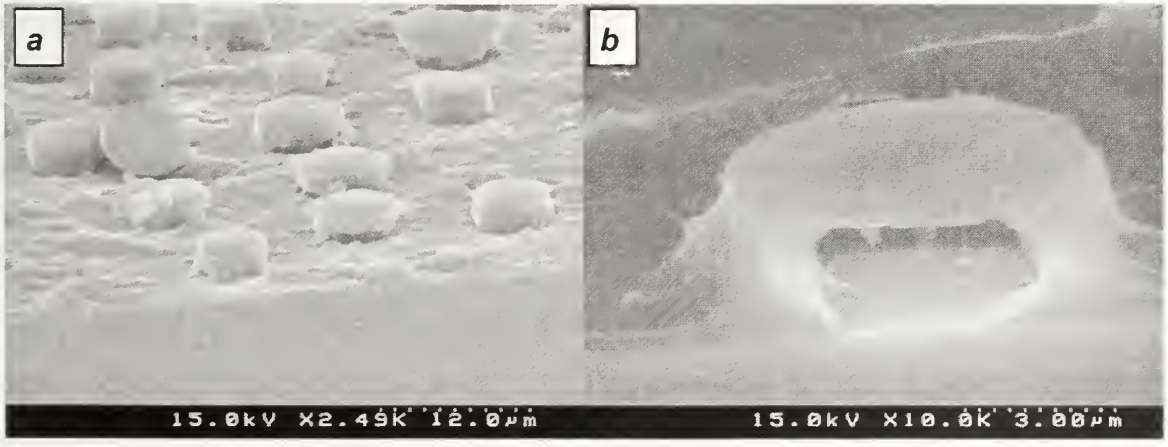

Figure 2.9: a) Acetic acid rinse reveals PS cores b) Cyclohexane rinse reveals complementary PMMA shell.

These observations can be explained if the interfacial dynamics at the PMMA/PS, PMMA/air and PS/substrate interface are studied. When an electric field is applied across two dielectric layers, a Maxwell stress, T_{ij}, is produced and is given by[15]

$$T_{ij} = \frac{1}{4\pi}\left[\varepsilon E_i E_j - \frac{1}{2}\varepsilon E^2 \delta_{ij}\right]$$

where E_i is the component of the electric field, ε is the dielectric constant of the medium with respect to the environment and δ is kronecker delta. When a low dielectric material is placed next to a high dielectric material, under the electric field, the interface is pushed towards the lower dielectric material. Since PMMA has a higher dielectric constant than both PS and air, the PMMA/air interface is pulled towards the glass electrode and the PS/PMMA interface is pulled towards the substrate. At the fluid/fluid interface, the Maxwell stress destabilizes the smooth interface and leads to growth of instabilities which are referred to as electrohydrodynamic because they involve interplay between the electric forces and hydrodynamic forces. These instabilities have been well studied and the characteristic spacing for the structures formed can be derived and are a function of interfacial tension and electric field strength[5,6,7]. Also, the dispersion forces at the PS/PMMA interface and PS/substrate interface are repulsive which will lead to dewetting of the fluids at these interfaces.

The Maxwell stress at the PMMA/air interface is higher than at the PMMA/PS interface because of larger mismatch in dielectric constant between air and PMMA than between PMMA and PS; therefore the characteristic time for the instability to grow at PMMA/air interface should be smaller. The characteristic time for electrohydrodynamic instabilities is furthermore dependent upon the viscosities of the fluids[5], which should

make it smaller for the PMMA/air interface than the PMMA/PS interface because of the negligible viscosity of air. However, we find the PS/PMMA interface becomes unstable initially, allowing PS to push through the PMMA film. The negative disjoining pressure at the PS/substrate interface accelerates the dewetting of the PS nucleated by the electrohydrodynamic instability. This is well represented in Figure 2.10a, which shows an SEM image of the undulations on a polymer film at an early time period, i.e. before the structures could span the air gap. The molecular weight of PMMA was increased to 99 kg/mol to slow down the kinetics of the instability. It can be observed that the PS/PMMA interface has undulations and some of them are fully grown. Figure 2.10b shows an image of a fracture surface, which illustrates that the PS forms a cone while the film thickness of PMMA has not changed much, consequently the PS/PMMA interface is destabilized first. At later time scales, these undulations develop into 'pillars' that have a PS core and a sheath of PMMA. The formation of a PS core is facilitated by both PS dewetting as well as the Maxwell pressure exerted at the PS/PMMA interface. From Figure 2.9a, it is observed that the PS has dewetted the silicon substrate and is only present in the cores of the pillars, while Figure 2.9b suggests the PMMA film is continuous and also covers the pillars, as expected because of favorable interactions between PMMA with silicon substrate.

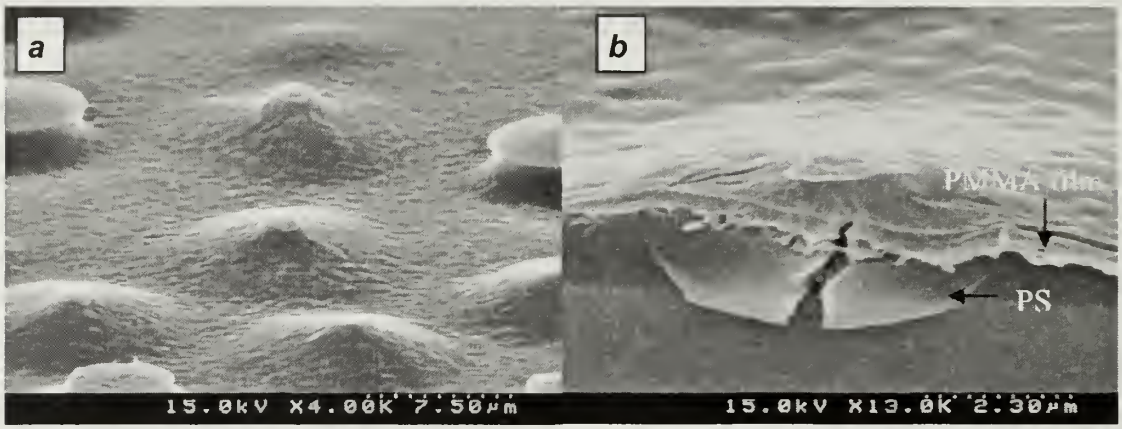

Figure 2.10: a) Overview of 99 kg/mol PMMA on 8 kg/mol PS shows undulations with several PS breakthroughs. b) Fractured surface of sample. PS film has dewet and filled the void created by undulations. The PMMA film blankets this cone shape.

Figure 2.11: PMMA dewetting determines the regions where pillars form in bilayers of 32 kg/mol PMMA on 157 kg/mol PS.

When the molecular weight of polystyrene was changed to 157 kg/mol, which increased the viscosity by about 10 times, while keeping the molecular weight of the PMMA at 32 kg/mol, the kinetics of dewetting of PS on silicon surface under the

electric field was retarded. Figure 2.11 shows an SEM image of the film surface where circular rings are observed with some structures within them, while no structures are present outside these rings. These rings result from the PMMA dewetting the PS and this circular ring pattern is reminiscent of nucleation and growth dewetting. During dewetting, the PMMA receding layer has a thicker rim as can be seen in the image and, hence, magnifies the electric field due to the height and curvature associated with the front. This amplifies the instability at PS/PMMA interface which nucleates the dewetting of PS from silicon wafer and give structures as observed in Figure 2.12a, where PMMA has been removed before taking the image. The PMMA rim continues to recede and the structures are generated along the way, hence no structures are formed outside the rings. PMMA forms a wetting layer on the exposed silicon wafer after PS has dewetted thus forming mounds around the PS pillars as seen in Figure 2.12b.

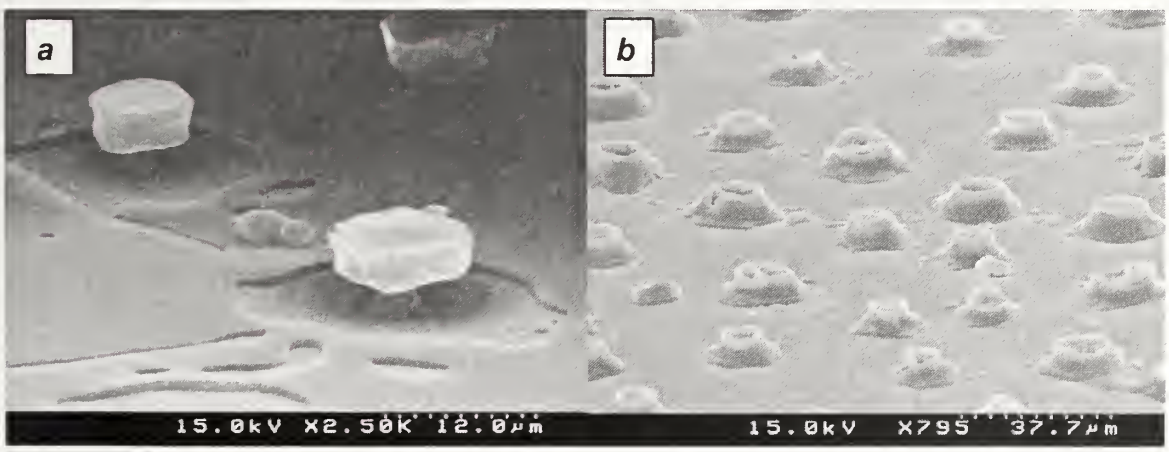

Figure 2.12: 157 kg/mol PS on 32 kg/mol PMMA. a) Acetic acid rinse reveals PS cores and a residual PS film b) Cyclohexane rinse reveals PMMA bases with no residual layer.

In conclusion, electrohydrodynamic instabilities in polymer thin films were studied where a higher dielectric constant polymer film was sandwiched between two lower dielectric constant fluids. Along with the electrostatic forces, the dewetting forces

at two of the interfaces played a major role in the type of structures obtained. The size and spacing of the structures are controlled by the electrostatic forces while the dewetting kinetics dictated the interface at which the instabilities were grown. When a low molecular weight PS was used, the PS/PMMA interface was destabilized, leading to the formation of novel structures. Pillars were formed which span across the air gap and have a PS core with a PMMA sheath. By selectively removing the PS core, hollow structures can be obtained that are difficult to produce by other existing techniques.

2.3 Conclusion

In summary, a route to fabricate three-dimensional microscopic structures in thin films has been shown by coupling electrohydrodynamic instabilities with preferential wetting. Cage-like structures were shown to be that produced by instabilities enhanced by the applied electric field. This methodology has the potential of producing arrays of closed-cell structures, with controlled size scale and spacing that cannot be produced at present.

2.4 References

1. Lambooy, P.; Phelan, K. C.; Haugg, O. and Krausch, G., Dewetting at the liquid-liquid interface. *Physical Review Letters* 1996, **76**, (7), 1110-1113.

2. Sferrazza, M.; Heppenstall-Butler, M.; Cubitt, R.; Bucknall, D.; Webster, J. and Jones, R. A. L., Interfacial instability driven by dispersive forces: The early stages of spinodal dewetting of a thin polymer film on a polymer substrate. *Physical Review Letters* 1998, **81**, (23), 5173-5176.

3. Chou, S. Y. and Zhuang, L., Lithographically induced self-assembly of periodic polymer micropillar arrays. *Journal of Vacuum Science & Technology B* 1999, **17**, (6), 3197-3202.

4. Schaffer, E.; Thurn-Albrecht, T.; Russell, T. P. and Steiner, U., Electrically induced structure formation and pattern transfer. *Nature* 2000, **403**, (6772), 874-877.

5. Lin, Z. Q.; Kerle, T.; Baker, S. M.; Hoagland, D. A.; Schaffer, E.; Steiner, U. and Russell, T. P., Electric field induced instabilities at liquid/liquid interfaces. *Journal of Chemical Physics* 2001, **114**, (5), 2377-2381.

6. Pease, L. F. and Russel, W. B., Linear stability analysis of thin leaky dielectric films subjected to electric fields. *Journal of Non-Newtonian Fluid Mechanics* 2002, **102**, (2), 233-250.

7. Verma, R.; Sharma, A.; Kargupta, K. and Bhaumik, J., Electric field induced instability and pattern formation in thin liquid films. *Langmuir* 2005, **21**, (8), 3710-3721.

8. Lin, Z. Q.; Kerle, T.; Russell, T. P.; Schaffer, E. and Steiner, U., Electric field induced dewetting at polymer/polymer interfaces. *Macromolecules* 2002, **35**, (16), 6255-6262.

9. Morariu, M. D.; Voicu, N. E.; Schaffer, E.; Lin, Z. Q.; Russell, T. P. and Steiner, U., Hierarchical structure formation and pattern replication induced by an electric field. *Nature Materials* 2003, **2**, (1), 48-52.

10. Qu, S.; Clarke, C. J.; Liu, Y.; Rafailovich, M. H.; Sokolov, J.; Phelan, K. C. and Krausch, G., Dewetting dynamics at a polymer-polymer interface. *Macromolecules* 1997, **30**, (12), 3640-3645.

11. Wyart, F. B.; Martin, P. and Redon, C., Liquid-Liquid Dewetting. *Langmuir* 1993, **9**, (12), 3682-3690.

12. Harris, M.; Appel, G. and Ade, H., Surface morphology of annealed polystyrene and poly(methyl methacrylate) thin film blends and bilayers. *Macromolecules* 2003, **36**, (9), 3307-3314.

13. Troian, S. M.; Herbolzheimer, E.; Safran, S. A. and Joanny, J. F., Fingering Instabilities of Driven Spreading Films. *Europhysics Letters* 1989, **10**, (1), 25-30.

14. Fox, T. G. and Flory, P. J., 2nd-Order Transition Temperatures and Related Properties of Polystyrene .1. Influence of Molecular Weight. *Journal of Applied Physics* 1950, **21**, (6), 581-591.

15. Melcher, J. R. and Taylor, G. I., Electrohydrodynamics - a Review of Role of Interfacial Shear Stresses. *Annual Review of Fluid Mechanics* 1969, **1**, 111-&.

CHAPTER 3

PATTERNED POLYMER THIN FILMS USING ELECTROHYDRODYNAMIC INSTABILITIES

3.1 Patterned polymer films using ultrasonic vibrations and electric field

3.1.1 Introduction

Surface waves on a liquid due to an oscillating gravitational force were first observed by Faraday in 1831[1]. Therefore these waves are also termed as Faraday waves. Faraday waves are generally excited by vibrating the surface of a liquid vertically. These waves were further studied by Lord Rayleigh and confirmed that the waves had a frequency equal to one-half that of the excitation and that the resonant response is sub-harmonic[2]. These capillary waves are termed as parametrically forced surface waves. These waves can be understood by considering the case of a simple pendulum that is subjected to a vertical oscillation of its pivot. If the acceleration of the pivot is $\alpha g \cos(\omega t)$, where α is a parameter and ω is the frequency and the angular displacement θ is assumed to be small, the motion of the pendulum is given by

$$\ddot{\theta} + \omega_0^2 (1 + \alpha \cos \omega t)\theta = 0$$

where $\omega_0 = (g/l)^{1/2}$ is the frequency of small oscillations when $\alpha = 0$. $\theta = 0$ is one solution to this equation, but for $0<\alpha<<1$, $\theta = A\cos\frac{1}{4}\omega t$ with $\omega^2 = \omega_0^2(1 \pm \frac{1}{2}\alpha)$ is also a solution to the equation. To ascertain the real solution, stability analysis has to be performed, which shows the null solution is not stable and the sub-harmonic solution is stable in the frequency interval of $\omega_0^2(1-\frac{1}{2}\alpha) < \omega^2 < \omega_0^2(1+\frac{1}{2}\alpha)$. Further, since the

physical systems are dissipative, the vibrations will be damped. This puts another limitation on the values of α for which the sub-harmonic response is possible. Therefore, there is a critical value of α, below which there will be no waves at the surface. This critical value of α will depend upon the dissipative component of the physical system and, therefore, will be dictated by the viscosity of the fluid.

Faraday waves have been of special interest in recent years in the fluid mechanics community since it provides a problem which can be solved by modern theories of chaos and bifurcation and, therefore, can be compared to experimental results[3]. In addition to advancing the understanding of granular and soft matter physics, this phenomenon also provides us with ordered surface patterns. Several patterns such as radial waves, square symmetry waves and hexagons can be produced on the surface of the liquids[4], which can be really useful in the field of optics, communications, etc. Various studies have been done to find the criterion for pattern selection[5]. It has been observed that different patterns are observed at the onset of the instability for different values of the excitation frequency. The patterns are generally related to the eigenmodes of the free surface that are further dictated by the boundary conditions[4]. Further, the amplitude of the vibrations also dictates the pattern obtained at the surface. For vibrations, where amplitudes are large enough and the cell or film surface size is much larger than the wavelength of the instabilities, square symmetric waves are favored. But, if the amplitude of vibrations is reduced; hexagons and quasi-crystals states are favored. Some of the observed patterns are shown in the Figure 3.1. The patterns are generally produced due to presence of pairs of opposite moving plane waves which leads to standing waves. Two standing waves give square symmetry structures, three standing

waves give hexagon or honey-comb lattices, four standing waves form a quasi-crystal, due to the absence of translational symmetry, while single standing waves are not supported due to two dimensional nature of surface.

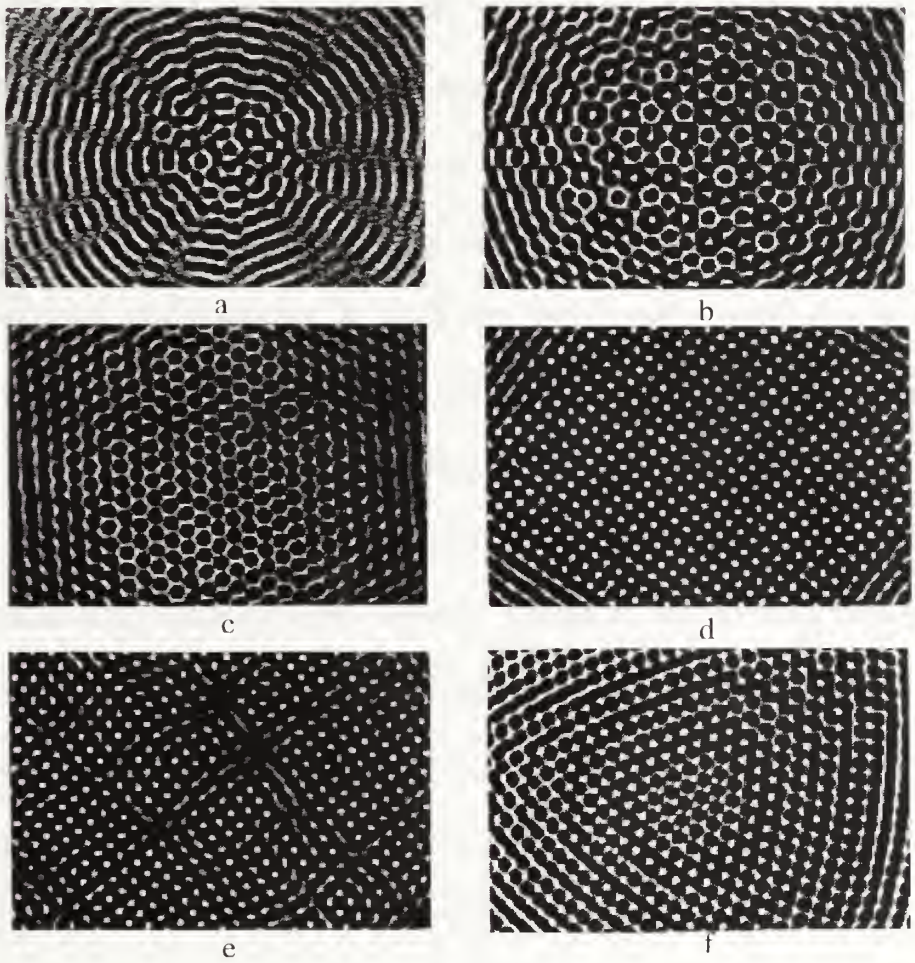

Figure 3.1: Images of capillary waves produced at 340 Hz. a) Disordered pattern, b) patterns produced by four standing waves, c) pattern produced by three standing waves, d) pattern produced by two standing waves, These patterns are produced at same frequency but amplitude of vibrations is higher and e) and f) patterns produced at higher amplitudes. The size of each image is around 4 cm. From ref (5)

Since these patterns are highly ordered, it is desirable to freeze-in these patterns in fluid surface, so as to use these patterned surfaces for different applications. Further the wavelength, λ, of the standing waves is governed by following relation[3],

$$\omega^2 = 4gk(1 + \frac{4\pi^2\sigma}{\lambda^2\rho g})$$

where σ is the surface tension of the fluid, ρ is the density of the fluid, and ω is the frequency of the vibrations. From this equation, it is clear that the wavelength can be easily varied by varying the frequency of the vibrations. This allows us to control the length scale of the structures in the pattern. Since these patterns are formed by standing waves, these structures are vibrating at high frequency. Therefore, it will be difficult to freeze-in these patterns. One can think of freezing-in the patterns by exposing a photocurable fluid to light, once the instabilities have set in or freezing the fluid by decreasing the temperature. These procedures may work out for waves vibrating at very small frequencies as the curing time for the photocurable fluid is of the order of seconds. But in order to produce patterns where structures have micron length scales, vibrations of the order of one hundred kilohertz are required. At these frequencies, it is impossible to freeze the structures by using above mentioned techniques. Therefore, to freeze-in the patterned structures at small length scales, an electric field was used.

As we have discussed in the previous chapter, electrohydrodynamic instabilities are produced when an electric field is applied across the interface of two fluids. The electric field develops displacement charges at the interface of the two fluids, due to the difference in the dielectric constants of the two fluids. These displacement charges lead to Maxwell stresses at the interface due to the attraction of these charges toward the oppositely charged electrode. In other words, the film surface is pulled towards the electrode on application of the electric field. Now both of these instabilities i.e. parametrically forced surface waves and electric field instabilities can be coupled

together. The free surface of polymer melt film can be patterned by using vibrations and then these waves can be frozen by applying an electric field which pulls up the cusps of the standing waves towards the electrode. The details of the experiment and the results will be discussed in the following sections.

3.1.2 Experiment

Polystyrene of molecular weight 8000 g/mol was used in this study. Thin films were coated from toluene solution on the substrate. The electric field was applied as shown in the Figure 3.2. A glass slide was etched using 5% HF solution so that there is a recess with a depth of 2 μm in the middle of the glass slide. The glass slide was coated with gold on the other side using thermal vapor deposition. The polymer film was removed from the edges such that the polymer film fit under the recess. Around 100 volts potential difference was used to apply the electric field. Lead zirconium titanate (PZT) based piezo crystals were used to apply the vibrations. Discs of PZT crystals of 1 inch diameter with bull's eye electrode pattern were used. The resonant frequency of the discs is controlled by varying the thickness of the discs. Three different frequencies were used in these experiments namely 1.3, 2.6 and 5.6 MHz. A 200 watt power source with variable frequency output was used to power the PZT crystals. Poly dimethyl siloxane (PDMS) was used to couple the vibrations from the piezo crystal to the substrate. The electric field was turned on approximately one-half minute after starting the vibrations so that the patterned structures can be frozen-in.

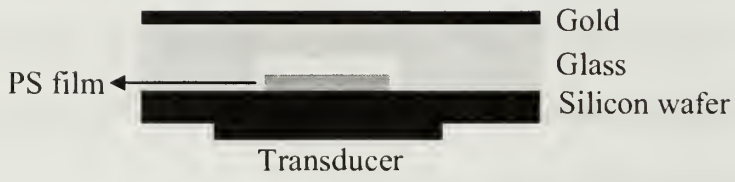

Figure 3.2: Schematic of the experimental set up. There is a layer of PDMS in between transducer and silicon wafer to couple vibrations from ultrasonic transducer to silicon wafer.

3.1.3 Results and Discussion

Figures 3.3, 3.4 and 3.5 represent the optical microscopic images of structures obtained by using vibrations with frequencies of 1.3, 2.6 and 5.6 MHz respectively. The electric field strength in each of these experiments was kept at ~10^7 volts/m. From Figure 3.3, the characteristic spacing was found out to be 3.3 ± 0.2 μm. For the similar conditions i.e. same electric field strengths and in the absence of vibrations, the characteristic spacing was ~15 μm. Further, it can be seen that the structures are packed in a square pattern with some defects. On changing the frequency of vibrations from 1.3 MHz to 2.6 MHz, a drop in the structure spacing is observed. As shown in Figure 3.4 the characteristic spacing, which is dictated by the wavelength of the capillary waves, is reduced to 2.2 ±0.2 μm. The wavelength of the excited capillary waves at the surface is given by the dispersion relation developed by Kelvin and is

$$\lambda = \sqrt[3]{\frac{8\pi\sigma}{\omega^2\rho}}$$

Therefore, the wavelength λ should decrease as $\omega^{2/3}$. The structure spacing was plotted against the frequency of vibration in a log-log plot and is shown in Figure 3.6. The

slope of the curve is -2/3 which is expected from the Kelvin relation. This confirms that the structures are produced by vibration driven capillary waves which are then stabilized by electric field.

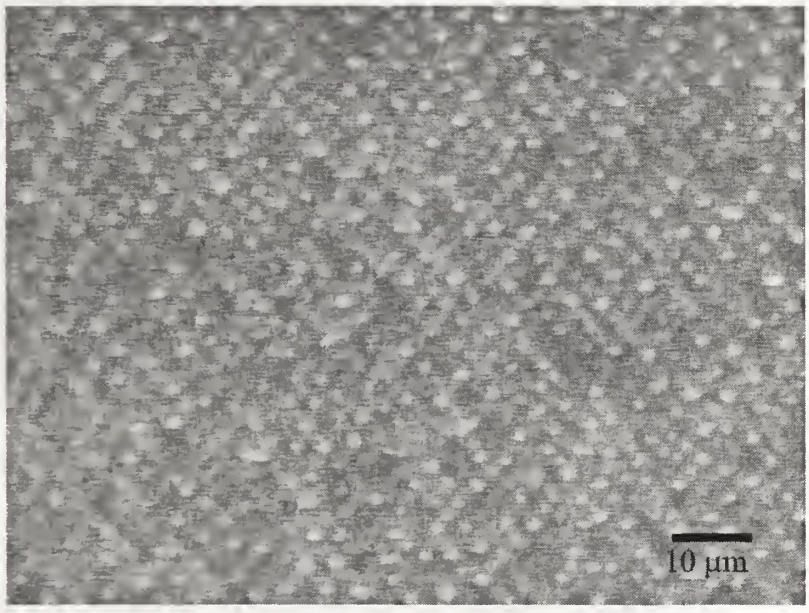

Figure 3.3: Optical microscopy image of structures produced by using 1.3 MHz vibrations and electric field.

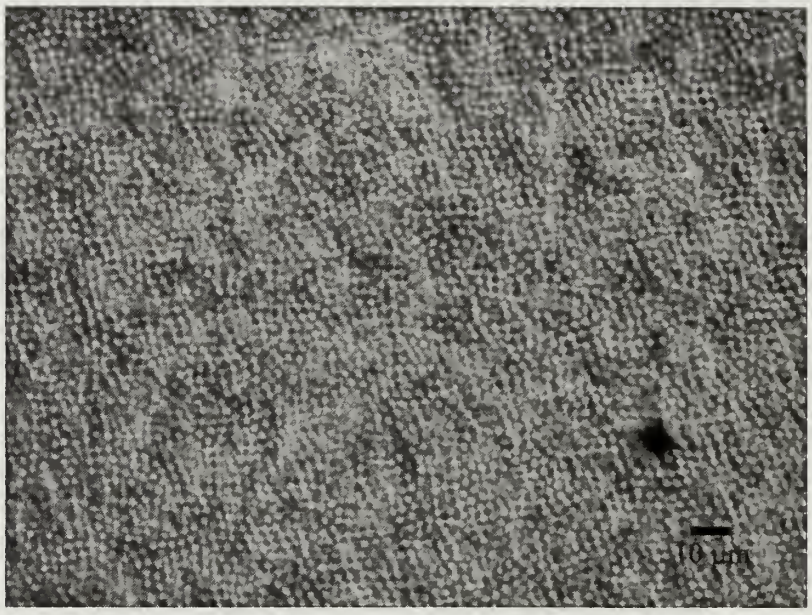

Figure 3.4: Optical microscopy image of structures produced by using 2.6 MHz vibrations and electric field.

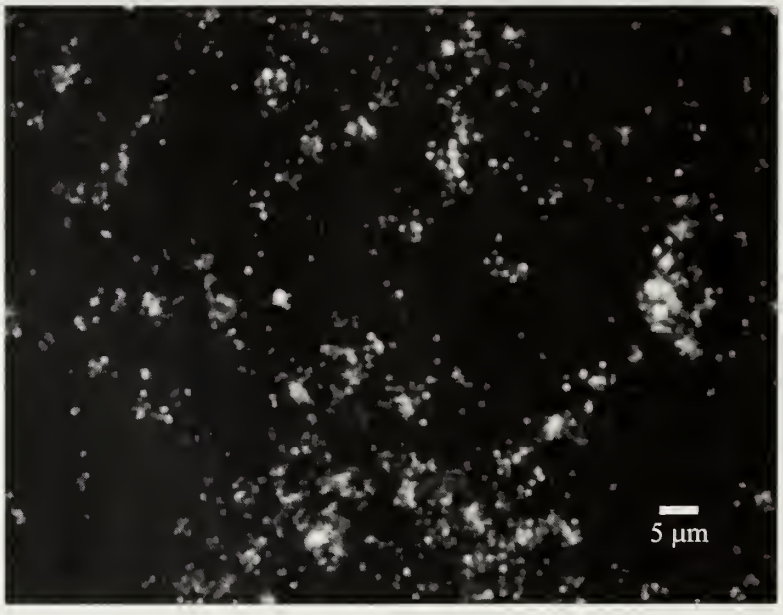

Figure 3.5: Optical microscopy image of structures produced by using 5.6 MHz vibrations and electric field.

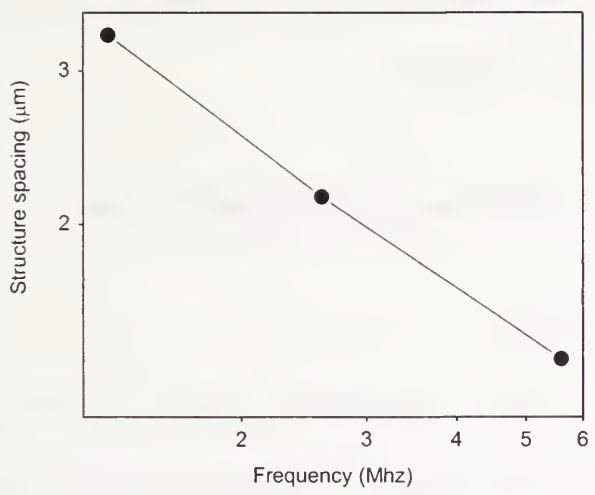

Figure 3.6: Log-log plot of structure spacing and frequency of vibrations used to produce them.

Further the images show patterned structures in square symmetry with defects. It has been shown before that to obtain square symmetry in structures, the amplitude of vibrations have to be large[5]. Also, since a polymer was used in this study, the viscosity is higher than fluids which have been studied before. Although a very low molecular weight polymer was used, the viscosity is still higher than water, which is mostly used in previous studies. It was also shown that the amplitude of vibration has to be large to excite capillary waves and obtain patterns in viscous fluids[6]. But, in this study the amplitude of the vibrations that can be applied is limited by the availability of piezo-crystals that can provide large amplitude vibrations.

3.1.4 Conclusion

In summary, it is shown that the capillary waves can be excited in polymer thin films by using ultrasonic vibrations. The patterns produced by these vibrations can be

stabilized by applying electric field. The pattern spacing can be controlled by changing the frequency of vibration.

3.2 Pattern replication using patterned electrode

3.2.1 Introduction

The interest in alternative patterning techniques has grown recently due to fundamental physical barriers in photolithography to pattern structures in sub-40 nm length scales. Directed self-assembly patterning techniques are appealing because of their ability to harness natural phenomena to form structures at such smaller length scales. Electrohydrodynamic instabilities are such a directed-assembly technique that is capable of forming polymeric columnar arrays. These arrays may find application in technologies such as micro-electro-mechanical systems, microfluidic devices, patterned magnetic media, and photonic band gap materials. The structures obtained by applying electric field across a polymer thin film can be directed by using a patterned top electrode.

Extensive research on the electrohydrodynamic instabilities under topographically patterned electrode has been done[7]. Electrodes with diverse types of patterns such as lines, circles, triangles, and squares have been used. Typically, the mask is held in close proximity to the polymer surface, leaving an air gap, and the system is heated above the glass transition temperature and an electric field is applied. The protrusions in the electrode due to the topographic pattern produce a non-uniform field across the polymer resulting in the nucleation of the instability in the polymer film under the pattern initially. This shifts the spacing from the natural wavelength of the

instability and guides the polymer into structures that can conform completely to the pattern on the mask. Thus, by using a patterned electrode, the location and domain orientation of the structures can be well controlled.

In this study patterned electrodes are formed by coating a film of phase separated PS-*b*-PMMA diblock copolymer on the electrode. This provides a non-topographic pattern on the electrode. Since the dielectric constant of PMMA is higher than PS, therefore the electric field strength is higher under the PMMA domains. This leads to nucleation of the instability under the PMMA domains and hence the pattern is replicated onto the polymer film.

3.2.2 Experiment

Patterned electrodes were prepared by spin coating 40 nm thick film of PS-*b*-PMMA diblock copolymer from toluene onto a glass slide that was modified with a neutral brush. Two PS-*b*-PMMA block copolymers with different volume fractions of PMMA were used. One block copolymer had 50 % PMMA volume fraction with total molecular weight of 66,000 g/mol and gave lamella morphology with normal orientation of the lamellae. Second diblock copolymer had 25% PMMA volume fraction and molecular weight was 60,000 g/mol. This block copolymer had cylindrical microdomain morphology with the cylindrical microdomains oriented normal to the substrate. A ~100 nm thick film of PMMA with a molecular weight of 25,000 g/mol was coated onto a doped silicon wafer that acted as the second electrode. These two electrodes were sandwiched together and electric field was applied at 110 ^{o}C.

3.2.3 Results and Discussion

Figure 3.7 shows a scanning force microscope (SFM) image of the patterned electrode. This image shows PMMA cylinders in a PS matrix with cylinders oriented normal to the surface. The spacing between two cylinders is around 40 nm and cylinder diameter is around 20 nm. This electrode was sandwiched with the other electrode having a PMMA film such that there was an air gap of 1 μm. Then the electrodes were heated and an electric field was applied for 1 hr. After separating the electrodes, the sample was examined in SFM. There was no pattern transferred. To understand these results, calculations were carried out to determine the electric field strengths at the homopolymer surface. Since the basis of the experiment lies at the nucleation of the instabilities under the higher dielectric constant PMMA, Gauss law was applied and the electric field strengths were determined. In the calculations the dielectric constant of PMMA was kept 7 and that of PS was 3. Further, the effect of separation between the patterned surface and the homopolymer film was studied. FlexPDE software was used to solve the partial differential equations numerically and to determine the electric field strengths.

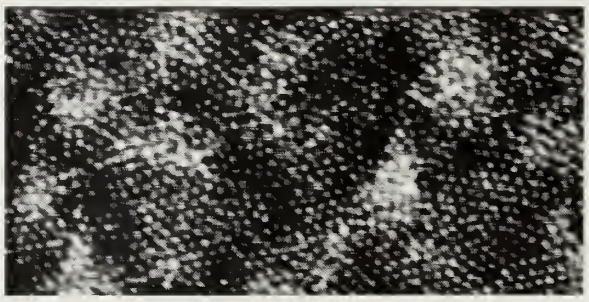

Figure 3.7: SFM image of PS-*b*-PMMA copolymer thin film with PMMA cylinders oriented normal to surface.

The results from the calculations indicated that the separation between the two electrodes is very important. When the separation between the patterned surface and the homopolymer film was more than twice the pattern spacing, the electric field contrast under the high dielectric constant region and lower dielectric strength was smeared and the electric field strength was essentially uniform. The electric field strength under PS region was 85% of that of under PMMA region when the spacing between two electrodes was kept equal to the pattern size. Since the Maxwell stress acting on the polymer interface depends upon the square of the electric field strength, the contrast in the stress was even higher. From the calculations, it is clear that the separation can not be larger than the pattern size for the pattern to be replicated onto the homopolymer using electric field. The contrast in the electric field strengths increased further on decreasing the separation distances. Therefore, to replicate structures with sizes of 20 nm, the separation between the electrodes has to be at most 20 nm. Since the separation was kept at 1 μm initially, therefore the patterns were not replicated onto the surface of homopolymer surface.

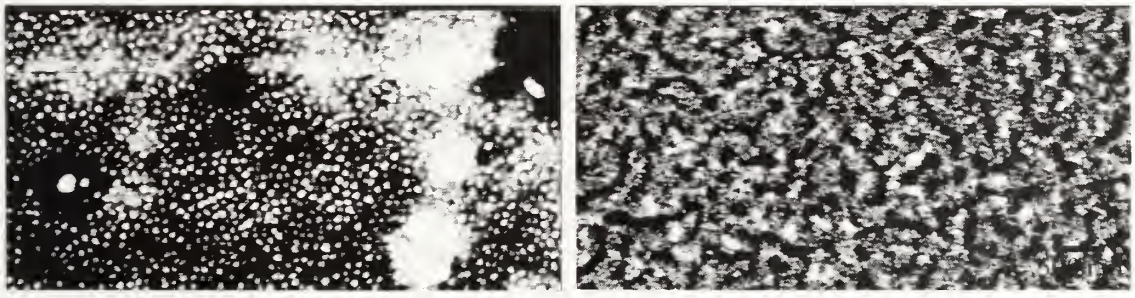

a b

Figure 3.8: SFM images of replicated patterns on the PMMA homopolymer thin films.

It is very difficult to keep an air gap of 20 nm between the two surfaces of electrodes. To overcome this difficulty air can be replaced with some other fluid. Any fluid can be used as long it has a low dielectric constant and low viscosity. PDMS was used as the fluid layer and 20 nm thick PDMS film was spin coated on PMMA from hexane and afterwards the two electrodes were sandwiched. The dielectric constant of PDMS is around 2.3 and also the PDMS is not miscible with PS or PMMA. This approach further decrease the interfacial tension at PMMA interface, which is beneficial in getting smaller size scale structures. After heating the setup to 110 ^{c}o and applying an electric field of 500 volts/μm for 1 hr, the electrodes were removed and the homopolymer was examined with SFM. Figure 3.8a shows SFM image of the surface of the PMMA homopolymer after washing with hexane to remove PDMS. It can be seen that the pattern was formed with features having sizes similar to that of diblock copolymer used. Further, from the height image columns are observed, which shows that the instabilities, in fact, began under the PMMA cylindrical microdomains. Figure 3.8b shows an SFM image of another sample which was prepared similarly. It can be seen that the film has been ripped from some areas. Since very thin PDMS layer was used, the removal of the two electrodes becomes very difficult and sometimes lead to the structures being ripped from the surface.

After the dot pattern, produced by cylinders oriented normal to surface, was successfully replicated onto the polymer film, the line pattern was also tried. In order to produce the line pattern, a thin film having lamellar microdomains oriented normal to the film surface was prepared on the top electrode. Figure 3.9a shows a SFM image of the pattern present on the top electrode. Experiment was performed as described

before. Figure 3.9b shows a SFM image of the pattern replicated onto the homopolymer surface. The pattern is replicated but the lines seem to disintegrate into smaller pillars.

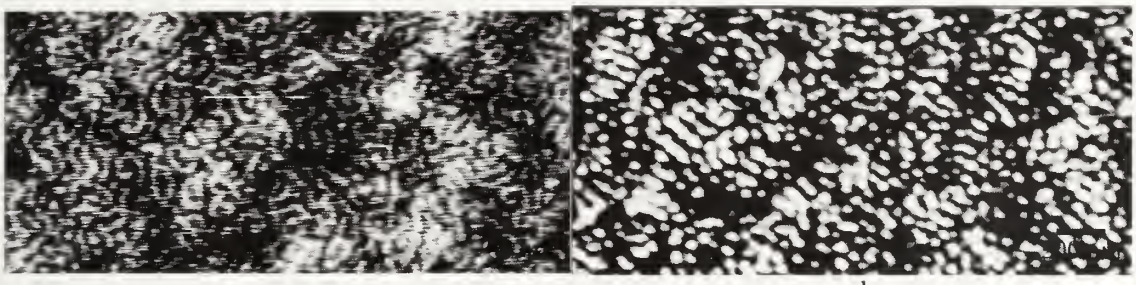

a b

Figure 3.9: a) SFM images of lamella pattern on the top electrode and b) replicated pattern on the PMMA film

3.2.4 Conclusion

In conclusion, it has been shown that the structures with size of 20 nm can be replicated successfully using electric field. The patterns with a contrast in the dielectric constant can also be used. In order to successfully replicate the pattern, the spacing between the two electrodes has to be same or smaller than the pattern size.

3.3 References

1. Kumar, K. and Tuckerman, L. S., Parametric-Instability of the Interface between 2 Fluids. *Journal of Fluid Mechanics* 1994, **279**, 49-68.

2. Rayleigh, L., On the crispations of fluid resting upon a vibrating support. *Philosophical Magazine* 1883, **16**, 50-58.

3. Miles, J. and Henderson, D., Parametrically Forced Surface-Waves. *Annual Review of Fluid Mechanics* 1990, **22**, 143-165.

4. Douady, S. and Fauve, S., Pattern Selection in Faraday Instability. *Europhysics Letters* 1988, **6**, (3), 221-226.

5. Christiansen, B.; Alstrom, P. and Levinsen, M. T., Ordered Capillary-Wave States - Quasi-Crystals, Hexagons, and Radial Waves. *Physical Review Letters* 1992, **68**, (14), 2157-2160.

6. Lang, R. J., Ultrasonic Atomization of Liquids. *Journal of the Acoustical Society of America* 1962, **34**, (1), 6-&.

7. Voicu, N. E.; Harkema, S. and Steiner, U., Electric-field-induced pattern morphologies in thin liquid films. *Advanced Functional Materials* 2006, **16**, (7), 926-934.

CHAPTER 4

SELF-HEALING NANOPARTICLE FILLED SYSTEMS

4.1 Introduction

Nanoparticle-filled systems are generating significant interest due to the unique mechanical and photophysical properties imparted to materials based on the small size of the filler particles.[1,2,3] Advances in nanoparticle synthesis have led to a wide variety of particles with tunable properties and narrow size distributions that enable the assembly of the nanoparticles into two or three dimensional superlattices[4]. The dispersion of nanoparticles in a polymer matrix and their surface activity will, of course, depend upon the interactions between the polymer and the ligands attached to the nanoparticles and the size of the nanoparticles relative to the radius of gyration of the polymer. Consequently, both enthalpic interactions and the entropy of the polymer contribute to the spatial distribution of the particles in a host polymer. This is perhaps best demonstrated by the addition of nanoparticles to microphase separated block copolymers. By manipulating the interactions between the ligands attached to the nanoparticles and the two blocks of the copolymer, a selective segregation of the nanoparticles to either microdomain or to the interfaces between the microdomains can be obtained so that the copolymer morphology dictates the spatial distribution of the nanoparticles in the material[5,6]. Alternatively, by minimizing the interactions between the nanoparticles and the blocks of the copolymer, the entropic constraints placed on the copolymer chains by the presence of the nanoparticles can force an exclusion of the nanoparticles to the interfaces of the film, thereby modifying interfacial interactions and

inducing a re-orientation of the copolymer microdomains[7,8]. Consequently, the system self-assembles and self-orients.

In general, designing systems that can automatically perform a specific function or respond to stimuli or environmental changes without external intervention are highly desirable. This is particularly important in cases where a mechanical failure of a system, as in the case of a cracking in multilayered systems, can have catastrophic consequences. Theory indicates that nanoparticle-filled systems represent one case where self-healing conditions can be realized[9]. Here, we provide experimental evidence of a self-healing system that relies on an entropically driven assembly of nanoparticles to crack interfaces in a layered composite material. When a crack is introduced into a brittle layer in a mutilayered system, the nanoparticles are found to migrate to and assemble at the crack interface, so that the particle concentration is high in the region of the crack. By manipulating the chemical nature of the ligands, the defect introduced by the crack can be ameliorated by the aggregation of the nanoparticles to the crack. Multilayered composites of ductile polymers and brittle films (ceramics or metals) are widely used in packaging, coatings, solid-state devices, and biomedical engineering. The results shown here provide a simple means of imparting a self-healing characteristic to systems that can substantially prolong structural and device life-times.

4.2 Experimental

CdSe/ZnS core/shell nanoparticles were synthesized according to published procedures[10]. The synthetic protocol yielded CdSe/ZnS nanoparticles covered with tri-n-octylphosphine oxide (TOPO)/hexadecylamine (HDA) ligands. In order to study the

effect of anisotropy of the nanoparticles on the diffusion of nanoparticles, nanorods were also synthesized as per published procedures. The nanorods were also initially covered with TOPO. To change the surface properties of the nanoparticles, thiolated poly (ethylene oxide) (Molecular weight - 2,100 Polymer Source Inc, Quebec, Canada) was exchanged with TOPO/HDA. To prepare the composite layer, nanoparticles were dissolved in chloroform solution of PMMA (Molecular weight of 25,000 and $R_g \sim 5$ nm, Polymer Source Inc, Quebec, Canada) to give a solution having 1 wt% PMMA and 0.1 wt% nanoparticles. A thin film of this composite material was prepared by spin coating the solution onto a silicon wafer. A layer of silicon oxide was then thermally deposited onto the composite film, as shown schematically in Figure 4.1. This bilayer film was heated to 170°C for a short period of time (less than one minute) which, due to the differences in the thermal expansion coefficients of the layers, produced cracks in the silicon oxide layer. This bilayer film was further annealed at 170°C under high vacuum (10^{-6} torr) to prevent oxidation of particles. The lateral distribution of nanoparticles in the film was monitored by fluorescence microscopy (Olympus BX51). A super wide band filter (420-440 nm) was used for excitation and a 475 nm filter was used for emission. Transmission electron microscopy (TEM) (JEOL 2000FX) was used to observe the distribution of nanoparticles in a cross-section of the polymer film.

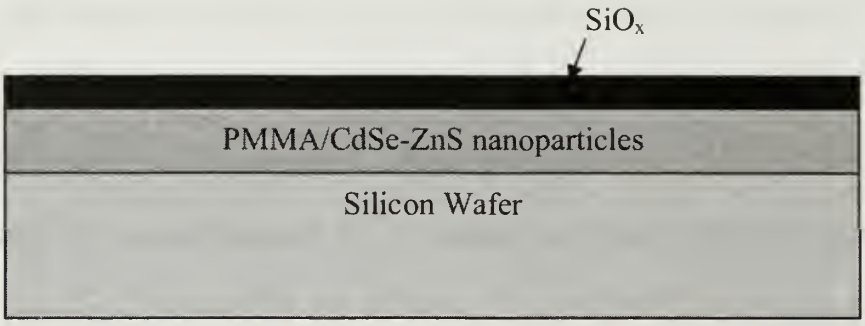

Figure 4.1: Schematic showing the bilayer with SiO_x as one layer and polymer/nanoparticle nanocomposite as the second layer on silicon wafer.

4.3 Results and Discussion

Figure 4.2 shows a fluorescence microscope image of a bilayer composite film with a crack in the 500 nm thick silicon oxide layer deposited on 300 nm thick PMMA and TOPO covered CdSe nanoparticle composite film. After annealing at 170 °C for 20 hrs, a localization of the nanoparticles into the crack did not occur. However, at the edge of the crack there is a bright fluorescent band that outlines the edge, a dark region (or depletion layer) behind this bright edge and uniform fluorescence intensity under the remaining intact silicon oxide layer. The behavior observed here is in contrast to theoretical predictions, where a segregation of the nanoparticles to the crack would be expected [9].

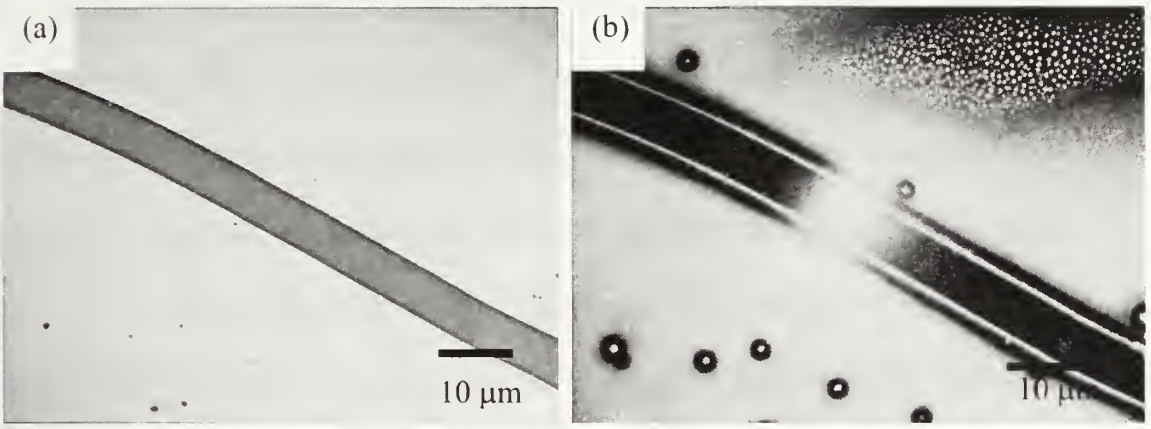

Figure 4.2: Crack in 500nm thick SiOx layer. (a) is the bright field image and (b) is the corresponding fluorescence image.

Cross-sectional TEM studies were performed on the PMMA/nanoparticle composite film prior to the deposition of the silicon oxide, to examine the distribution of nanoparticles within the film. Figure 4.3a shows a cross-section of a TOPO-CdSe/ZnS-PMMA film, where it is seen that most of the nanoparticles are located at the top of the film (air/polymer interface), while very few are in the bulk. The segregation of the nanoparticles to the air interface arises from the non-favorable interactions between the alkane ligands attached to the nanoparticles and the PMMA matrix and the lower surface energy of the alkanes. Upon evaporation of the silicon oxide, the nanoparticles form an intermediate layer between the silicon oxide and the PMMA. When the crack is produced in the silicon oxide, the nanoparticles are drawn along with the silicon oxide, exposing bare PMMA to air. While the segregation of the nanoparticles to the exposed surface would be expected, this would require the diffusion of the nanoparticles either along the interface between the PMMA and silicon oxide layers or the diffusion of the nanoparticles through the PMMA to the exposed surface.

The latter is highly unfavorable, due to the strong non-favorable interactions between the ligands and the PMMA. Diffusion of the nanoparticles along the PMMA/silicon oxide occurs initially, as evidenced by the enhanced fluorescence intensity at the crack edge, and the trailing depletion zone, as evidenced by the lack of fluorescence immediately behind the edge. However, there is no further driving force to cause a migration of the particles along the interface to complete a healing of the crack. Any further motion of the particles would increase the energy of the system and, as such, the system is trapped in this state.

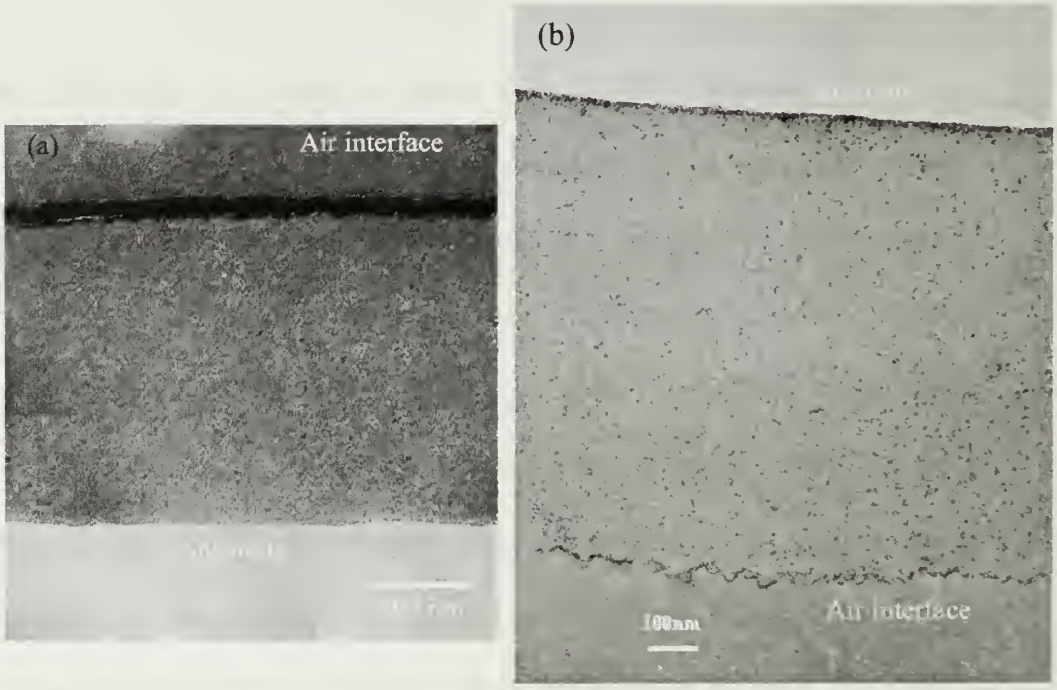

Figure 4.3: TEM images of the cross-section of films with (a) TOPO covered nanoparticle in PMMA with a black carbon marker at the air polymer interface and (b) PEO covered nanoparticles in PMMA.

A uniform distribution of nanoparticles in the PMMA film can be achieved by attaching poly(ethylene oxide), PEO, to the nanoparticles. PEO and PMMA are known to be miscible, but the segmental interactions between the PEO and PMMA are quite

small[11], virtually eliminating enthalpic interactions of the nanoparticles with the host matrix. PEO covered CdSe/ZnS core-shell nanoparticles were prepared and blended with PMMA in a chloroform solution. Thin films were spin coated onto a silicon substrate, annealed under vacuum at 170 °C, above the glass transition temperature of PMMA for 24 hrs. Figure 4.3b, shows a TEM cross-sectional image of the composite where the nanoparticles are seen to be uniformly dispersed in the PMMA matrix. Very slight enhancements of the nanoparticles at the substrate and air interfaces are seen. A 60 nm layer of silicon oxide was then evaporated onto the surface of the composite, and the layered sample was annealed under vacuum at 170 °C. Figure 4.4 shows the bright field and fluorescence microscopic images of the sample after 20 hrs annealing. In the bright field image, cracks are clearly seen in the silicon oxide over layer arising from the difference in the thermal expansion coefficients of the two layers. In the fluorescence image, the higher intensity in the cracks indicates the nanoparticles have migrated to the cracks, in agreement with predictions[9]. The fluorescence intensity under the remaining silicon oxide demonstrates that there are still nanoparticles dispersed in the PMMA matrix. This behavior is completely different from the TOPO covered particles. Since the interactions between the nanoparticles and the PMMA matrix is virtually zero, a migration of the nanoparticles to the exposed film surface at the crack arises from the lower surface energy of the PEO than PMMA. However, this alone is not sufficient to achieve the segregation observed. Rather, an equally dominant factor is the entropic penalty imposed on the PMMA chains due to the presence of the particles. Since the individual PMMA chains must wrap around the nanoparticles to achieve a uniform dispersion, there is an entropic gain in expelling the nanoparticles to

the free surface[12]. This depletion attraction pushes the nanoparticles out of the film even though the particles are 'soluble' in polymer film. It should also be noted that PMMA preferentially wets the silicon oxide layer, which has the desirable effect of precluding a segregation of the nanoparticles to the silicon oxide/polymer interface[13], thereby promoting a dispersion of the nanoparticles in the PMMA matrix. Thus, in the presence of a crack, which exposes a fresh air/polymer interface, the nanoparticles easily migrate to the exposed crack surface.

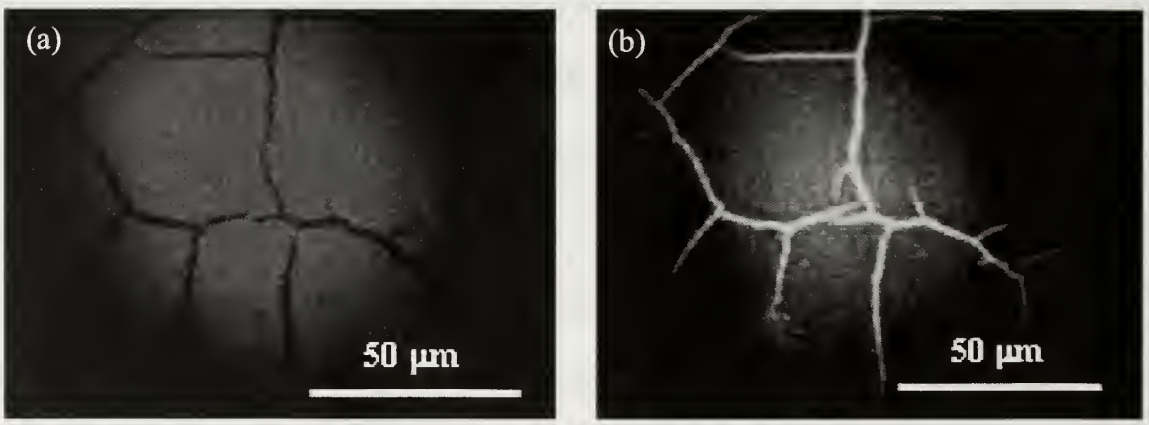

Figure 4.4: Fluorescence microscope image of crack in 60nm SiOx layer on a PMMA/ CdSe-ZnS nanoparticle. (a) is the bright field image and (b) is the corresponding fluorescence image.

The dominant driving force for this observed segregation is argued to be entropic in origin. If this is correct, then there must be a dependence of the segregation on the relative size of the nanoparticles to the size of the polymer chains. Consequently, studies were performed on both 3 nm and 5.2 nm PEO coated nanoparticles dispersed in the PMMA matrix. The rate of increase in the fluorescence intensity within the crack was monitored as a function of time and the results obtained at 140 °C, which is above the glass transition temperature of the PMMA, are shown in

Figure 4.5 and Figure 4.6. While in the solid state the intensity increase cannot be directly correlated with an increase in the absolute number of nanoparticles in the crack, it does provide a relative measure of the diffusion of the nanoparticles to this interface. It is interesting to note that the fluorescence intensity in the cracks for the 3 nm nanoparticles was invariant with time as shown in Figure 4.6, though the fluorescence intensity in the cracks was always higher than the surrounding areas. With the 5.2 nm nanoparticles, however, a large increase in the relative fluorescence intensity was seen as shown in Figure 4.5. This can be understood strictly in terms of the entropic cost to the PMMA chains due to the presence of the nanoparticles. If the nanoparticles are small in comparison to the radius of gyration of the polymer, the constraints placed on the configuration of the chains are small and, as such, the entropic penalty to incorporate the nanoparticles in the polymer matrix is small. However, as the particles become larger, comparable to the radius of gyration of the polymer, the entropic penalty increases and the nanoparticles will be driven from the matrix and, in this case, to the exposed crack area.

If we assume that the fluorescence intensity is proportional to the concentration of nanoparticles, the diffusion coefficient, D, of 5.2 nm nanoparticles in PMMA can be calculated by

$$D = 0.925034 \frac{a^2}{t_h - t_0}$$

where a is the crack width measured by optical microscopy; t_h is the diffusion time to reach half of the saturated fluorescence intensity; and t_o is the starting time. The average width of the crack, a, was determined to be 6 μm which yields a diffusion

constant, D, 7.8 × 10^{-3} μm^2/sec for 5.2 nm diameter CdSe/ZnS nanoparticles covered with PEO in PMMA at 140 °C. This diffusion constant represents predominantly the lateral diffusion of nanoparticles into the cracks rather than the vertical diffusion, since the diffusion of the nanoparticles normal to the film surface would not produce a change in the fluorescence intensity due to the depth of field of the microscope objective. It should be noted that the diffusion coefficient calculated here is very close to the diffusion coefficient of CdSe nanoparticles confined to immiscible interfaces as reported by Lin et al. [14]

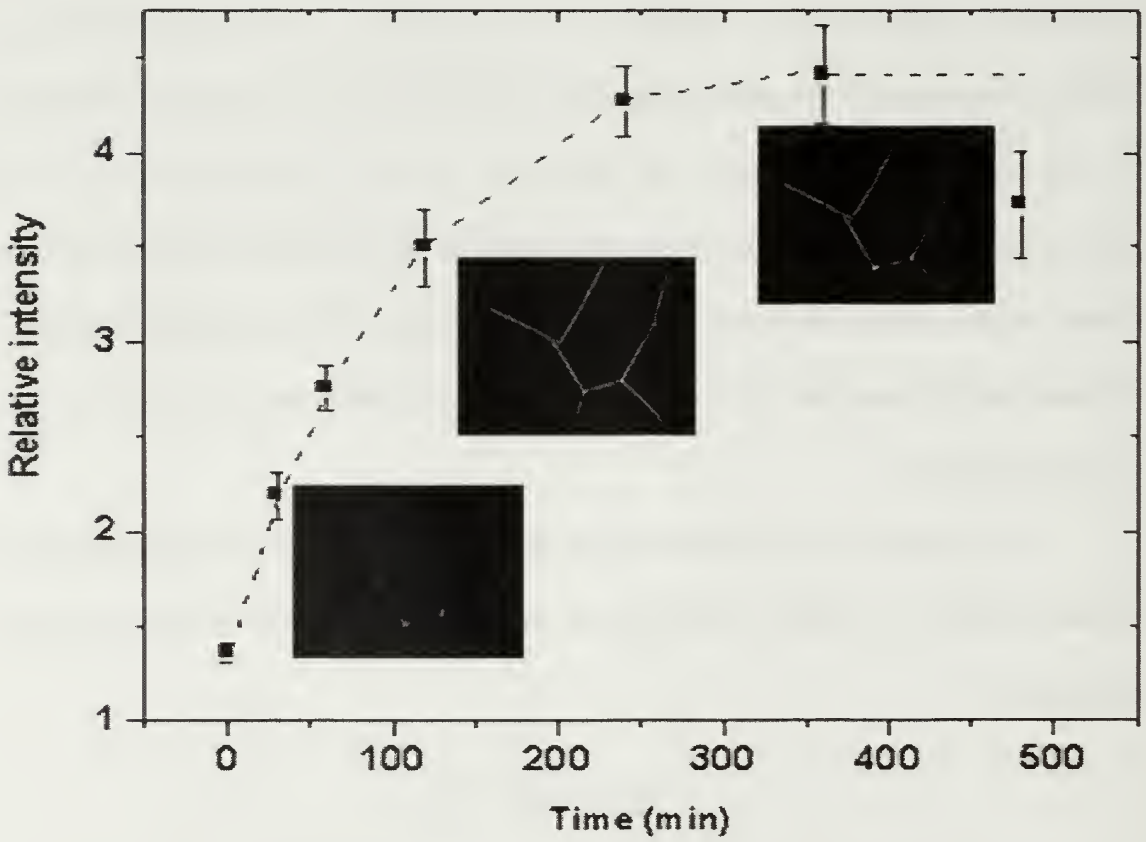

Figure 4.5: Plot for the relative intensity in cracks and time for 5.2 nm diameter PEO covered CdSe nanoparticles at 140oC. The images inserted in the graph show relative increase in fluorescence intensity in the cracks with increase in time.

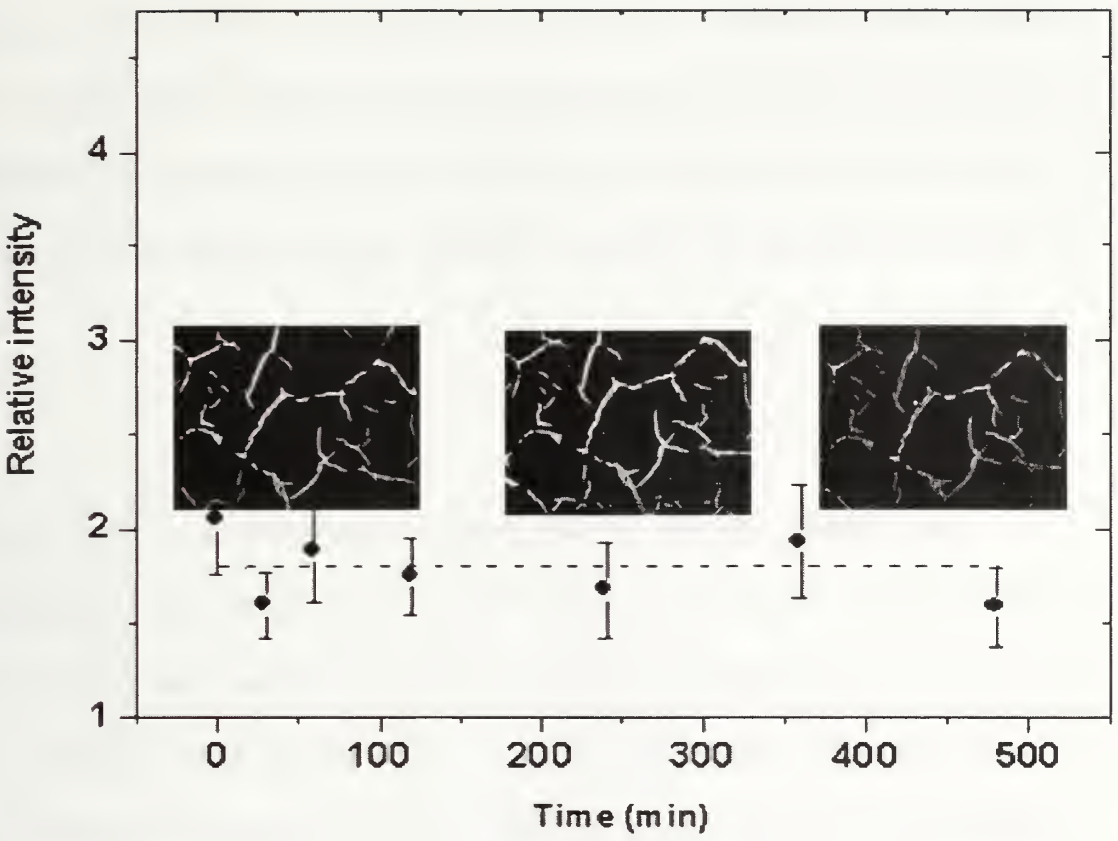

Figure 4.6: Plot for the relative intensity in cracks and time for 3 nm diameter PEO covered CdSe nanoparticles at 140°C. The images inserted in the graph shows constant fluorescence intensity in the cracks with time.

In order to study the effect of anisotropy of the nanoparticle shape on the rate of diffusion, nanorods were used instead of spherical nanoparticles. Previously it has been shown that the one dimensional nature of nanorods (with diameter ~ 8 nm and length 40 nm) causes the concentration of nanorods in the cracks to be higher when compared to nanoparticles.[15] But to study the effect of anisotropy on diffusion, experiments were carried out by replacing the nanoparticles with nanorods that were 40 nm long and 8 nm in diameter. These nanorods were also covered with PEG and were dispersed in PMMA film. The diffusion studies were carried out and the diffusion constant was found out to be 4.7 x 10^{-2} μm^2/sec. This value of diffusion coefficient is an order higher than

observed for nanoparticles. This was expected because the entropic penalty is higher in the case of nanorods than the nanoparticles due to their higher volume but the viscous drag is similar in both cases due to similarity in sizes of nanoparticle and the diameter of nanorods. Therefore the diffusion of nanorods should be higher than the spherical nanoparticles.

4.4 Conclusion

Two different examples of nanoparticle composites in a multilayered system have been shown. In one case, where enthalpic interactions between the nanoparticles and matrix are non-favorable, a segregation of the nanoparticles to the surface is found. In a multilayered system with cracks in the adjoining layer, diffusion of the nanoparticles to the crack area is precluded due to the unfavorable interactions of the nanoparticles with the matrix. In a second case, where the nanoparticles are uniformly dispersed in the polymer matrix and the interactions between the nanoparticles and matrix are small, entropic factors lead to a migration of the nanoparticles to the crack area, essentially healing the crack formed in the adjoining layers. This segregation is dependent on the relative size of the nanoparticles to the polymer host and, if the entropic driving force to exclude the nanoparticles is too small, the migration of the nanoparticles to the crack does not occur. Further, on changing the shape of nanoparticles from spherical to rods increase the diffusion rate of particles to cracks. The behavior observed is in keeping with theoretical predictions and provides a simple means of designing self-healing systems. These systems, depending on the functionalization of the nanoparticles, has potential use in optical communications,

biological engineering and microelectronic systems, where multilayer composites, that include brittle layer and polymer layer, are used.

4.5 References

1. Brust, M.; Fink, J.; Bethell, D.; Schiffrin, D. J. and Kiely, C., Synthesis and Reactions of Functionalized Gold Nanoparticles. *Journal of the Chemical Society-Chemical Communications* 1995, (16), 1655-1656.

2. Alivisatos, A. P., Semiconductor clusters, nanocrystals, and quantum dots. *Science* 1996, **271**, (5251), 933-937.

3. Puntes, V. F.; Krishnan, K. M. and Alivisatos, A. P., Colloidal nanocrystal shape and size control: The case of cobalt. *Science* 2001, **291**, (5511), 2115-2117.

4. Murray, C. B.; Kagan, C. R. and Bawendi, M. G., Synthesis and characterization of monodisperse nanocrystals and close-packed nanocrystal assemblies. *Annual Review of Materials Science* 2000, **30**, 545-610.

5. Bockstaller, M. R.; Lapetnikov, Y.; Margel, S. and Thomas, E. L., Size-selective organization of enthalpic compatibilized nanocrystals in ternary block copolymer/particle mixtures. *Journal of the American Chemical Society* 2003, **125**, (18), 5276-5277.

6. Misner, M. J.; Skaff, H.; Emrick, T. and Russell, T. P., Directed deposition of nanoparticles using diblock copolymer templates. *Advanced Materials* 2003, **15**, (3), 221-+.

7. Thompson, R. B.; Ginzburg, V. V.; Matsen, M. W. and Balazs, A. C., Predicting the mesophases of copolymer-nanoparticle composites. *Science* 2001, **292**, (5526), 2469-2472.

8. Lin, Y.; Boker, A.; He, J. B.; Sill, K.; Xiang, H. Q.; Abetz, C.; Li, X. F.; Wang, J.; Emrick, T.; Long, S.; Wang, Q.; Balazs, A. and Russell, T. P., Self-directed self-assembly of nanoparticle/copolymer mixtures. *Nature* 2005, **434**, (7029), 55-59.

9. Lee, J. Y.; Buxton, G. A. and Balazs, A. C., Using nanoparticles to create self-healing composites. *Journal of Chemical Physics* 2004, **121**, (11), 5531-5540.

10. Chen, Y. F.; Ji, T. H. and Rosenzweig, Z., Synthesis of glyconanospheres containing luminescent CdSe-ZnS quantum dots. *Nano Letters* 2003, **3**, (5), 581-584.

11. Ito, H.; Russell, T. P. and Wignall, G. D., Interactions in Mixtures of Poly(Ethylene Oxide) and Poly(Methyl Methacrylate). *Macromolecules* 1987, **20**, (9), 2213-2220.

12. Kim, J. U. and O'Shaughnessy, B., Morphology selection of nanoparticle dispersions by polymer media. *Physical Review Letters* 2002, **89**, (23).

13. Krausch, G., Dewetting at the interface between two immiscible polymers. *Journal of Physics-Condensed Matter* 1997, **9**, (37), 7741-7752.

14. Lin, Y.; Boker, A.; Skaff, H.; Cookson, D.; Dinsmore, A. D.; Emrick, T. and Russell, T. P., Nanoparticle assembly at fluid interfaces: Structure and dynamics. *Langmuir* 2005, **21**, (1), 191-194.

15. Smith, K. A.; Tyagi, S. and Balazs, A. C., Healing surface defects with nanoparticle-filled polymer coatings: Effect of particle geometry. *Macromolecules* 2005, **38**, (24), 10138-10147.

CHAPTER 5

ASSEMBLY OF CDSE NANORODS IN BLOCK COPOLYMER TEMPLATES

5.1 Introduction

Metallic, semiconductor and magnetic nanoparticles are of great interest due to their novel electronic, luminescent and magnetic properties that are not present in the bulk[1,2,3,4,5]. The combination of unique nanoparticle properties with their small size, leads to a wide array of potential applications that could be realized from high density arrays of such functional components. Nanoparticles can be made in various shapes, e.g. spherical, cylindrical, pyramidal, or star-like; moreover, a significant control over nanoparticle size and size distribution can be achieved[5]. However, optimal utilization of the unique properties of nanoparticles requires the level of positional control enabled by self-assembly.

Assembly of spherical nanoparticles has been pursued actively over the last few years. The preferential chemical attraction of functionalized nanoparticles has been utilized in their preferred assemble into one of the blocks of microphase separated diblock copolymers[6]. Capillary force[7,8,9] and electrophoretic deposition[10] have also been used to assemble the nanoparticles on patterned templates. Lin et al. used the interface of immiscible fluids to assemble nanoparticles, finding that nanoparticles form a liquid-like monolayer at fluid interfaces[11].

Changing the shape of nanoparticles from isotropic spheres to anisotropic rods can dramatically change the properties of nanoparticles[12]. Anisotropic CdSe nanorods are especially interesting for applications in photovoltaic since the long axis of rod-like

structure may provide a continuous channel for electron transfer compared to the spherical nanoparticles where electrons have to hop from one particle to another[13]. However, methods to manipulate nanorods are few and limited in scope. Nanorods have been shown to self-assemble into liquid crystalline phases in a manner similar to rigid rod molecules, due to anisotropic shape[14,15,16]. Another interesting recent example of nanorod assembly is the formation of strings of Au nanorods using multiwall carbon nanotubes as templates via a polyelectrolyte layer-by-layer deposition approach[17]. To utilize these rods to their full potential for applications, further control is needed over their assembly, such as positional and orientational correlation between rods.

Here, various routes to nanorod assembly are discussed, where both positional and orientational control over the rods can be achieved. Described here is the use of polystyrene-*block*-poly(methyl methacrylate) (PS-*b*-PMMA) diblock copolymer thin films to generate templates having hollow cylindrical pores or channels[10]. CdSe nanorods covered with poly(ethylene oxide) (PEO) were then assembled within the templates and confined within the pores and channels by 1) spin coating the nanorods along with diblock copolymer and annealing, 2) "surface reconstruction" of diblock copolymer template[18] and 3) floating the template film onto an aqueous solution of nanorods. The nature of the ligands on the rods is very important to enable the assembly of the rods. Alkane-covered nanorods are not compatible with these approaches since 1) alkane-covered nanorods are not miscible with either component of the diblock copolymer and 2) they are not water-soluble which is required for flotation technique. Therefore, PEG covered nanorods are used that are soluble in water and as well as miscible with PMMA matrix.

5.2 Experimental

CdSe nanorods were synthesized according to published procedures[19] and were obtained from Qingling Zhang at University of Massachusetts, Amherst. The nanorods were covered with PEO ligands and dispersity in size of the nanorods was less than 10 %. Films of PS-*b*-PMMA copolymer (MW 260,000 g/mol, PS weight fraction of 50%, Polymer Source, Inc), 50 nm in thickness, were prepared by spin-casting toluene solution of the polymer onto cleaned silicon substrates. Thin films of PS-*b*-PMMA copolymer (MW 140,000 g/mol and PS weight fraction of 68 %) were similarly prepared. For the block copolymer-nanorod composite films, a co-solution of nanorods along with block copolymer was prepared in toluene. The concentration of nanorods was 5% by weight and was 1 % by weight for the block copolymer. These films were annealed at 170 ^{o}C under vacuum for 1 hr.

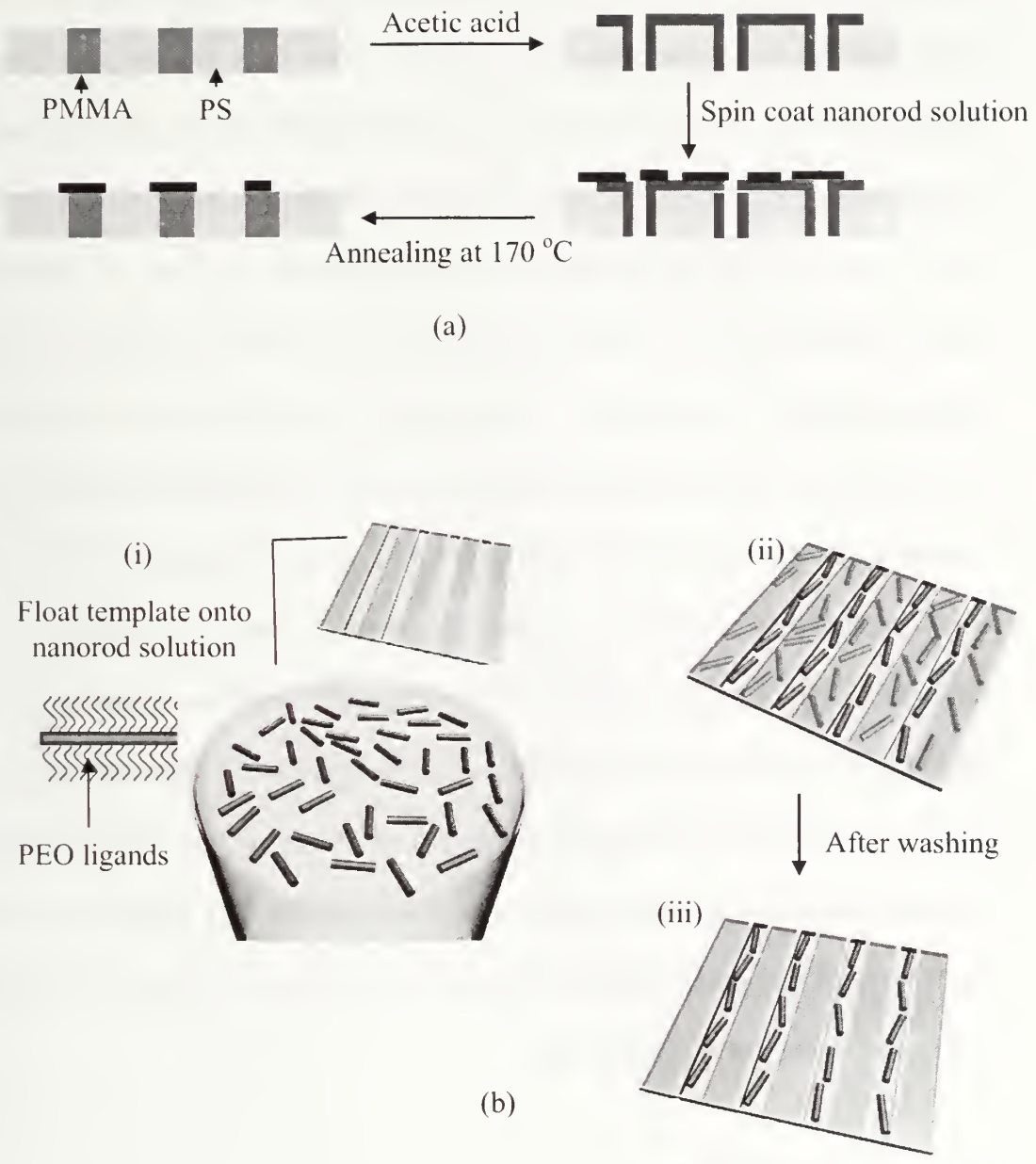

Figure 5.1: (a) Schematic showing 'surface reconstruction' of PS-*b*-PMMA template to selectively incorporate nanorods in PMMA domains. (b) Schematic showing floating a PS-*b*-PMMA template on TEM copper grid onto the aqueous solution of PEO covered nanorods.

After annealing films of block copolymer-nanorods composites, the films were floated onto aqueous hydrofluoric acid solution (5 vol %) (warning: 5 % hydrofluoric acid is dangerous and safety precautions including use of personal protective equipment

is recommended) and were examined under transmission electron microscopy (TEM) (JEOL 2000FX). For the template films used for surface reconstruction, the films were immersed in acetic acid for 5 min and were then washed with ethanol. The nanorods were deposited on the film from ethanol solution and the film was annealed for 1 hr at 170 ^{o}C. Later, the films were floated and examined under the TEM. The schematic is shown in Figure 5.1(a). To prepare templates for the flotation technique, films were exposed to deep UV irradiation (λ = 254 nm) for 30 min and washed with acetic acid for 5 min, which removed PMMA and cross-linked PS. The film was then floated onto hydrofluoric acid solution and retrieved with a 400 mesh TEM copper grid. In this way, cross-linked polystyrene films with pores of diameter ~30 nm and channels of ~30 nm width were obtained. The copper grid with template was floated onto an aqueous solution of PEO covered CdSe nanorods, with the template film facing the solution as shown in Figure 5.1(b). The template supported by the copper grid was left floating on the nanorod solution overnight, then removed and washed with water for one minute. Transmission electron microscopy (TEM) (JEOL 2000FX) was used to examine the distribution of nanorods in the template.

5.3 Results and Discussion

It has been shown previously that the nanoparticles tend to assemble in the domains of a phase separated diblock thin copolymer film with which they have favorable interactions.[6] Further, it has been shown that the nanoparticles can even mediate the interactions of the block copolymer with the surfaces and can help orient the domains in thin copolymer films.[20] The previous studies were carried out with

spherical nanoparticles. Therefore, the effect of anisotropic particles on diblock copolymer domains orientation was not studied. In this study, PS-*b*-PMMA block copolymer was mixed with PEO covered nanorods. It is well known that the PEO and PMMA are miscible and therefore PEO covered nanorods are expected to go to the PMMA domains. Unlike in previous studies, the effect of block copolymer domain alignment on nanorods orientation is studied. A neutral surface was used to spincoat the film so as to have the normal orientation of cylinder domains. Figure 5.2 shows TEM micrographs of the thin films after annealing for 1 hr at 170 °C. It can be observed that the PMMA domains are oriented normal to surface and some of the domains have nanorods dispersed in them. Further it can be observed that the nanorods are present mostly in PMMA domains but most of them are still oriented perpendicular to the domains. Although the PMMA domains are less than 15 nm in diameter and nanorods are 30 nm long, still the nanorods stretch the PMMA domains and lie parallel to surface.

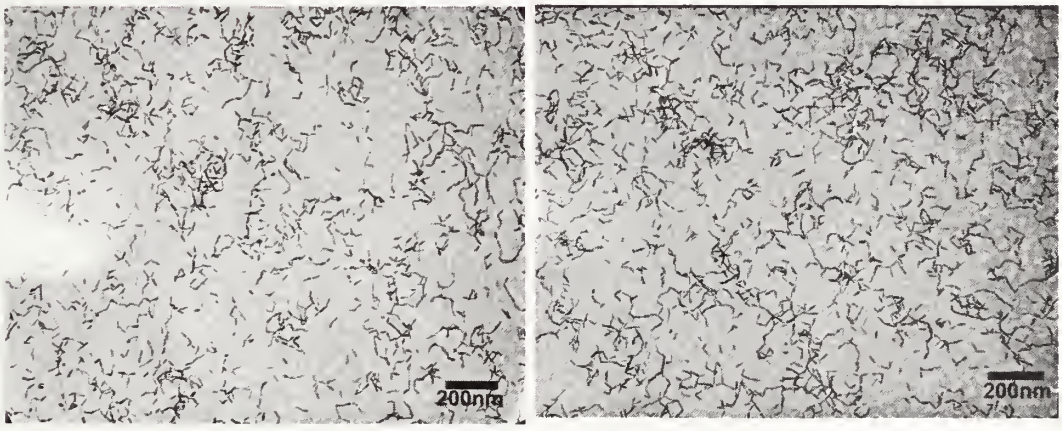

Figure 5.2: TEM micrographs of diblock copolymer and nanorods composite thin film after annealing for 1 hr at 170 °C.

Therefore, in order to have a better segregation of nanorods in PMMA domains, surface reconstruction technique was used. In surface reconstruction a phase separated

thin block copolymer film is swollen with a solvent which is preferable for the minority component and is shown in Figure 5.1(a). In this case acetic acid was used to swell the PMMA domains such that on removing the solvent, PMMA covers the whole surface of the polymer thin film. Afterwards nanorods are deposited on the surface and the film is annealed so that the equilibrium is achieved and the PMMA chains retract to their domains. Since the PEO is miscible with PMMA, it is expected that the nanorods will be dragged along the retracting PMMA chains and the nanorods will be accommodated in the PMMA domains. Figure 5.3 shows TEM images of the films which have been annealed after depositing the nanorods on the top. It can be observed that the nanorods do not go to the PMMA domains and are arranged on the top of film randomly. Since there is no strong interaction between PMMA and PEO, therefore it is possible that the retracting PMMA chains could not drag the PEO covered nanorods along with them in the cylinder domains. Therefore, in order to have a better separation of nanorods in one domain of a diblock copolymer, flotation technique was used and is shown in Figure 5.1(b).

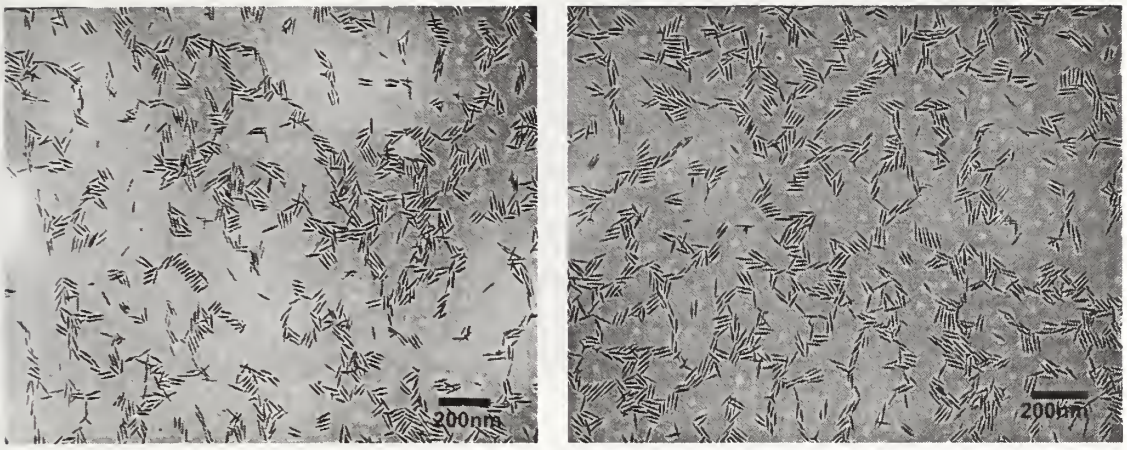

Figure 5.3: TEM micrographs of annealed 'surface reconstructed' thin films with nanorods deposited on it.

The solubility of the PEO-covered nanorods is characteristic of PEO, as the nanorods were dispersible effectively in both water and organic solvents, such as chloroform, toluene, and methanol. Since PEO is well known to be surface-active[21] which means PEO can act as a surfactant, it is expected that the PEO-covered CdSe nanorods will segregate to the water-air interface, forming a layer of nanorods at the water-air interface. Therefore, the block copolymer templates with pores and channels floating on the surface, will limit the surface area accessible for adsorption, and, control the lateral placement of the nanorods. Figure 5.4(a) shows the distribution of 40 nm CdSe nanorods on the template, and within the channels of the template, after floating on the aqueous nanorod solution overnight. Figure 5.4(b) shows the same sample after rinsing with water for 1 minute where the nanorods that were initially present on the template surface rather than within the channels, have been removed. From these results, it is clear that the nanorods on the template surface are loosely bound, while those embedded within the channels are held more strongly.

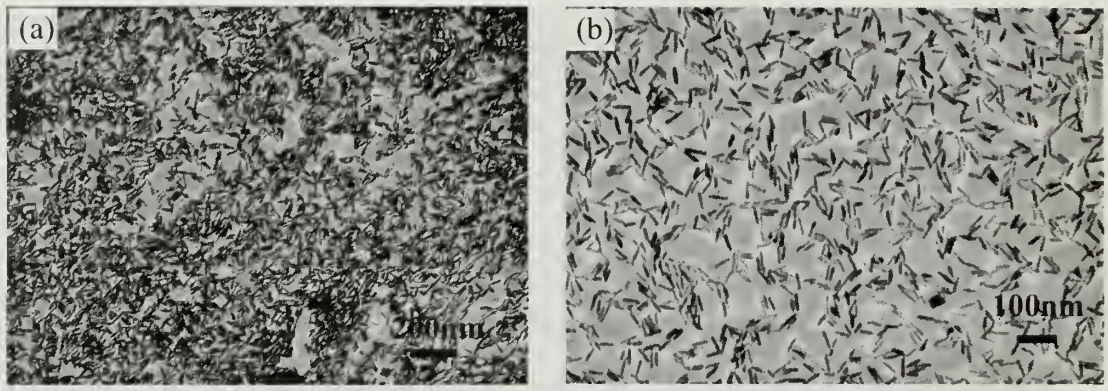

Figure 5.4: TEM micrographs showing the distribution of nanorods on lamellar template film with channels (a) after deposition, and (b) after washing with water.

The incorporation of the nanorods within the channels of the template was observed for all nanorods length studied (20, 30, 35, and 60 nm), as shown in Figure 5.5. It should also be noted that the nanorods align themselves along the wall of channels. This tendency becomes more obvious when the nanorods are confined laterally as the rod length becomes comparable to or larger than the width of the channels (Figure 5.5 (b) and (c)). It should be noted that the average separation distance between the confined nanorods can be varied by changing the channel-to-channel separation distance, which is dictated by the molecular weight of the diblock copolymers used to prepare the templates.

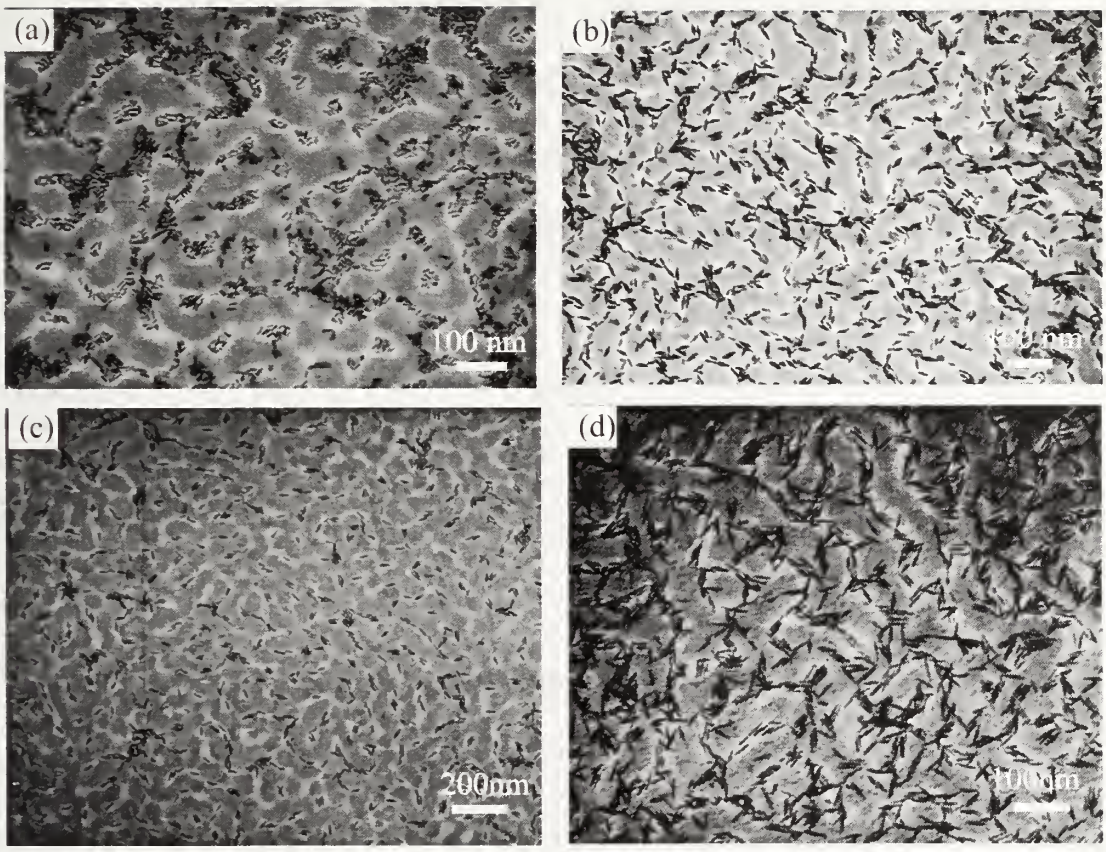

Figure 5.5: TEM micrographs showing distribution of nanorods on lamella template film after washing in water. Length of nanorod is (a) 20 nm, (b) 30 nm, (c) 35nm and (d) 60nm

Similar behavior was observed using nanoporous templates prepared from diblock copolymers having cylindrical microdomains. Here, circular areas on the surface are available for adsorption. When the nanorod length is smaller than the diameter of the pores in the template, the nanorods segregate to the surface within the pores. The high fidelity of this assembly is apparent in Figure 5.6(a), for 20 nm nanorods in a template with 30 nm diameter pores. Each of the pores contains several nanorods, although no preferred orientation of the nanorods is observed, due to the symmetry of a cross-section of the circular pore. Figure 5.6(b) shows 40 nm CdSe nanorods in the same nanoporous template. Apparently, as the rod length exceeds the

diameter of pores, it is difficult for the nanorods to fit into the pores. Due to packing constraints, each pore can only hold one or two nanorods.

The segregation and ordering of PEO-covered nanorods in the channels and pores of the template can be understood by considering the interfacial energy of the system. The low surface energy of PEO directs the PEO-covered nanorods to the water/air interface within the template, and orients the nanorods with respect to one another, to maximize the number of nanorods in the confined area. The channels and pores in the copolymer templates are hydrophobic and, as such, are not wet by water. However, the segregation of PEO to the template-water interface allows the nanorod solution to enter the channels/pores. In order to maximize contact with the walls of the channels, the nanorods orient parallel to the walls. The anisotropy of the nanorods and the more favorable interactions between the ligands, as opposed to with water, enhances the packing between the rods. In turn, a dense packing of the nanorods within the channels would limit the access of water into the channels, and consequently, retard desorption of the nanorods. In addition, the ligands within the channels may have more contact with the pore walls which would also slow desorption. Therefore, the nanorods within the channels and pores were not washed away with water while the nanorods on the template surface were removed upon washing with water.

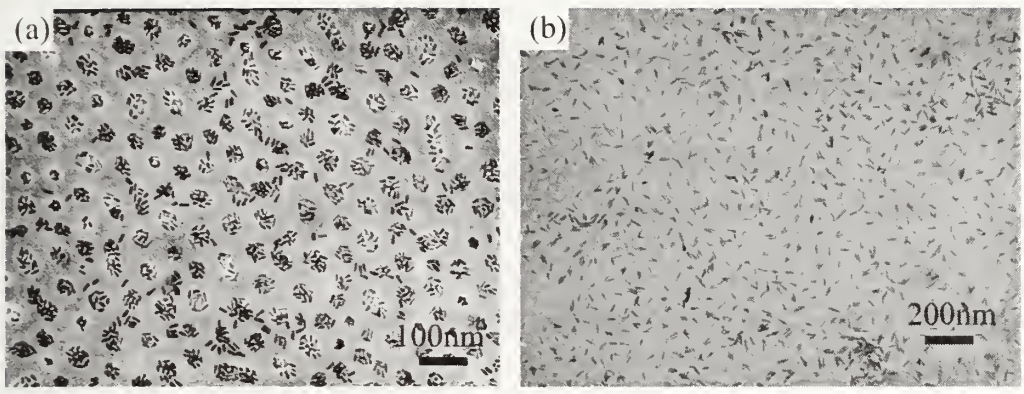

Figure 5.6: TEM micrographs showing the distribution of nanorods in cylindrical template a) length of the nanorod is 20 nm and b) length of nanorod is 40 nm.

5.4 Conclusion

We have shown that the PEO-covered CdSe nanorods can be assembled in two dimensions in block copolymer templates with control over both position and orientation. Of all the three techniques used, flotation technique worked best. The nanorods are parallel to the template surface and are present selectively in the channels with orientation along the channels. This has been further extended to nanoporous templates such that the nanorods were confined within the nanopores. The lower surface energy of PEO as compared to water surface energy, rod-rod interaction within the channels and pores, and rod-wall interaction are believed to give the selective presence of nanorods within the channels and pores. These findings may create new avenues for advancement in the fields of photovoltaic and microelectronics where 2-dimensional assembly of nanorods with control over position and orientation is desired.

5.4 References

1. Alivisatos, A. P., Semiconductor clusters, nanocrystals, and quantum dots. *Science* 1996, **271**, (5251), 933-937.

2. Frank, S.; Poncharal, P.; Wang, Z. L. and de Heer, W. A., Carbon nanotube quantum resistors. *Science* 1998, **280**, (5370), 1744-1746.

3. Sun, S. H.; Murray, C. B.; Weller, D.; Folks, L. and Moser, A., Monodisperse FePt nanoparticles and ferromagnetic FePt nanocrystal superlattices. *Science* 2000, **287**, (5460), 1989-1992.

4. Maier, S. A.; Brongersma, M. L.; Kik, P. G.; Meltzer, S.; Requicha, A. A. G. and Atwater, H. A., Plasmonics - A route to nanoscale optical devices. *Advanced Materials* 2001, **13**, (19), 1501-+.

5. Cushing, B. L.; Kolesnichenko, V. L. and O'Connor, C. J., Recent advances in the liquid-phase syntheses of inorganic nanoparticles. *Chemical Reviews* 2004, **104**, (9), 3893-3946.

6. Bockstaller, M. R.; Lapetnikov, Y.; Margel, S. and Thomas, E. L., Size-selective organization of enthalpic compatibilized nanocrystals in ternary block copolymer/particle mixtures. *Journal of the American Chemical Society* 2003, **125**, (18), 5276-5277.

7. Yin, Y. D.; Lu, Y.; Gates, B. and Xia, Y. N., Template-assisted self-assembly: A practical route to complex aggregates of monodispersed colloids with well-defined sizes, shapes, and structures. *Journal of the American Chemical Society* 2001, **123**, (36), 8718-8729.

8. Misner, M. J.; Skaff, H.; Emrick, T. and Russell, T. P., Directed deposition of nanoparticles using diblock copolymer templates. *Advanced Materials* 2003, **15**, (3), 221-+.

9. Cui, Y.; Bjork, M. T.; Liddle, J. A.; Sonnichsen, C.; Boussert, B. and Alivisatos, A. P., Integration of colloidal nanocrystals into lithographically patterned devices. *Nano Letters* 2004, **4**, (6), 1093-1098.

10. Zhang, C. L.; Xu, T.; Butterfield, D.; Misner, M. J.; Ryu, D. Y.; Emrick, T. and Russell, T. P., Controlled placement of CdSe nanoparticles in diblock copolymer templates by electrophoretic deposition. *Nano Letters* 2005, **5**, (2), 357-361.

11. Lin, Y.; Skaff, H.; Emrick, T.; Dinsmore, A. D. and Russell, T. P., Nanoparticle assembly and transport at liquid-liquid interfaces. *Science* 2003, **299**, (5604), 226-229.

12. Hu, J. T.; Li, L. S.; Yang, W. D.; Manna, L.; Wang, L. W. and Alivisatos, A. P., Linearly polarized emission from colloidal semiconductor quantum rods. *Science* 2001, **292**, (5524), 2060-2063.

13. Huynh, W. U.; Dittmer, J. J. and Alivisatos, A. P., Hybrid nanorod-polymer solar cells. *Science* 2002, **295**, (5564), 2425-2427.

14. Kim, F.; Kwan, S.; Akana, J. and Yang, P. D., Langmuir-Blodgett nanorod assembly. *Journal of the American Chemical Society* 2001, **123**, (18), 4360-4361.

15. Li, L. S.; Walda, J.; Manna, L. and Alivisatos, A. P., Semiconductor nanorod liquid crystals. *Nano Letters* 2002, **2**, (6), 557-560.

16. Li, L. S. and Alivisatos, A. P., Semiconductor nanorod liquid crystals and their assembly on a substrate. *Advanced Materials* 2003, **15**, (5), 408-+.

17. Correa-Duarte, M. A.; Perez-Juste, J.; Sanchez-Iglesias, A.; Giersig, M. and Liz-Marzan, L. M., Aligning an nanorods by using carbon nanotubes as templates. *Angewandte Chemie-International Edition* 2005, **44**, (28), 4375-4378.

18. Xu, T.; Stevens, J.; Villa, J. A.; Goldbach, J. T.; Guarim, K. W.; Black, C. T.; Hawker, C. J. and Russell, T. R., Block copolymer surface reconstuction: A reversible route to nanoporous films. *Advanced Functional Materials* 2003, **13**, (9), 698-702.

19. Peng, Z. A. and Peng, X. G., Nearly monodisperse and shape-controlled CdSe nanocrystals via alternative routes: Nucleation and growth. *Journal of the American Chemical Society* 2002, **124**, (13), 3343-3353.

20. Lin, Y.; Boker, A.; He, J. B.; Sill, K.; Xiang, H. Q.; Abetz, C.; Li, X. F.; Wang, J.; Emrick, T.; Long, S.; Wang, Q.; Balazs, A. and Russell, T. P., Self-directed self-assembly of nanoparticle/copolymer mixtures. *Nature* 2005, **434**, (7029), 55-59.

21. Dewhurst, P. F.; Lovell, M. R.; Jones, J. L.; Richards, R. W. and Webster, J. R. P., Organization of dispersions of a linear diblock copolymer of polystyrene and poly(ethylene oxide) at the air-water interface. *Macromolecules* 1998, **31**, (22), 7851-7864.

CHAPTER 6

"SELF-CORRALLING" NANORODS UNDER AN APPLIED ELECTRIC FIELD

6.1 Introduction

Orienting and packing nano-scale anisotropic objects, such as conducting and semi-conducting nanorods, is highly desirable for fundamental studies in charge transport, as well as photovoltaic and field emission devices.[1,2] Organic-inorganic hybrid photovoltaic devices, while having advantages of low cost, processibility, and flexibility, suffer from lower efficiency than silicon-based photovoltaics.[3] The efficiency of nanorod-based photovoltaics may be enhanced by a controlled orientation, and close-packing, of the rods. However, at low concentration nanorods tend to pack randomly when deposited from solution onto a substrate, while at higher concentration, liquid crystalline packing is achieved.[4,5,6] By adding a non-solvent to the nanorod solution, crystalline aggregates of nanorods have been observed.[7] The deposition of these nanorod aggregates onto a substrate produces densely packed, but unoriented, arrangements of the rods.

In this chapter, the orientation and packing of anisotropic nanoparticles, specifically CdSe nanorods is controlled by a combination of an external field and interfacial interactions. Prior studies have shown that polymer domains in diblock copolymer templates can be oriented in a pre-determined direction using an electric field, due to the anisotropic domains having different dielectric properties.[8] In this work, the permanent dipole moment in CdSe nanorods, as well as the anisotropy in the

dielectric properties of CdSe nanorods in solution, leads to nanorod alignment, along their long axes, in the presence of an electric field. Moreover, by addition of a polymer to the nanorod solution, the rods can be "corralled," due to non-favorable polymer-ligand interactions. Such interactions can be tailored by varying the polymer matrix and the ligands on the nanorod surface, and used to self-corral nanorods into densely packed arrays with controlled orientation.

6.2 Experimental

CdSe nanorods (~8 nm in diameter and ~40 nm in length) were prepared according to published procedures[9] that afford nanorods with a surface ligand coverage of tetradecylphosphonic acid (TDPA) and tri-*n*-octylphosphine oxide (TOPO). Transmission electron microscopy (TEM, JEOL 2000 FX, operated at 200kV) showed a nanorod length distribution of ~10%. A chloroform solution of these CdSe nanorods (0.5 wt %) and poly(methyl methacrylate) (PMMA, 0.5 wt %, molecular weight 25,000 g/mol) was prepared, and a droplet (~20 μl) of this solution was placed on a silicon oxide coated silicon wafer. Beside PMMA, poly(3-hexyl thiophene) was also used and was acquired form Aldrich. An electric field **E** (10^7 V/m) was applied while the chloroform evaporated over a ~8 hour period. This is shown schematically in Figure 6.1. The thin nanorod/polymer composite film obtained in this process was transferred onto a copper grid by floating the film onto a 5% HF(aq) solution to remove the silicon substrate, then examined by TEM.

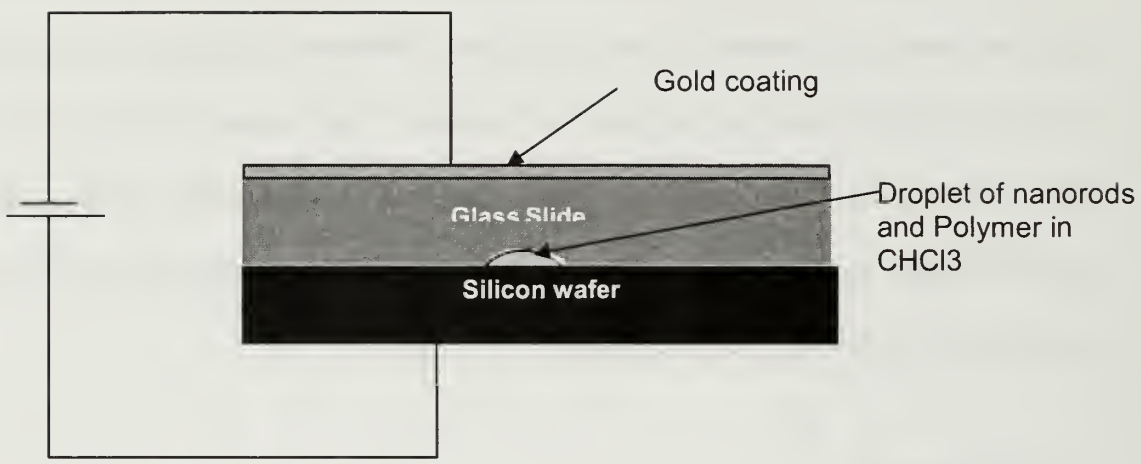

Figure 6.1: Schematic representation of the experimental setup for application of an electric field during solvent evaporation of nanorod-polymer composites. A silicon wafer serves as one electrode, and gold-coated soda lime glass serves as the second electrode.

Further in order to control the placement of the nanorods on the substrate, chemically patterned substrates were used. These were prepared by soft lithography.[10] The schematic of the process to prepare chemically patterned substrate is shown in Figure 6.2. A PDMS stamp was prepared by curing PDMS in a silicon mold and was 1 mM solution of dodecanethiol in ethanol was deposited on it. After evaporating the solvent, PDMS stamp was placed on a gold coated silicon wafer. This transfer the pattern onto the substrate and a pattern of dodecanethiol is obtained.

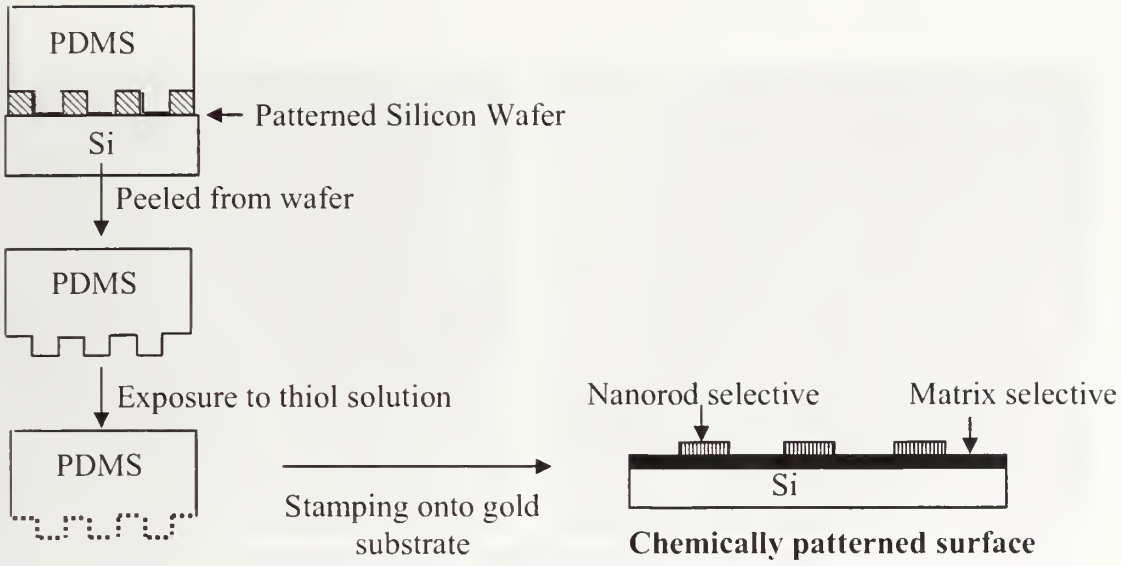

Figure 6.2: Schematic showing preparation of chemically patterned substrates using soft lithography.

6.3 Results and Discussion

The TEM image of Figure 6.3a shows a self-corralled nanorod-polymer composite film, using the procedure described above, to obtain a hexagonally close-packed array of nanorods aligned normal to the film surface. The average center-to-center distance between the nanorods is ~18 nm, with a separation distance between the rods of ~2 nm, or approximately twice the length of the attached TOPO ligands. In the absence of an applied field, the nanorods were found to aggregate in an orientation parallel to the film surface, as shown in Figure 6.3b.

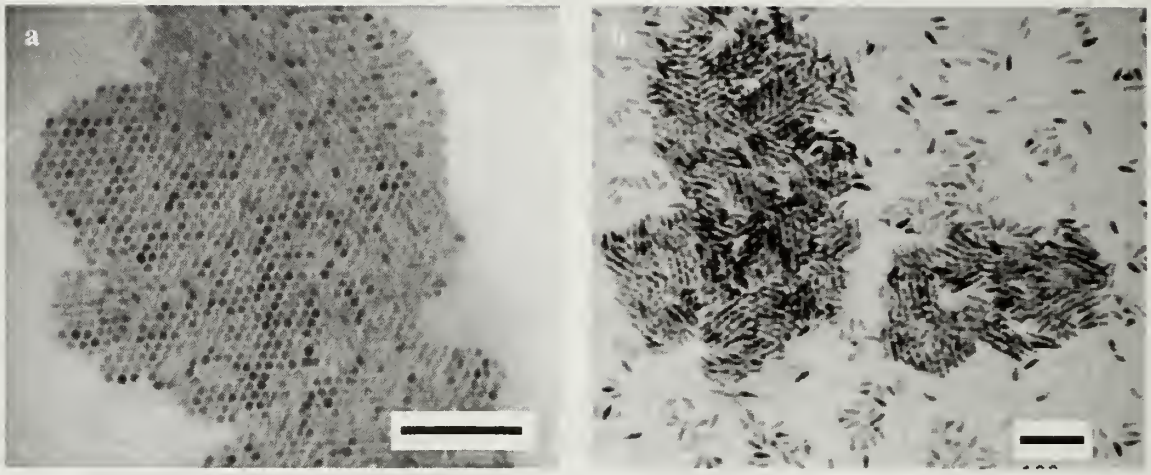

Figure 6.3: TEM images of "self-corralling" of alkane-covered CdSe nanorods in PMMA: (a) after solvent evaporation under an applied electric field, and (b) after solvent evaporation without an applied electric field. The scale bar is 100 nm.

The non-centrosymmetric, Wurtzite lattice of CdSe nanorods leads to a permanent dipole that increases linearly with increasing volume of the nanorods.[11] The unscreened dipole moment **P** of the nanorods used in our experiments is calculated to be ~1450 Debye, based on reported dipole moments of the CdSe nanorods, [10] assuming that the nanorods comprise a single crystal. There is a torque **T** exerted on a permanent dipole when placed in an electric field that aligns the dipole in the direction of the applied electric field. If the rods and electric field lines are orthogonal, the strength of the torque on the nanorods (**T** = **P** x **E**) is 4.872 x 10^{-20} Nm, or ten times the thermal energy at room temperature that would otherwise randomize the orientation of the nanorods. The dipole moment **P** is along the length of the nanorods as described in ref 10. In addition, the difference between the dielectric constants of CdSe nanorods and chloroform, used here as the solvent, gives rise to a polarization charge that exerts a force on the nanorods in the presence of the applied field. The sum of these forces causes the alignment of the nanorods in the direction of the applied electric field.

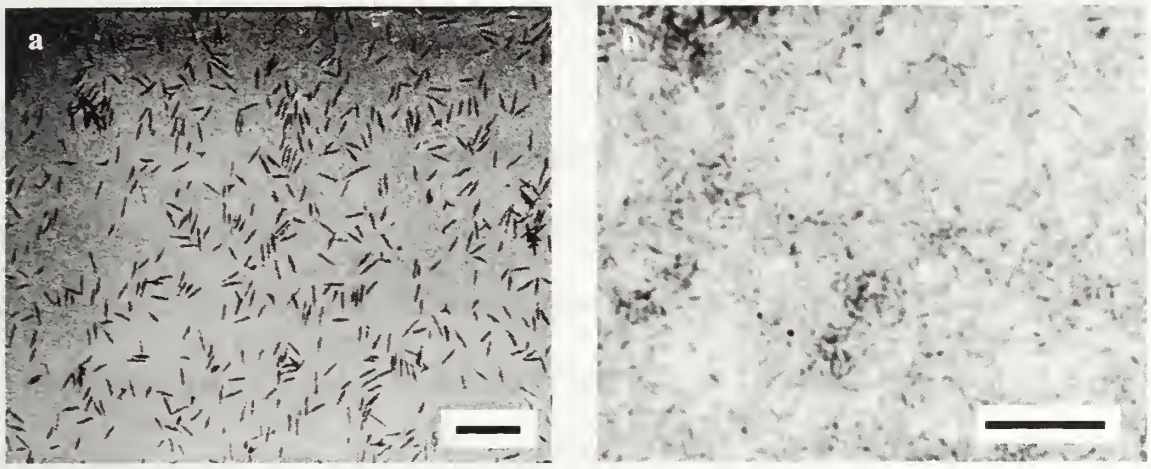

Figure 6.4: TEM images of unsuccessful "self-corralling": (a) PEO-covered CdSe nanorods in a PMMA matrix; and (b) PS-covered CdSe nanorods in PMMA matrix. All the samples were prepared under electric field. The scale-bar is 100 nm.

When self-corralling experiments were performed without polymer in the solution, nanorod alignment normal to the underlying substrate was not observed, even when the solvent was allowed to evaporate in the presence of an electric field. While in solution the nanorods become oriented in the direction of the applied electric field, as shown by Li *et al.*,[12] the orientation is lost when the solvent evaporates and the field is removed. This can be understood by considering that the ligands attached to the nanorods are highly solvent swollen and, upon solvent evaporation, the large volume loss and removal of the field cause the nanorods to collapse onto the substrate and assume an orientation parallel to the substrate. In the presence of a polymer, minimization of the interfacial tension, arising from the highly non-favorable interactions between the ligands and the polymer matrix, forces a phase separation and dense packing of the nanorods, *i.e.* a "corralling" that is frozen in by the polymer matrix upon solvent evaporation. It should also be noted that there is a large enthalpic energy

cost for isolated nanorods to be dispersed in the polymer matrix, further underscoring the concept of corralling.

By changing the chemical composition of either the polymer matrix or the ligands attached to the nanorods, the driving force for the corralling can be altered or even removed, though the dipolar properties of the nanorods remain unchanged. For example, alkane ligands on CdSe nanorods were replaced with poly(ethylene oxide) (PEO, molecular weight 2,000), keeping PMMA as the corralling polymer matrix. As in the prior case, a chloroform solution of these PEO-functionalized CdSe nanorods and PMMA was prepared, and a droplet of this solution was allowed to dry under an applied electric field. As shown in Figure 6.4a, the nanorods did not aggregate, due to the miscibility between the PEO ligands and the surrounding PMMA matrix[11] that promotes homogeneous dispersion of the nanorods in the polymer matrix. The lack of orientation observed for these nanorods in the applied field direction indicates that not only is it necessary to have an applied field to orient the nanorods, but an additional force, acting in the plane of the film, is necessary to force a dense packing of oriented nanorods and to retain the desired alignment.

With interfacial energy playing a key role in corralling the nanorods, studies were performed to determine if systems with a low interfacial energy would behave similarly. Figure 6.4b shows a TEM image of a mixture of PMMA with nanorods having polystyrene (PS) ligands (molecular weight ~2,000, thiol chain-end), in which the film was solution cast under an applied field. As expected, the PS-covered nanorods phase separate from the PMMA matrix. However, the nanorods remain oriented parallel to the surface of the film, normal to the applied field. Consequently,

while the non-favorable interactions between the PS ligands and the PMMA matrix cause a phase separation, the magnitude of the segmental interactions is too weak[13,14] to force a close packing of the nanorods. Hence, during solvent evaporation, volume contraction is sufficiently large such that when the field is removed, orientation of the nanorods in the direction of the field is lost. Strong, non-favorable polymer-ligand interactions are thus necessary to attain a sufficient packing density of the oriented nanorods so that alignment is not lost when the field is removed.

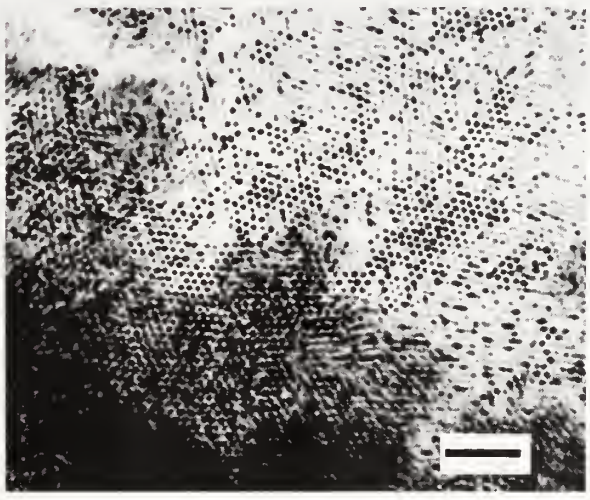

Figure 6.5: "Self-corralling" of Alkane-covered CdSe nanorods in a P3HT matrix. The nanorods phase separate and align perpendicular to the substrate upon application of an electric field. The scale-bar is 100 nm.

Figure 6.5 shows another example of self-corralling, in this case, arrays of densely-packed CdSe nanorods oriented normal to the film surface, where the nanorods are covered with alkane ligands, and the polymer matrix is regioregular poly(3-hexylthiophene) (P3HT). P3HT is a photoactive polymer that has generated considerable interest in photovoltaic devices, making this type of nanorod assembly especially encouraging. In future studies we will examine the effect of corralled nanorods where the photoactive polymer is attached directly to the rods,[15,16] an

appealing structure from the standpoint of potentially improving charge transport efficiency in photovoltaic applications.[17]

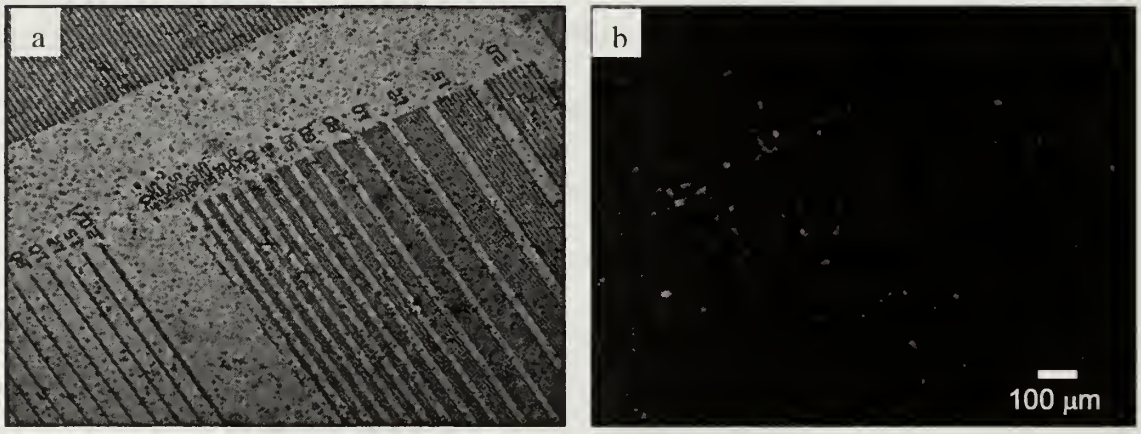

Figure 6.6: (a) Optical microscope image of nanorods corralled on thiol covered areas after selectively removing poly (vinyl pyridine). (b) Florescence microscope image of fluorescent nanorods selectively 'corralled' on alkane-thiol covered areas.

For the device fabrication, it will be crucial to control the area under nanorod aggregates and for photovoltaic applications it will be useful to maximize the areas under the nanorods. To achieve a control on self corralling, chemically patterned substrates were tried. For these experiments, chemically patterned substrates were prepared which have gold and thiol patterns. A solution of alkane covered nanorods along with poly(2-vinyl pyridine) (P2VP) in chloroform was deposited on a chemically patterned substrate. Then the chloroform was removed under electric field. Since there is a strong interaction between gold and P2VP and between alkane covered nanorods and dodecanethiol, the nanorods should corral onto the dodecanethiol covered areas. This was observed by optical microscopy as well fluorescence microscope also. Figure 6.6a shows the optical micrograph in which nanorods are shown to cover the areas

where dodecanethiol was deposited and Figure 6.6b shows the fluorescence micrograph. Since the nanorods are fluorescent, the bright areas have higher concentration of nanorods.

6.4 Conclusion

In summary, phase separation phenomena in combination with an applied electric field is shown to effectively corral CdSe nanorods into densely packed arrays that stand perpendicular to the underlying substrate. A coupling of the phase separation and the field alignment is critically important to achieving the desired assemblies. The strength of the force corralling the nanorods is governed by the interfacial energy between the ligands attached to the nanorods and the polymer matrix. If the interfacial energy is not sufficiently large, then alignment of the nanorods is not achieved. When extrapolating to the use of photoactive ligands on the nanorods, a viable route to highly efficient photovoltaic devices is conceivable.

6.5 References

1. Huynh, W. U.; Dittmer, J. J. and Alivisatos, A. P., Hybrid nanorod-polymer solar cells. *Science* 2002, **295**, (5564), 2425-2427.

2. Fan, S. S.; Chapline, M. G.; Franklin, N. R.; Tombler, T. W.; Cassell, A. M. and Dai, H. J., Self-oriented regular arrays of carbon nanotubes and their field emission properties. *Science* 1999, **283**, (5401), 512-514.

3. Coakley, K. M. and McGehee, M. D., Conjugated polymer photovoltaic cells. *Chemistry of Materials* 2004, **16**, (23), 4533-4542.

4. Kim, F.; Kwan, S.; Akana, J. and Yang, P. D., Langmuir-Blodgett nanorod assembly. *Journal of the American Chemical Society* 2001, **123**, (18), 4360-4361.

5. Li, L. S.; Walda, J.; Manna, L. and Alivisatos, A. P., Semiconductor nanorod liquid crystals. *Nano Letters* 2002, **2**, (6), 557-560.

6. Li, L. S. and Alivisatos, A. P., Semiconductor nanorod liquid crystals and their assembly on a substrate. *Advanced Materials* 2003, **15**, (5), 408-+.

7. Talapin, D. V.; Shevchenko, E. V.; Murray, C. B.; Kornowski, A.; Forster, S. and Weller, H., CdSe and CdSe/CdS nanorod solids. *Journal of the American Chemical Society* 2004, **126**, (40), 12984-12988.

8. Morkved, T. L.; Lu, M.; Urbas, A. M.; Ehrichs, E. E.; Jaeger, H. M.; Mansky, P. and Russell, T. P., Local control of microdomain orientation in diblock copolymer thin films with electric fields. *Science* 1996, **273**, (5277), 931-933.

9. Peng, Z. A. and Peng, X. G., Nearly monodisperse and shape-controlled CdSe nanocrystals via alternative routes: Nucleation and growth. *Journal of the American Chemical Society* 2002, **124**, (13), 3343-3353.

10. Zhao, X. M.; Xia, Y. N. and Whitesides, G. M., Soft lithographic methods for nano-fabrication. *Journal of Materials Chemistry* 1997, **7**, (7), 1069-1074.

11. Li, L. S. and Alivisatos, A. P., Origin and scaling of the permanent dipole moment in CdSe nanorods. *Physical Review Letters* 2003, **90**, (9).

12. Ito, H.; Russell, T. P. and Wignall, G. D., Interactions in Mixtures of Poly(Ethylene Oxide) and Poly(Methyl Methacrylate). *Macromolecules* 1987, **20**, (9), 2213-2220.

13. Russell, T. P.; Hjelm, R. P. and Seeger, P. A., Temperature-Dependence of the Interaction Parameter of Polystyrene and Poly(Methyl Methacrylate). *Macromolecules* 1990, **23**, (3), 890-893.

14. Strobl, G. R. (1997). The physics of Polymers: Concepts for Understanding Their Structures and Behavior. Berlin, Springer-Verlag.

15. Liu, J. S.; Tanaka, T.; Sivula, K.; Alivisatos, A. P. and Frechet, J. M. J., Employing end-functional polythiophene to control the morphology of nanocrystal-polymer composites in hybrid solar cells. *Journal of the American Chemical Society* 2004, **126**, (21), 6550-6551.

16. Skaff, H.; Sill, K. and Emrick, T., Quantum dots tailored with poly(para-phenylene vinylene). *Journal of the American Chemical Society* 2004, **126**, (36), 11322-11325.

17. Scher, E. C.; Manna, L. and Alivisatos, A. P., Shape control and applications of nanocrystals. *Philosophical Transactions of the Royal Society of London Series a-Mathematical Physical and Engineering Sciences* 2003, **361**, (1803), 241-255.

CHAPTER 7

CONCLUSION AND FUTURE WORK

In this thesis various projects have been described that deal with manipulating interactions between polymer thin films and substrates, as well as polymer and inorganic particles at length scales that vary from the microscopic to nanoscopic. Novel structures on microscopic length scale were made in polymer thin films using an electric field. By using multi-layered polymer thin films and applying an electric field, novel 3D cage like structures were obtained. These 'cage' like structures were formed because one of the polymers was encapsulated by the other polymer and upon selective removal of one of the polymers, cage-like structures were obtained. Electric fields were also used in conjunction with ultrasonic vibrations to produce structures having square symmetry in polymer thin films. The size of the structures was varied by changing the frequency of the vibrations. These square symmetric structures have length scales that are appropriate for planar photonic band gap devices. Further, electric fields were used to replicate nanoscopic structures in polymer thin films by using a patterned top electrode. PS-*b*- PMMA diblock copolymer thin film was used to pattern the electrode and provide the contrast in the electric field at the polymer film on the lower electrode. The areas under the PMMA domains have higher electric field strength and thus, were pulled towards the top electrode leading to replication of the pattern.

The interactions between polymer and inorganic particles were manipulated at nanoscopic length scales to produce composites that 'self heal'. The interactions were manipulated by varying the ligands present on the nanoparticles. When a polymer-

nanoparticle composite thin film is sandwiched between two brittle layers, the nanoparticles migrate to a crack created in the brittle layer. This fills up the crack with nanoparticles and potentially heals the crack. The nanoparticles diffuse to the crack only when their enthalpic interactions with polymer was negligible and they are big enough to provide an entropic penalty to the polymer chains by limiting the conformational states available to polymer chains. When 5.2 nm PEO-covered nanoparticles were used with a PMMA matrix, they satisfy both the conditions and diffuse to the cracks, while smaller nanoparticles, 3 nm in size did not diffuse due to the negligible entropic penalty. TOPO-covered nanoparticles were found to be fully excluded from a PMMA matrix due to large, non-favorable enthalpic interactions between the PMMA and the alkane ligands. The shape of the nanoparticles also affected the rate of diffusion of nanoparticles to the cracks, with rod-like nanoparticles having higher diffusion constants. Anisotropic nanoparticles were co-assembled with PS-*b*-PMMA by a variety of techniques. When PEO-covered nanorods were used, the nanorods assembled in PMMA domains. PEO-covered nanorods were assembled in PMMA domains by a 'surface reconstruction' method. Here, PMMA domains in PS-*b*-PMMA copolymer thin films were highly swollen by acetic acid, pulling the PMMA chains to the surface and, upon drying PMMA covered the entire surface. Nanorods were deposited on to the film and the film was annealed so that PMMA chains retracted back into the pores pulling along the PEO-covered nanorods. Also PEO-covered nanorods were deposited in the channels and pores made by the selective removal of PMMA in thin films of PS-*b*-PMMA with lamella and cylindrical microdomain. This was done by a floatation technique where the porous thin films were floated on an

aqueous solution of PEO-covered nanorods. Due to low surface energy of the PEO-covered nanorods, nanorods get trapped in the channels/pores present in the film. This technique provides positional control over the assembly of the nanorods in thin polymer films but orientational control was absent i.e. nanorods were always parallel to polymer film and could not be oriented normal to surface. To orient the nanorods normal to surface, a 'self-corralling' technique was developed. Here, the phase separation of nanorods a in polymer matrix along with an applied electric field was used to obtain hexagonally close packed nanorods oriented normal to film surface. The phase separation of the nanorods in the polymer matrix forces the nanorods to be corralled so as to minimize ligand/polymer contacts. The electric field oriented the CdSe nanorods along the field lines due to the permanent dipole moment along the length of the nanorods. Thus, close-packed nanorods oriented normal to the film surface were obtained. Further 'self corralling' of nanorods can be directed by using a chemically patterned surface such that the nanorods can be preferentially directed to one area of a patterned surface and the polymer to the other. Such patterned substrates were made by soft lithography where a PDMS stamp was used to pattern a gold substrate followed by the self-assembly of dodecane thiol on the gold substrate. By using such a patterned substrate along with nanorods covered with alkanes and using poly (2-vinyl pyridine) as matrix, self-corralling of nanorods was directed to thiol covered areas where as P2VP covered the gold covered areas. These normally oriented semiconductor CdSe nanorods have potential applications in photovoltaic devices.

A lot of work has been done in studying the electrohydrodynamic instabilities in thin polymer films. Structures with sizes varying from nanoscopic to microscopic

length scales have been made using the electrohydrodynamic instabilities. However, some areas remain with numerous opportunities. One can think of altering the dielectric constant of polymer films by doping with ionic salts so that the dielectric constant of the polymer can be increased. Under DC voltage conditions, the dielectric constant of the polymer can be made infinite by doping with an ionic salt that dissociates in the polymer. To attain this one has to use polar polymers like PEO or PMMA. Since structure spacing depends on the dielectric constant of the polymer film, smaller structures should be formed.

In 'self healing' composites, we have shown that the nanoparticles can migrate to a crack. Whether they really heal the crack is still unanswered. Experiments have to be done to determine the mechanical properties of the brittle layer and compared to the mechanical properties of cracks where nanoparticles have aggregated. Further, in order to improve the mechanical properties of the cracked brittle layer one can think of crosslinking the nanoparticles after they assemble in the crack. In order to enable it, novel ligands have to be designed.

'Self-corralling' experiments open up avenues to obtain structures suitable for photovoltaic applications. However, it is left to be proven that photovoltaic devices made by using this technique have high photoconversion efficiencies. To fabricate photovoltaic devices, CdSe nanorods have to be synthesized with attached photoactive polymer ligands. Since this will give maximum interface between hole and electron transport domains, excitons can be harvested efficiently while the normally oriented CdSe nanorods will provide efficient route for electrons to travel to the electrode.

BIBLIOGRAPHY

Alivisatos, A. P., Semiconductor clusters, nanocrystals, and quantum dots. *Science* 1996, **271**, (5251), 933-937.

Black, C. T.; Guarini, K. W.; Milkove, K. R.; Baker, S. M.; Russell, T. P. and Tuominen, M. T., Integration of self-assembled diblock copolymers for semiconductor capacitor fabrication. *Applied Physics Letters* 2001, **79**, (3), 409-411.

Bockstaller, M. R.; Lapetnikov, Y.; Margel, S. and Thomas, E. L., Size-selective organization of enthalpic compatibilized nanocrystals in ternary block copolymer/particle mixtures. *Journal of the American Chemical Society* 2003, **125**, (18), 5276-5277.

Bockstaller, M. R. and Thomas, E. L., Proximity effects in self-organized binary particle-block copolymer blends. *Physical Review Letters* 2004, **93**, (16).

Brandrup, J. and Immergut, E. H. (1989). Polymer handbook. New York, Wiley.

Brust, M.; Fink, J.; Bethell, D.; Schiffrin, D. J. and Kiely, C., Synthesis and Reactions of Functionalized Gold Nanoparticles. *Journal of the Chemical Society-Chemical Communications* 1995, (16), 1655-1656.

Buxton, G. A.; Lee, J. Y. and Balazs, A. C., Computer simulation of morphologies and optical properties of filled diblock copolymers. *Macromolecules* 2003, **36**, (25), 9631-9637.

Cahn, J. W. and Hilliard, J. E., Free Energy of a Nonuniform System .1. Interfacial Free Energy. *Journal of Chemical Physics* 1958, **28**, (2), 258-267.

Chen, X. X.; Dam, M. A.; Ono, K.; Mal, A.; Shen, H. B.; Nutt, S. R.; Sheran, K. and Wudl, F., A thermally re-mendable cross-linked polymeric material. *Science* 2002, **295**, (5560), 1698-1702.

Chen, Y. F.; Ji, T. H. and Rosenzweig, Z., Synthesis of glyconanospheres containing luminescent CdSe-ZnS quantum dots. *Nano Letters* 2003, **3**, (5), 581-584.

Chiu, J. J.; Kim, B. J.; Kramer, E. J. and Pine, D. J., Control of nanoparticle location in block copolymers. *Journal of the American Chemical Society* 2005, **127**, (14), 5036-5037.

Chou, S. Y. and Zhuang, L., Lithographically induced self-assembly of periodic polymer micropillar arrays. *Journal of Vacuum Science & Technology B* 1999, **17**, (6), 3197-3202.

Christiansen, B.; Alstrom, P. and Levinsen, M. T., Ordered Capillary-Wave States - Quasi-Crystals, Hexagons, and Radial Waves. *Physical Review Letters* 1992, **68**, (14), 2157-2160.

Coakley, K. M. and McGehee, M. D., Conjugated polymer photovoltaic cells. *Chemistry of Materials* 2004, **16**, (23), 4533-4542.

Colburn, M.; Bailey, T.; Choi, B. J.; Ekerdt, J. G.; Sreenivasan, S. V. and Willson, C. G., Development and advantages of step-and-flash lithography. *Solid State Technology* 2001, **44**, (7), 67-+.

Correa-Duarte, M. A.; Perez-Juste, J.; Sanchez-Iglesias, A.; Giersig, M. and Liz-Marzan, L. M., Aligning an nanorods by using carbon nanotubes as templates. *Angewandte Chemie-International Edition* 2005, **44**, (28), 4375-4378.

Cui, Y.; Bjork, M. T.; Liddle, J. A.; Sonnichsen, C.; Boussert, B. and Alivisatos, A. P., Integration of colloidal nanocrystals into lithographically patterned devices. *Nano Letters* 2004, **4**, (6), 1093-1098.

Cushing, B. L.; Kolesnichenko, V. L. and O'Connor, C. J., Recent advances in the liquid-phase syntheses of inorganic nanoparticles. *Chemical Reviews* 2004, **104**, (9), 3893-3946.

Dewhurst, P. F.; Lovell, M. R.; Jones, J. L.; Richards, R. W. and Webster, J. R. P., Organization of dispersions of a linear diblock copolymer of polystyrene and poly(ethylene oxide) at the air-water interface. *Macromolecules* 1998, **31**, (22), 7851-7864.

Douady, S. and Fauve, S., Pattern Selection in Faraday Instability. *Europhysics Letters* 1988, **6**, (3), 221-226.

Fan, S. S.; Chapline, M. G.; Franklin, N. R.; Tombler, T. W.; Cassell, A. M. and Dai, H. J., Self-oriented regular arrays of carbon nanotubes and their field emission properties. *Science* 1999, **283**, (5401), 512-514.

Fox, T. G. and Flory, P. J., 2nd-Order Transition Temperatures and Related Properties of Polystyrene .1. Influence of Molecular Weight. *Journal of Applied Physics* 1950, **21**, (6), 581-591.

Frank, S.; Poncharal, P.; Wang, Z. L. and de Heer, W. A., Carbon nanotube quantum resistors. *Science* 1998, **280**, (5370), 1744-1746.

Harris, M.; Appel, G. and Ade, H., Surface morphology of annealed polystyrene and poly(methyl methacrylate) thin film blends and bilayers. *Macromolecules* 2003, **36**, (9), 3307-3314.

Hu, J. T.; Li, L. S.; Yang, W. D.; Manna, L.; Wang, L. W. and Alivisatos, A. P., Linearly polarized emission from colloidal semiconductor quantum rods. *Science* 2001, **292**, (5524), 2060-2063.

Huynh, W. U.; Dittmer, J. J. and Alivisatos, A. P., Hybrid nanorod-polymer solar cells. *Science* 2002, **295**, (5564), 2425-2427.

Ito, H.; Russell, T. P. and Wignall, G. D., Interactions in Mixtures of Poly(Ethylene Oxide) and Poly(Methyl Methacrylate). *Macromolecules* 1987, **20**, (9), 2213-2220.

Kim, F.; Kwan, S.; Akana, J. and Yang, P. D., Langmuir-Blodgett nanorod assembly. *Journal of the American Chemical Society* 2001, **123**, (18), 4360-4361.

Kim, J. U. and O'Shaughnessy, B., Morphology selection of nanoparticle dispersions by polymer media. *Physical Review Letters* 2002, **89**, (23).

Krausch, G., Dewetting at the interface between two immiscible polymers. *Journal of Physics-Condensed Matter* 1997, **9**, (37), 7741-7752.

Kumar, K. and Tuckerman, L. S., Parametric-Instability of the Interface between 2 Fluids. *Journal of Fluid Mechanics* 1994, **279**, 49-68.

Lambooy, P.; Phelan, K. C.; Haugg, O. and Krausch, G., Dewetting at the liquid-liquid interface. *Physical Review Letters* 1996, **76**, (7), 1110-1113.

Lang, R. J., Ultrasonic Atomization of Liquids. *Journal of the Acoustical Society of America* 1962, **34**, (1), 6-&.

Lee, J. Y.; Buxton, G. A. and Balazs, A. C., Using nanoparticles to create self-healing composites. *Journal of Chemical Physics* 2004, **121**, (11), 5531-5540.

Li, L. S.; Walda, J.; Manna, L. and Alivisatos, A. P., Semiconductor nanorod liquid crystals. *Nano Letters* 2002, **2**, (6), 557-560.

Li, L. S. and Alivisatos, A. P., Origin and scaling of the permanent dipole moment in CdSe nanorods. *Physical Review Letters* 2003, **90**, (9).

Li, L. S. and Alivisatos, A. P., Semiconductor nanorod liquid crystals and their assembly on a substrate. *Advanced Materials* 2003, **15**, (5), 408-+.

Lin, Y.; Skaff, H.; Emrick, T.; Dinsmore, A. D. and Russell, T. P., Nanoparticle assembly and transport at liquid-liquid interfaces. *Science* 2003, **299**, (5604), 226-229.

Lin, Y.; Boker, A.; He, J. B.; Sill, K.; Xiang, H. Q.; Abetz, C.; Li, X. F.; Wang, J.; Emrick, T.; Long, S.; Wang, Q.; Balazs, A. and Russell, T. P., Self-directed self-assembly of nanoparticle/copolymer mixtures. *Nature* 2005, **434**, (7029), 55-59.

Lin, Y.; Boker, A.; Skaff, H.; Cookson, D.; Dinsmore, A. D.; Emrick, T. and Russell, T. P., Nanoparticle assembly at fluid interfaces: Structure and dynamics. *Langmuir* 2005, **21**, (1), 191-194.

Lin, Z. Q.; Kerle, T.; Baker, S. M.; Hoagland, D. A.; Schaffer, E.; Steiner, U. and Russell, T. P., Electric field induced instabilities at liquid/liquid interfaces. *Journal of Chemical Physics* 2001, **114**, (5), 2377-2381.

Lin, Z. Q.; Kerle, T.; Russell, T. P.; Schaffer, E. and Steiner, U., Electric field induced dewetting at polymer/polymer interfaces. *Macromolecules* 2002, **35**, (16), 6255-6262.

Lin, Z. Q.; Kerle, T.; Russell, T. P.; Schaffer, E. and Steiner, U., Structure formation at the interface of liquid liquid bilayer in electric field. *Macromolecules* 2002, **35**, (10), 3971-3976.

Liu, J. S.; Tanaka, T.; Sivula, K.; Alivisatos, A. P. and Frechet, J. M. J., Employing end-functional polythiophene to control the morphology of nanocrystal-polymer composites in hybrid solar cells. *Journal of the American Chemical Society* 2004, **126**, (21), 6550-6551.

Maier, S. A.; Brongersma, M. L.; Kik, P. G.; Meltzer, S.; Requicha, A. A. G. and Atwater, H. A., Plasmonics - A route to nanoscale optical devices. *Advanced Materials* 2001, **13**, (19), 1501-+.

McGuigan, A. P.; Briggs, G. A. D.; Burlakov, V.; Yanaka, M. and Tsukahara, Y., An elastic-plastic shear lag model for fracture of layered coatings. *Thin Solid Films* 2003, **424**, (2), 219-223.

Miles, J. and Henderson, D., Parametrically Forced Surface-Waves. *Annual Review of Fluid Mechanics* 1990, **22**, 143-165.

Misner, M. J.; Skaff, H.; Emrick, T. and Russell, T. P., Directed deposition of nanoparticles using diblock copolymer templates. *Advanced Materials* 2003, **15**, (3), 221-+.

Monch, W. and Herminghaus, S., Elastic instability of rubber films between solid bodies. *Europhysics Letters* 2001, **53**, (4), 525-531.

Morariu, M. D.; Voicu, N. E.; Schaffer, E.; Lin, Z. Q.; Russell, T. P. and Steiner, U., Hierarchical structure formation and pattern replication induced by an electric field. *Nature Materials* 2003, **2**, (1), 48-52.

Morkved, T. L.; Lu, M.; Urbas, A. M.; Ehrichs, E. E.; Jaeger, H. M.; Mansky, P. and Russell, T. P., Local control of microdomain orientation in diblock copolymer thin films with electric fields. *Science* 1996, **273**, (5277), 931-933.

Murray, C. B.; Kagan, C. R. and Bawendi, M. G., Synthesis and characterization of monodisperse nanocrystals and close-packed nanocrystal assemblies. *Annual Review of Materials Science* 2000, **30**, 545-610.

Nikoobakht, B.; Wang, Z. L. and El-Sayed, M. A., Self-assembly of gold nanorods. *Journal of Physical Chemistry B* 2000, **104**, (36), 8635-8640.

Pease, L. F. and Russel, W. B., Linear stability analysis of thin leaky dielectric films subjected to electric fields. *Journal of Non-Newtonian Fluid Mechanics* 2002, **102**, (2), 233-250.

Peng, Z. A. and Peng, X. G., Nearly monodisperse and shape-controlled CdSe nanocrystals via alternative routes: Nucleation and growth. *Journal of the American Chemical Society* 2002, **124**, (13), 3343-3353.

Puntes, V. F.; Krishnan, K. M. and Alivisatos, A. P., Colloidal nanocrystal shape and size control: The case of cobalt. *Science* 2001, **291**, (5511), 2115-2117.

Qu, S.; Clarke, C. J.; Liu, Y.; Rafailovich, M. H.; Sokolov, J.; Phelan, K. C. and Krausch, G., Dewetting dynamics at a polymer-polymer interface. *Macromolecules* 1997, **30**, (12), 3640-3645.

Rayleigh, L., On the crispations of fluid resting upon a vibrating support. *Philosophical Magazine* 1883, **16**, 50-58.

Reiter, G., Dewetting of Thin Polymer-Films. *Physical Review Letters* 1992, **68**, (1), 75-78.

Reiter, G., Unstable Thin Polymer-Films - Rupture and Dewetting Processes. *Langmuir* 1993, **9**, (5), 1344-1351.

Russell, T. P.; Hjelm, R. P. and Seeger, P. A., Temperature-Dependence of the Interaction Parameter of Polystyrene and Poly(Methyl Methacrylate). *Macromolecules* 1990, **23**, (3), 890-893.

Schaffer, E.; Thurn-Albrecht, T.; Russell, T. P. and Steiner, U., Electrically induced structure formation and pattern transfer. *Nature* 2000, **403**, (6772), 874-877.

Schaffer, E.; Thurn-Albrecht, T.; Russell, T. P. and Steiner, U., Electrohydrodynamic instabilities in polymer films. *Europhysics Letters* 2001, **53**, (4), 518-524.

Schaffer, E.; Harkema, S.; Roerdink, M.; Blossey, R. and Steiner, U., Morphological instability of a confined polymer film in a thermal gradient. *Macromolecules* 2003, **36**, (5), 1645-1655.

Scher, E. C.; Manna, L. and Alivisatos, A. P., Shape control and applications of nanocrystals. *Philosophical Transactions of the Royal Society of London Series a-Mathematical Physical and Engineering Sciences* 2003, **361**, (1803), 241-255.

Sferrazza, M.; Heppenstall-Butler, M.; Cubitt, R.; Bucknall, D.; Webster, J. and Jones, R. A. L., Interfacial instability driven by dispersive forces: The early stages of spinodal dewetting of a thin polymer film on a polymer substrate. *Physical Review Letters* 1998, **81**, (23), 5173-5176.

Shchukin, D. G.; Zheludkevich, M.; Yasakau, K.; Lamaka, S.; Ferreira, M. G. S. and Mohwald, H., Layer-by-layer assembled nanocontainers for self-healing corrosion protection. *Advanced Materials* 2006, **18**, (13), 1672-+.

Shchukin, D. G. and Mohwald, H., Self-repairing coatings containing active nanoreservoirs. *Small* 2007, **3**, (6), 926-943.

Skaff, H.; Sill, K. and Emrick, T., Quantum dots tailored with poly(para-phenylene vinylene). *Journal of the American Chemical Society* 2004, **126**, (36), 11322-11325.

Smith, K. A.; Tyagi, S. and Balazs, A. C., Healing surface defects with nanoparticle-filled polymer coatings: Effect of particle geometry. *Macromolecules* 2005, **38**, (24), 10138-10147.

Strobl, G. R. (1997). The physics of Polymers: Concepts for Understanding Their Structures and Behavior. Berlin, Springer-Verlag.

Sun, S. H.; Murray, C. B.; Weller, D.; Folks, L. and Moser, A., Monodisperse FePt nanoparticles and ferromagnetic FePt nanocrystal superlattices. *Science* 2000, **287**, (5460), 1989-1992.

Suo, Z. and Liang, J., Theory of lithographically-induced self-assembly. *Applied Physics Letters* 2001, **78**, (25), 3971-3973.

Suo, Z.; Prevost, J. H. and Liang, J., Kinetics of crack initiation and growth in organic-containing integrated structures. *Journal of the Mechanics and Physics of Solids* 2003, **51**, (11-12), 2169-2190.

Talapin, D. V.; Shevchenko, E. V.; Murray, C. B.; Kornowski, A.; Forster, S. and Weller, H., CdSe and CdSe/CdS nanorod solids. *Journal of the American Chemical Society* 2004, **126**, (40), 12984-12988.

Thompson, R. B.; Ginzburg, V. V.; Matsen, M. W. and Balazs, A. C., Predicting the mesophases of copolymer-nanoparticle composites. *Science* 2001, **292**, (5526), 2469-2472.

Thurn-Albrecht, T.; Schotter, J.; Kastle, C. A.; Emley, N.; Shibauchi, T.; Krusin-Elbaum, L.; Guarini, K.; Black, C. T.; Tuominen, M. T. and Russell, T. P., Ultrahigh-density nanowire arrays grown in self-assembled diblock copolymer templates. *Science* 2000, **290**, (5499), 2126-2129.

Trau, M.; Saville, D. A. and Aksay, I. A., Assembly of colloidal crystals at electrode interfaces. *Langmuir* 1997, **13**, (24), 6375-6381.

Troian, S. M.; Herbolzheimer, E.; Safran, S. A. and Joanny, J. F., Fingering Instabilities of Driven Spreading Films. *Europhysics Letters* 1989, **10**, (1), 25-30.

Tyagi, S.; Lee, J. Y.; Buxton, G. A. and Balazs, A. C., Using nanocomposite coatings to heal surface defects. *Macromolecules* 2004, **37**, (24), 9160-9168.

Verma, R.; Sharma, A.; Kargupta, K. and Bhaumik, J., Electric field induced instability and pattern formation in thin liquid films. *Langmuir* 2005, **21**, (8), 3710-3721.

Voicu, N. E.; Harkema, S. and Steiner, U., Electric-field-induced pattern morphologies in thin liquid films. *Advanced Functional Materials* 2006, **16**, (7), 926-934.

White, S. R.; Sottos, N. R.; Geubelle, P. H.; Moore, J. S.; Kessler, M. R.; Sriram, S. R.; Brown, E. N. and Viswanathan, S., Autonomic healing of polymer composites. *Nature* 2001, **409**, (6822), 794-797.

Wyart, F. B.; Martin, P. and Redon, C., Liquid-Liquid Dewetting. *Langmuir* 1993, **9**, (12), 3682-3690.

Xu, T.; Stevens, J.; Villa, J. A.; Goldbach, J. T.; Guarim, K. W.; Black, C. T.; Hawker, C. J. and Russell, T. R., Block copolymer surface reconstuction: A reversible route to nanoporous films. *Advanced Functional Materials* 2003, **13**, (9), 698-702.

Yin, Y. D.; Lu, Y.; Gates, B. and Xia, Y. N., Template-assisted self-assembly: A practical route to complex aggregates of monodispersed colloids with well-defined sizes, shapes, and structures. *Journal of the American Chemical Society* 2001, **123**, (36), 8718-8729.

Yu, G.; Gao, J.; Hummelen, J. C.; Wudl, F. and Heeger, A. J., Polymer Photovoltaic Cells - Enhanced Efficiencies Via a Network of Internal Donor-Acceptor Heterojunctions. *Science* 1995, **270**, (5243), 1789-1791.

Zhang, C. L.; Xu, T.; Butterfield, D.; Misner, M. J.; Ryu, D. Y.; Emrick, T. and Russell, T. P., Controlled placement of CdSe nanoparticles in diblock copolymer templates by electrophoretic deposition. *Nano Letters* 2005, **5**, (2), 357-361.

Zhao, X. M.; Xia, Y. N. and Whitesides, G. M., Soft lithographic methods for nano-fabrication. *Journal of Materials Chemistry* 1997, **7**, (7), 1069-1074.